STORM SURGE SIMULATION OF HURRICANE IVAN AND HURRICANE DENNIS

By

YANFENG ZHANG

A DISSERTATION PRESENTED TO THE GRADUATE SCHOOL
OF THE UNIVERSITY OF FLORIDA IN PARTIAL FULFILLMENT
OF THE REQUIREMENTS FOR THE DEGREE OF
DOCTOR OF PHILOSOPHY

UNIVERSITY OF FLORIDA

2007

To my parents, my wife, and my son

ACKNOWLEDGMENTS

First, I want to express my sincere appreciation to my advisor and supervisory committee chairman, Dr. Y. Peter Sheng, for his support and guidance through all these years. I also thank the members of my supervisory committee, Dr. Robert G. Dean, Dr. Ramesh K. Reddy, Dr. Robert J. Thieke, and Dr. Gary R. Consolazio for reviewing my dissertation.

I thank the sponsors of several University of Florida research projects for providing funding and data for my research study: Florida Sea Grant, South Florida Water Management District and UCITSS (Florida Atlantic University).

I thank Justin Davis, Vadim Alymov, Vladimir Paramygin, Taeyun Kim, Jun Lee, Jeff King, Kijin Park, Detong Sun for their help and moral support during my study. I would also like to thank Nancy, Kim, Ketty, Doretha and Lucy who make my life easier.

My sincere thanks, with my heart and soul, go to my parents and my wife for their love and endless support.

TABLE OF CONTENTS

LIST OF TABLES

LIST OF FIGURES

Abstract of Dissertation Presented to the Graduate School
of the University of Florida in Partial Fulfillment of the
Requirements for the Degree of Doctor of Philosophy

STORM SURGE SIMULATION OF HURRICANES IVAN AND HURRICANE DENNIS

By

Yanfeng Zhang

December 2007

Chair: Dr. Peter Y. Sheng
Major: Coastal and Oceanographic Engineering

This dissertation investigates the development, testing, and application of numerical models for simulating hurricane-induced storm surges and waves in coastal waters, with particular application to storm surges and inundation during Hurricanes Ivan (2004) and Dennis (2005) within the northeast Gulf of Mexico. This study also includes an assessment of the vulnerability of coastal highways and bridges during hurricane event.

Recent development in storm surge modeling was briefly reviewed followed by a detailed discussion of the high-resolution, curvilinear-grid coastal storm surge modeling system CH3D-SSMS. By dynamically coupling with a local wave model SWAN and a regional surge model ADCIRC, CH3D-SSMS is able to simulate wave, storm surge, and inundation during tropical storms driven by wind, atmospheric pressure, radiation stress, and freshwater discharge. For application to Hurricane Ivan (2004) and Hurricane Dennis (2005), a curvilinear grid with grid spacing of 100 m to 1,000 m was generated for the northeast Gulf of Mexico to resolve the complex shoreline as defined by the combined bathymetry/topography available from NOAA and USGS. NOAA HRD wind, NCEP WNA wind, and analytical Holland wind with land reduction effect are used in the model. CH3D-SSMS successfully reproduced both the magnitude and phase of storm surge and wave transport over extensive Northeast Gulf domain for both

hurricanes. The extent of flooding is found to be significant around Pensacola Bay during Category four Hurricane Ivan. Wave heights are reduced significantly from open water to coastal bay areas, but they are still sufficient to cause coastal structure damages. Various tests were conducted to investigate the model sensitivity to wind, land dissipation on wind, atmospheric pressure, wave, tide, bottom friction coefficient, open boundary condition, and time step. The results reveal that wind field is the dominant factor affecting storm surge development. Atmospheric pressure, wave-induced radiation stress, bottom friction coefficient, and water level at open boundary also have significant effects on simulated surge level. It is found that the water level at open boundary from shelf wave may contribute up to half of total storm surge at some coastal stations for Hurricane Dennis simulation. Other factors are found to be not very sensitive.

The coastal highways risk analysis during storm event, aimed to improve highway and bridge safety and security, is conducted for Hurricane Ivan in Florida and nearby states. The methodology of wave load calculation is described and then applied to the I-10 Bridge over Escambia Bay during Hurricane Ivan. The results confirmed that the big waves on top of the high surge during Ivan were sufficient to cause the breakdown of bolted connection, overcome of span weight and total damage of the bridge deck. With slightly decreased surge levels, the total wave force would be significantly reduced and result in no threat to the bridge. The risk analysis tests are conducted by varying hurricane parameters of intensity, size, landfall location, speed, and direction of approach for Hurricane Ivan. All these parameters are found to be important. A ranking system for assessing the vulnerability of coastal highways and bridges along the northeast Gulf coasts to storm surge and wave damages in extreme storm events are presented.

CHAPTER 1
INTRODUCTION

Hurricanes are storms with strong winds rotating counter-clockwise around a moving center of low atmospheric pressure. The strong wind can not only cause severe damage to structures, but also induce storm surges and cause devastating flooding over miles inland. According to Bureau of Meteorology Research Center, Australia (BMRC, 2006), a storm surge is a long gravity wave with a length scale similar to the size of the generating tropical cyclone and can lasts from several hours to days depending on the cyclone size and speed of movement. It is of a similar scale to an astronomical tide and should not be confused with short gravity wind waves which have wave-lengths of meters and periods of seconds. The surge usually consists of a single passing wave that elevates or depresses the still water height. In some special situations, especially for cyclones moving parallel to the coast, secondary waves or resurgences can form behind the tropical cyclone.

The ocean response to tropical cyclones is quite different in deep water and in shallow water. In deep water, far from a coast, the surface wind stress from a tropical cyclone creates a rotating mound of water by diffusing momentum downward. The ocean elevation is increased by approximately the hydrostatic uplift in response to the low central pressure and some minor long term Coriolis effects. Dynamic effects become pronounced as the tropical cyclone approaches a coast. On entering the shallow waters of a continental shelf, conservation of the potential vorticity of the mound requires development of marked divergence. Channeling by local bathymetry and reflections from the coast also contribute to substantially amplify the surge height (BMRC, 2006). Because of strong wind and high rising water, hurricanes are a huge threat to coastal areas. Billions of dollars and many lives can be lost.

With a quickly increasing population in coastal regions, hurricane caused damage becomes more and more devastating. In 2005, hurricane Katrina set a record-high of 81.2 billions dollars and nearly 2000 lives lost. It caused devastating catastrophe in New Orleans. The rising water caused the collapse of levees and left almost the entire city under water. Katrina also caused massive destruction on the coasts and great damage to coastal structures. Several coastal bridges have been completely destroyed. Among the five costliest hurricanes in history: (1) Hurricane Katrina (2005, $81.2B); (2) Hurricane Andrew (1992, $44.9B); (3) Hurricane Wilma (2005, $20.6B); (4) Hurricane Charlie (2004, $15.4B); (5) Hurricane Ivan (2004, $14.6B), four of them happened within recent three years (Wikipedia, 2006). Because of the devastating effect, government agencies are spending more money on hurricane-related studies and trying to prevent or reduce future loss. As most of the damage comes from flooding and flooding-related structure damage, more and more research, especially on storm surge modeling, has been conducted to determine the physical process and changes of sea level and the extent of coastal flooding.

Storm surge simulation is a complex task and involves multiple interacting science and engineering fields. It requires atmospheric scientists to provide accurate hurricane track and wind fields over a large domain. It requires a good set of topography and bathymetry in high resolution. Most of all, it requires an efficient, and robust model to incorporate all major physical processes affecting storm surge. Some storm surge models contain rather simple physics and only consider a few hurricane parameters (e.g., atmospheric pressure deficit, size of the storm, translation speed, and direction) and coarse grid resolution. Some models, however, include ok physical processes, such as wave, tide and their interaction with surge, and use higher grid

resolution. The next section contains a brief review of the development of storm surge models over the past thirty years.

Storm surge modeling began in the 1970's with the National Oceanic and Atmospheric Administration's (NOAA) Special Program to List Amplitudes of Surges from Hurricane (SPLASH) (Jelesnianski, 1972), which was adopted by the National Weather Service (NWS). This early stage model was a 2D storm surge model without nonlinear terms and a fixed boundary on water-land interface. It does not work well in shallow water domains with complex shoreline and bathymetry and is only suitable for open water. Next, a popular model of Sea, Lake, and Overland Surges from Hurricanes (SLOSH) was developed by NOAA (Jelesnianski, et al, 1984 and Jelesnianski, et al, 1992) and was widely used along Atlantic and Gulf Coasts of the U.S. to estimate storm surge heights resulting from historical, hypothetical, or predicted hurricanes. As the primary use of the SLOSH model is to define flood-prone areas for evacuation planning, the forecasting of storm surge and inundation is designed for a large domain to capture the main feature and is not suitable for a specific hurricane. The grid resolution is relatively coarse (0.5-7 km), therefore it can not resolve complex shoreline and bathymetry. In addition, the advection terms are not explicitly incorporated in SLOSH (Jelesnianski, et al, 1992), which may underestimate storm surge and inundation in shallow water regions.

The Arbiter of Storms (TAOS) model is a 2-D integrated hazards model (Watson, 1995; Watson and Johnson, 1999) that simulates storm surge, wave height, maximum winds, inland flooding, debris, and structural damage. Since tide and wave effect is not included in TAOS, it is similar to SLOSH.

The Princeton Ocean Model (POM) is a sigma coordinate, free surface, 3-D ocean model developed by Blumberg and Mellor (1987). It has been used for modeling of estuaries, coastal

regions and global oceans. An explicit finite difference scheme is used in POM to calculate horizontal differential terms and an implicit scheme is implemented for vertical differentiation. A flooding & drying scheme was recently incorporated in POM (Xie, et al, 2004) and then applied to simulate storm surge and inundation in Charleston Harbor, South Carolina for Hurricane Hugo and some hypothetical hurricane events (Peng, et al., 2006), as well as in Chesapeake Bay for Hurricane Isabel (Peng, et al., 2006). Moon (2000, 2005) coupled a third-generation wave model WAVEWATCH-II with POM to study wave-current interaction in open water during Typhoon Winnie (1997) in the Yellow and East China Seas.

The ADvanced CIRCulation Model (ADCIRC) for oceanic, coastal, and estuarine waters (Westerink and Luettich, 1991, 1992; Luettich and Westerink, 2000) is a finite element model for simulating astronomical tide and storm surge. ADCIRC solves the time dependent, free surface circulation and transport problems in two and three dimensions using flexible unstructured grids. Typical ADCIRC applications use the 2D instead of the 3D simulations.

MIKE 21 is an engineering software package for 2D free-surface flows developed by Danish Hydraulic Institute (DHI) (DHI, 2002). MIKE 21 is applicable to the simulation of hydraulic and related phenomena in lakes, estuaries, bays, coastal areas, and seas where stratification can be neglected. The contained hydrodynamic module for floodplain modeling in MIKE21 can be used for storm surge simulation in coastal regions when coupled with a storm cyclone wind model.

Recently, tropical cyclones have shown strong activities and caused much more damage, especially in North America. Much more attention has been paid by researchers to study storm surges for disaster planning, prevention, and management using numerical models. Along with the rapid advance of computing capacities, the modeling of storm surge has been under

development for both real-time forecasting and hindcasting. Newer models and techniques have been developed and applied to improve storm surge simulation accuracy and efficiency. Advances in storm surge modeling come in four different areas: model physics, model grid system, wind models used, and inclusion of wave and other (e.g., tide) influences.

1.1 Structured Grid Model

There are two kinds of numerical models being used for storm surge simulation. The first group models are developed based on circulation models, such as POM, ADCIRC and MIKE21, etc. By implementing new features; including flooding & drying capability, deficit air pressure term, hurricane wind stress term, these models are reconstructed, updated, and are more suitable for storm surge and inundation simulation. The most recent applications of these models include the 1939 storm simulation along Australia Coast using GEMS (Hubbert & McInnes,1999); 1953 North Sea storm simulation using GEMS (Wolf & Flather, 2005); Hurricane Floyd (1999) simulation in the Chesapeake Bay using ADCIRC (Shen, 2006); Hurricane Hugo (1989) simulation in Charleston, SC using ADCIRC (Dietsche, et al., 2007); Wave effect on storm surge in Hurricane George (1994) using ADCIRC and SWAN (Weaver, 2004); 1991 cyclone simulation in the Bay of Bengal using MIKE21 (Madsen, H. & F. Jakobsen, 2004); Hurricane Winnie (1997) simulation along west coast of Korea using POM (Moon, I., et al., 2003); Hurricane Emily (1993) in the Croatan-Albemarle-Pamlico Estuarine, NC using POM (Peng, et al., 2004); and Hurricane Isabel (2003) in the Chesapeake Bay using POM (Peng, et al., 2006). As summarized in Table 1-1, most of these models use structured grid, either rectangular or curvilinear for discretization of mathematical equations. Three models in Table 1-1 use unstructured grid: UnTRIM, FVCON and ELCIRC are finite volume model while ADCIRC is a finite element model. Although 2D model cannot accurately represent the bottom friction and

represent the vertical flow structure, they can simulate the storm surge reasonably well. Hence, 2D models are generally used for storm surge simulation.

1.2 Unstructured Grid Model

The UnTRIM model is a semi-implicit finite difference (-volume) model based on the three-dimensional shallow water equations. UnTRIM (Casulli and Walters, 2000) is the unstructured-grid version of the tidal, residual, intertidal mudflat model (TRIM) developed by Casulli and Cheng (1992). Compared to the other traditional models discussed above, UnTRIM is capable of representing a modeling domain with a very high resolution unstructured grid while maintaining numerical stability and computation efficiency. UnTRIM was used to simulate Hurricane Andrew (1992) in Biscayne Bay, FL (Shen, et al., 2005) and Hurricane Isabel (2003) in the Chesapeake Bay (Shen, et al., 2006).

The MOG2D model is a two-dimensional depth-integrated hydrodynamic model for ocean and coastal water (Carrere and Lyard, 2003). It is a barotropic model based on the classical shallow water equations formulated in spherical coordinates with inclusion of nonlinear terms. The spatial variations are discretized by the continuous Galerkin finite element method which allows freely varying resolution and facilitates a smoothly resolved coastline. Because the drying and flooding is implemented using an explicit time scheme, it requires relatively smaller time step to keep stability. The MOG2D model has been applied to simulate the 1953 North Sea storm (Kleim, et al., 2006).

The ELCIRC model is another representative efficient and stable unstructured-grid model that is designed for the effective simulation of 3D baroclinic circulation across river-to-ocean scales (Zhang, et al., 2004; Baptista, et al., 2005). It uses a finite-volume/finite-difference Eulerian-Lagrangian algorithm to solve the shallow water equations with incorporation of wetting and drying schemes. While originally developed to meet specific modeling challenges

for the Columbia River, ELCIRC has been tested against the Columbia River data and other standard ocean/coastal benchmarks. ELCIRC has been applied to simulate Hurricane Floyd (1999) with success (NOAA, 2004f).

The validation of these case studies has shown the success of these unstructured models. However, they are still in their early stage of development. Many processes, e.g., waves are not incorporated into unstructured grid surge models.

1.3 Grid Resolution

In order to accurately simulate storm surge and inundation in shallow coastal region, coastal morphological features such as bathymetry, barrier islands, inlets, and shoreline configurations must be resolved reasonably well because of their important roles in affecting nonlinear transport, bottom friction, and flood water flux. To incorporate detailed morphological features, a high resolution grid system has to be used for storm surge models in the horizontal plane. This can be achieved by implementing refined structured curvilinear grid or unstructured grid. For a structured grid, high resolution in one particular domain requires similar resolution along both horizontal axes, which leads to a rapid increase of the total number of cells. Among the reviewed studies, the very fine grid goes from 150 m for Australia Coast (Hubbert, 1999) to around 50 m for storm simulation by Sheng et al. (2005).

With fast advances in compute technology, finer structured grids could be used with faster computer with more memory that becomes available every year. The unstructured grid is able to resolve complex shorelines with much finer elements/cells and open waters with coarser elements/cells simultaneously to keep the overall number of cells relatively low. The minimum grid resolution is as small as 50 m for the Hurricane Isabel (2003) simulation using UnTRIM (Shen, et al., 2006). The finite element model ADCIRC uses unstructured grids to represent the irregular shoreline. However, its computation speed is limited by a stringent stability condition

associated with the propagation of surface gravity wave and the nonlinear advection terms. Sometimes small time steps in the order of seconds have to be used for very fine grid, resulting in significantly increased simulation time. On the other hand, the UnTRIM model uses semi-implicit time integration and an Eulerian-Lagrangian for advection calculation, which allows larger time steps to be used without severely reducing accuracy.

1.4 Wind Model

Wind forcing is another important aspect in storm surge simulations. The review on recent storm surge applications shows that most models rely on Parametric Wind Models to provide hurricane wind to simulate storm surge (Table 1-1). The simplified parametric wind model by MYERs and MALmuN' (1961) has been adopted by the SLOSH model and some other researchers in their storm surge simulations (Shen, et al., 2005; Shen, et al., 2006). The wind and atmospheric pressure fields are generated with the parameters of atmospheric pressure drop and radius of maximum wind speed. The pressure, wind speed, and wind direction are computed for a stationary, circularly symmetric storm with a balance of forces along and perpendicular to a surface wind trajectory. Another popular parametric wind model is the Holland wind model (Holland, 1980), which is the most widely used model and needs only several input parameters such as deficit atmospheric pressure, radius of maximum wind, and maximum wind to reconstruct tropical cyclone wind speed (Moon, et al., 2003; Peng, et al., 2004; Xie, etc., 2004; Peng, et al., 2006; Weisberg & Zheng, 2006).

There are more sophisticated wind models that have been applied to simulate and provide wind for storm surge and wave simulation, such as the Planetary Boundary Layer (PBL) model and models by Ocean Weather and Numerical Weather Prediction systems (NWP, 2004). In general, these sophisticated wind models generate better wind fields than parametric wind models. However, additional parameters, such as sea surface temperature, horizontal temperature

gradient, etc., are necessary to provide boundary conditions and drive the wind model. In many cases, these parameters are not available and have to be estimated. As the result, uncertainty is introduced which may lead to errors in the simulated wind field. For hypothetical storm events in coastal hazard studies, storm surge forecasting, or real storms where detailed wind is not available, the parametric wind models are very useful as they require very limited cyclone input and at the same time rebuild the entire wind field with fairly good accuracy. Recent publications have not considered the land reduction effect on wind when hurricane wind blew over coastal land. Its effect has been recognized by US Army Corps of Engineers in their evaluation of the New Orleans and southeast Louisiana hurricane protection system for Hurricane Katrina (2005) (IPET, 2005). This is a factor that should be included in the future storm surge simulations.

1.5 Inclusion of Wave Effect

Most storm surge simulations do not include simulation of storm waves or the interaction between surges and waves. Storm wind and deficit atmospheric pressure are the only two major driving forces in these storm surge simulations. Among the limited studies with wave simulation, Choi (2003) established a coupled wave–tide–surge model in investigating the effect of tides, storm surges, and wind waves interactions during a winter monsoon in November 1983 in Yellow Sea. The coupled model is based on the synchronous dynamic coupling of a third-generation wave model, WAM-Cycle 4 (WAMDI group, 1988), and the two-dimensional tide–surge model developed at the Institute of Oceanographic Sciences (IOS) (Choi, 1980). The surface stress generated by interactions between wind and waves is calculated using the WAM-Cycle 4 directly based on an analytical approximation of the results obtained from the quasi-linear theory of wave generation. The changes of the bottom friction factor generated by waves and current interactions are calculated by using simplified bottom boundary layer model of

Grand and Madsen (1986). Their results showed that bottom velocity and bottom drag coefficient were affected by wave-current interaction in shallow waters during strong storm conditions.

Moon (2003) used a two-way-coupled ocean wave-circulation model to study the unusual coastal flooding by Typhoon Winnie on the west coast of Korea. The coupled model consists of a third-generation ocean wave model WAVEWATCH-II (Tolman, 1992) and a three-dimensional circulation model POM. In the coupling scheme of the two models, WAVEWATCH-II uses the new currents and elevations fed back from POM to consider wave-current interactions; POM uses a wave-dependent drag coefficient calculated from WAVEWATCH-II to consider the dependency of sea state (wave age) on the wind stress. The coupling process between the storm surge model and the wave model is important for both water level and wave simulation. Within shallow coastal regions, the elevated water level increases the flow field and total depth which may significantly change wave development and transport. At the same time, wave-induced radiation stress and its effect on surface and bottom friction will change circulation and ultimately the storm surge and inundation. Thus, the surge-wave coupling process should be considered for a complete storm surge simulation.

1.6 CH3D-SSMS Storm Surge Modeling System

The Curvilinear-grid Hydrodynamics 3D model (CH3D) was developed by Peter Sheng (1986, 1989). The CH3D model uses a horizontal boundary-fitted curvilinear grid and a vertically sigma grid and is therefore suitable for application to coastal and nearshore waters with complex shorelines and bathymetry. The non-orthogonal grid enables CH3D to more accurately represent the complex geometry than the orthogonal grid, which is used by many other ocean circulation models, e.g. POM and ROMS. CH3D was first used for storm surge simulation of Hurricanes Marco (1990) and Floyd (1999). Sheng et al. (2002, 2005) produced a CH3D-based storm surge modeling system CH3D-SSMS by adding flooding and drying process to the coastal

circulation model CH3D and coupling it with a coastal wave model SWAN, a large scale surge model ADCIRC and a large-scale wave model WaveWatch-III (WW3). CH3D-SSMS uses the model results of ADCIRC and WW3 for the entire Gulf of Mexico and the Western Atlantic to provide the open boundary conditions for the coastal surge model CH3D and coastal wave model SWAN. The forcing mechanisms for surge and flooding in CH3D-SSMS include wind, atmospheric pressure deficit, wave, tide, precipitation, and river flow. CH3D-SSMS has been applied to several major hurricanes, including Isabel (2003), Charley (2004), Frances (2004) and Wilma (2005).

In spite of recent progress, storm surge modeling is far from perfect and needs further improvement. The following are some examples:

- The difficulty of obtaining an accurate description of wind over the ocean - there is always a discrepancy between numerical wind simulations and observed measurements. In addition, most wind models do not include the land reduction effect for winds during and after landfall.
- The drag coefficient of wind over water is not well known for strong hurricane force winds.
- The flooding and drying process is not adequately understood and validated due to lack of data.
- The drag coefficient of water on the sea-floor is difficult to estimate.
- Spatial resolution is a limiting factor for accurate and efficient storm surge simulation.
- There is a lack of adequate field data for model validation including water level, wave and current.

1.7 Questions to be answered

Storm surge development along the coast is a complex process and is affected by many factors, hurricane wind intensity, atmospheric pressure, speed of approach, land fall location and direction, local shoreline, and bathymetry and topography characteristics, etc. To develop sound understanding and robust predictive model of storm surge, there are numerous questions and

uncertainties that must be addressed. For example, how do the bathymetry and topography and their slopes affect the surges and waves along the coast? The West Florida coast has a wide shelf and gentle bottom slope, but the East Florida coast has a narrow shelf and steeper slope. So how do these differences affect the surge and wave along the West and East coasts of Florida? What roles do estuaries play in affecting the storm surge and inundation in coastal zones? Do waves significantly affect the storm surge and inundation in coastal regions? How should a large scale model couple with a coastal model? What are the differences between 2D and 3D results for surge and inundation? Is 3D model necessary for surge simulation? How often (e,g., every minute or every hour) is it necessary to run wave model to get accurate surge-wave interaction? How sensitive are the storm surges to wind fields, method of wind field interpolation, tide, bottom friction coefficient, model grid resolution, and model time step? How efficient are the storm surge models? How to produce the "BEST" results for storm surge simulations? What are the different ways to calculate wave forces on bridges? All these topics will be discussed in the following chapters.

1.8 Goals and Objectives

In 2004, Florida suffered huge loss from four hurricanes: Charley, Frances, Jeanne, and Ivan. The severe surge generated in these storms caused severe flooding, as well as significant damage to coastal structures. Coastal highway roads and bridges are some of the structures vulnerable to storm surge and waves. During Hurricane Ivan, miles of coastal structures were damaged and pavement was washed away. The I-10 Bridge over Escambia Bay collapsed during the peak of the hurricane. In order to mitigate future economic losses to hurricanes in Florida, it is important to identify the vulnerability of Florida's coastal highways to storm surge and flooding and seek solutions to improve their safety. This is conducted in the study with focus on the I-10 Bridge during Hurricane Ivan using a storm surge modeling system, CH3D-SSMS,

which includes coupling with large scale surge model (ADCIRC) and regional wave model (SWAN) and large scale wave models WW3.

Hurricane Dennis in 2005 was a relatively weak hurricane and made a landfall on the west Florida panhandle, following a similar but slightly to the east track to Hurricane Ivan. Even though it was considered weak, Hurricane Dennis caused unexpected high surges (2-3 m) around Apalachee Bay. A thorough analysis on how the surge was generated is conducted using CH3D-SSMS.

The goals of this study are summarized as follows:

1. To enhance CH3D-SSMS by introducing a Lagrange-interpolation technique to remove artificial hurricane weakness around the hurricane center and land-reduction on the wind based on a land use map.

2. To validate CH3D-SSMS simulations on Hurricane Ivan by comparing water level, waves, and high water marks at coastal regions with available data.

3. To calculate force on the I-10 Bridge during Hurricane Ivan and determine the mechanism that caused the collapse of the bridge.

4. To conduct extensive sensitivity tests on Hurricane Ivan simulations to identify roles of key model parameters in storm surge simulation.

5. To conduct a set of risk assessment simulations to evaluate the vulnerability of highways and bridges in the Florida Panhandle, Alabama, and Mississippi.

6. To conduct a complete simulation on Hurricane Dennis and analyze the reason that caused the unexpected surges in Apalachicola Bay.

7. To answer the questions listed in the previous paragraph.

Table 1-1. Summary of recent development of storm surge model

Authors	Model Name	Dime -nsion	Application Domain	Case Study	Grid Type	Grid Res -olution	Wind	Wave Model	Storm Wave Coupling	Inund -ation	Data
Shen, et al. (2006a)	UnTRIM	2D	Chesapeake Bay	Isabel (2003)	Unstruc -tured	50 m – a few km	Parametric	N/A	N/A	Yes	NOAA
Shen, et al. (2006b)	UnTRIM	2D	Biscayne Bay	Andrew (1992)	Unstruc -tured	50 m - km	Parametric	N/A	N/A	Yes	HWM
Shen, et al. (2006c)	ELCIRC	2D	Chesapeake Bay	Floyd (1999)	Unstruc -tured	100 m – 10 km	Parametric	N/A	N/A	Yes	NOAA
Shen, et al. (2006c)	ADCIRC	2D	Chesapeake Bay	Floyd (1999)	Unstruc -tured	450 m – 10 km	Parametric	N/A	N/A	Yes	NOAA
Choi, et al. (2003)	IOS	2D	Yellow Sea	Monsoon (1983)	Rectang -ular	1/12 degree	PMBL model	WAM	Two-way	No	Current from buoy
Madsen & Jakobsen (2004)	Mike21	2D	Bay of Bengal	Cyclone (1991)	Structur -ed	600m - 54 km	Parametric	N/A	N/A	Yes	Water level
Moon, et al (2003)	POM	3D	West coast of Korea	Winnie (1997)	Structur -ed	N/A	Holland	WWII	Two-way	N/A	Water level
Peng, et al. (2006)	POM	3D	Chesapeake Bay	Isabel (2003) Charley(2004)	Structur -ed	N/A	Holland	N/A	N/A	Yes	Water level
Peng, et al. (2004)	POM	3D	Croatan-Albemarle-Pamlico, NC	Emily (1993)	Rectang -ular	325 m	Holland	N/A	N/A	Yes	HWM
Xie, et al. (2004)	POM	3D	Hypothetical domain	N/A	Structur -ed	600 m	Holland	N/A	N/A	Yes	N/A
Weisberg & Zhang (2006)	FVCOM	3D	Tampa Bay, FL	Hypothetical wind	Unstruc -tured	100m – 20 km	Holland	N/A	N/A	Yes	N/A
Dietsche, et al. (2007)	ADCIRC	2D	Charleston, SC	Hugo (1989)	Unstruc -tured	50 m – a few km	Ocean Weather Inc.	N/A	N/A	Yes	HWM
Kliem, et al. (2006)	MOG2D	2D	North Sea	N/A	Unstruc -tured	3 km – 20 km	NWP	N/A	N/A	Yes	Water level
Wolf & Flather (2005)	CS3	2D	North Sea	Storm (1953)	Structur -ed	12 km	Parametric	WAM	N/A	N/A	Water level
Hubbert & McInnes (1999)	GEMS	2D	Australia Coast	Storm (1939)	Rectang -ular	150 / 225 /300 m	Parametric	N/A	N/A	N/A	Water level
Sheng et al. (2002, 2005)	CH3D	3D	Chesapeake Bay, Tampa Bay, Charlotte Harbor	Isabel (2003) Charley(2004) Frances(2004) Wilma(2005)	Cuvilin -ear	50 m – a few km	HRD; WNA; WINDGEN; Holland	SWAN; WWII	Two-way	Yes	NOAA - Water level; Wave

CHAPTER 2
STORM SURGE MODELING SYSTEM - CH3D-SSMS

2.1 Introduction

The Storm Surge Modeling System, CH3D-SSMS (Sheng et al., 2002 and 2005; Alymov, 2005) is an integration of the circulation model, surge model, wind model and wave model. Unlike most other models, CH3D-SSMS includes the complete forcing mechanisms for storm surge simulation: wind, tide, atmospheric pressure, wave, precipitation and river flow. In CH3D-SSMS, the complicated interactions of physical processes are solved using the dynamic-coupling of each sub-model. A diagram that explains the coupling processes in CH3D-SSMS is shown in Figure 2.1. In general, the integrated modeling system can be divided into regional models and local models. Based on wind and atmospheric pressure fields from atmospheric model or wind snapshots (a1 and a2), regional circulation/surge model ADCIRC and regional wave model WaveWatch-III provide wave parameters to local wave model SWAN (b) and water elevation to local circulation model CH3D (c) at open boundaries. With additional precipitation, discharge and tide (e) together with wind and atmospheric pressure fields (a3 and a4), local models are used to calculate water level, current, wave and inundations over interested domain. The dynamic coupling process between SWAN and CH3D allows waves (d1) and total water depths (d2) to be updated at each time step. The following section first explains the detailed physical processes and governing equations of the key sub-model CH3D in CH3D-SSMS. Then the regional models and local wave model SWAN are introduced. The last part is the discussion on wind field used in CH3D-SSMS.

2.2 Local Circulation Model - CH3D

The Curvilinear-grid Hydrodynamics 3D model (CH3D) was developed by Peter Sheng (1986, 1989). With assumption of incompressible water, hydrostatic pressure, Boussinesq

approximation and turbulent Reynolds stresses approximation, the governing equations in CH3D was derived from Navier-Stokes equations using a horizontally boundary-fitted curvilinear grid and a vertically sigma grid. The non-orthogonal grid enables CH3D to more accurately represent the complex geometry than the orthogonal grid, which is used by most other ocean circulation models. With added additional features, such as flooding & drying and radiation stress, CH3D was updated to an integrated storm surge modeling system CH3D-SSMS and has been successfully applied to produce Flood Insurance Rate Mao (FIRM) of Pinellas County, FL and for simulating Hurricane Isabel, Charley, Frances and Wilma (Sheng et al., 2002 and 2005; Alymov, 2005).

2.2.1 Governing Equations

In Cartesian coordinate systems, the governing equations for water continuity, X-momentum, and Y-momentum equations are:

$$\frac{\partial u}{\partial x}+\frac{\partial v}{\partial y}+\frac{\partial w}{\partial z}=0 \tag{2-1}$$

$$\begin{aligned}&\frac{\partial u}{\partial t}+\frac{\partial uu}{\partial x}+\frac{\partial uv}{\partial y}+\frac{\partial uw}{\partial z}+\frac{1}{\rho_w}\frac{\partial S_{xx}}{\partial x}+\frac{1}{\rho_w}\frac{\partial S_{xy}}{\partial y}\\&=-g\frac{\partial \varsigma}{\partial x}-\frac{1}{\rho_w}\frac{\partial P_a}{\partial x}+fv+A_H(\frac{\partial^2 u}{\partial x}+\frac{\partial^2 u}{\partial y})+\frac{\partial}{\partial z}(A_V\frac{\partial u}{\partial z})\end{aligned} \tag{2-2}$$

$$\begin{aligned}&\frac{\partial v}{\partial t}+\frac{\partial uv}{\partial x}+\frac{\partial vv}{\partial y}+\frac{\partial vw}{\partial z}+\frac{1}{\rho_w}\frac{\partial S_{yx}}{\partial x}+\frac{1}{\rho_w}\frac{\partial S_{yy}}{\partial y}\\&=-g\frac{\partial \varsigma}{\partial y}-\frac{1}{\rho_w}\frac{\partial P_a}{\partial y}-fu+A_H(\frac{\partial^2 v}{\partial x}+\frac{\partial^2 v}{\partial y})+\frac{\partial}{\partial z}(A_V\frac{\partial v}{\partial z})\end{aligned} \tag{2-3}$$

where $u(x; y; z; t)$, $v(x; y; z; t)$, and $w(x; y; z; t)$ are the velocity vector components in x-, y-, and z-coordinate directions, respectively; t is time; $\varsigma(x; y; t)$ is the free surface elevation; g is the acceleration of gravity; A_H and A_V are the horizontal and vertical turbulent eddy coefficients,

respectively; S_{xx}, S_{xy}, S_{yy} are radiation stresses, ρ_w is the density of water, P_a is atmospheric pressure and f is the Coriolis component.

The following reference scales are used to non-dimensionalize the governing equations: X_r and Z_r are the references lengths in the horizontal and vertical direction; U_r is the reference velocity; ρ_r and ρ_0 are reference density and mean density; A_{Hr} and A_{Vr} are the reference eddy viscosities in the horizontal and vertical direction. Following Sheng (1986, 1987, and 1990), the non-dimensional form of above equations in curvilinear, boundary-fitted grid systems can be written as:

$$\frac{\partial \zeta}{\partial t} + \frac{\beta}{\sqrt{g_0}}\left[\frac{\partial}{\partial \xi}(\sqrt{g_0}Hu) + \frac{\partial}{\partial \eta}(\sqrt{g_0}Hv)\right] + \beta\frac{\partial H\omega}{\partial \sigma} = 0 \tag{2-4}$$

$$\begin{aligned}
\frac{1}{H}\frac{\partial Hu}{\partial t} &= -(g^{11}\frac{\partial \zeta}{\partial \xi} + g^{12}\frac{\partial \zeta}{\partial \eta}) + -(g^{11}\frac{\partial P}{\partial \xi} + g^{12}\frac{\partial P}{\partial \eta}) + (\frac{g_{12}}{\sqrt{g_0}}u + \frac{g_{22}}{\sqrt{g_0}}v) \\
&- \frac{R_0}{g_0}\left\{x_\eta\left[\frac{\partial}{\partial \xi}(y_\xi\sqrt{g_0}S_{xx} + y_\eta\sqrt{g_0}S_{xy}) + \frac{\partial}{\partial \eta}(y_\xi\sqrt{g_0}S_{xy} + y_\eta\sqrt{g_0}S_{yy})\right]\right. \\
&\left. - y_\eta\left[\frac{\partial}{\partial \xi}(x_\xi\sqrt{g_0}S_{xx} + x_\eta\sqrt{g_0}S_{xy}) + \frac{\partial}{\partial \eta}(x_\xi\sqrt{g_0}S_{xy} + x_\eta\sqrt{g_0}S_{yy})\right]\right\} \\
&- \frac{R_0}{g_0 H}\left\{x_\eta\left[\frac{\partial}{\partial \xi}(y_\xi\sqrt{g_0}Huu + y_\eta\sqrt{g_0}Huv) + \frac{\partial}{\partial \eta}(y_\xi\sqrt{g_0}Huv + y_\eta\sqrt{g_0}Hvv)\right]\right. \\
&\left. - y_\eta\left[\frac{\partial}{\partial \xi}(x_\xi\sqrt{g_0}Huu + x_\eta\sqrt{g_0}Huv) + \frac{\partial}{\partial \eta}(x_\xi\sqrt{g_0}Huv + x_\eta\sqrt{g_0}Hvv)\right] - g_0\frac{\partial Hu\omega}{\partial \sigma}\right\} \\
&+ \frac{E_v}{H^2}\frac{\partial}{\partial \sigma}(A_v\frac{\partial u}{\partial \sigma}) + E_H A_H(\text{Horizontal Diffusion of } u) \\
&- \frac{R_0}{F_r^2}\left[H\int_\sigma^0(g^{11}\frac{\partial \rho}{\partial \xi} + g^{12}\frac{\partial \rho}{\partial \eta})d\sigma + (g^{11}\frac{\partial H}{\partial \xi} + g^{12}\frac{\partial H}{\partial \eta})(\int_\sigma^0 \rho d\sigma + \sigma p)\right]
\end{aligned} \tag{2-5}$$

$$
\begin{aligned}
\frac{1}{H}\frac{\partial Hv}{\partial t} &= -(g^{21}\frac{\partial \zeta}{\partial \xi} + g^{22}\frac{\partial \zeta}{\partial \eta}) - (g^{21}\frac{\partial P}{\partial \xi} + g^{22}\frac{\partial P}{\partial \eta}) - (\frac{g_{11}}{\sqrt{g_0}}u + \frac{g_{21}}{\sqrt{g_0}}v) \\
&- \frac{R_0}{g_0}\left\{ x_\xi \left[\frac{\partial}{\partial \xi}(y_\xi \sqrt{g_0} S_{yx} + y_\eta \sqrt{g_0} S_{yy}) + \frac{\partial}{\partial \eta}(y_\xi \sqrt{g_0} S_{yx} + y_\eta \sqrt{g_0} S_{yy}) \right] \right. \\
&\left. - y_\eta \left[\frac{\partial}{\partial \xi}(x_\xi \sqrt{g_0} S_{xx} + x_\eta \sqrt{g_0} S_{yx}) + \frac{\partial}{\partial \eta}(x_\xi \sqrt{g_0} S_{yx} + x_\eta \sqrt{g_0} S_{yy}) \right] \right\} \\
&- \frac{R_0}{g_0 H}\left\{ x_\xi \left[\frac{\partial}{\partial \xi}(y_\xi \sqrt{g_0} Huv + y_\eta \sqrt{g_0} Hvv) + \frac{\partial}{\partial \eta}(y_\xi \sqrt{g_0} Huv + y_\eta \sqrt{g_0} Hvv) \right] \right. \\
&\left. - y_\eta \left[\frac{\partial}{\partial \xi}(x_\xi \sqrt{g_0} Huu + x_\eta \sqrt{g_0} Huv) + \frac{\partial}{\partial \eta}(x_\xi \sqrt{g_0} Huv + x_\eta \sqrt{g_0} Hvv) \right] - g_0 \frac{\partial Hv\omega}{\partial \sigma} \right\} \\
&+ \frac{E_v}{H^2}\frac{\partial}{\partial \sigma}(A_v \frac{\partial v}{\partial \sigma}) + E_H A_H (\text{Horizontal Diffusion of } v) \\
&- \frac{R_0}{F_r^2}\left[H\int_\sigma^0 (g^{21}\frac{\partial \rho}{\partial \xi} + g^{22}\frac{\partial \rho}{\partial \eta}) d\sigma + (g^{21}\frac{\partial H}{\partial \xi} + g^{22}\frac{\partial H}{\partial \eta})(\int_\sigma^0 \rho d\sigma + \sigma p) \right]
\end{aligned}
\tag{2-6}
$$

where

ξ, η and σ are transform coordinate system;
u, v, ω are non-dimensional contra-variant velocities in curvilinear grid (ξ,η,σ).
$\sqrt{g_0}$ is the Jacobian of horizontal transformation;
$g^{11}, g^{12}, g^{22}, g_{11}, g_{12}, g_{22}$ are the metric coefficients of coordinate transformations;
R_0 is the Rossby Number U_r/fX_r;
E_v is the vertical Ekman Number A_{vr}/fZ_r^2;
β is non-dimensional parameter $gZ_r/f^2X_r^2$;
ζ is water level;

By taking a vertical integral of the non-dimensional form of shallow water continuity and momentum equations, the two-dimensional vertically averaged form of equations can be written as:

$$
\frac{\partial \zeta}{\partial t} + \frac{\beta}{\sqrt{g_0}}\left[\frac{\partial}{\partial \xi}(\sqrt{g_0} H\bar{u}) + \frac{\partial}{\partial \eta}(\sqrt{g_0} H\bar{v}) \right] = 0 \tag{2-7}
$$

$$
\frac{\partial \bar{u}}{\partial t} + g^{11}\frac{\partial \zeta}{\partial \xi} - \frac{g_{12}}{\sqrt{g_0}}\bar{u} - \frac{g_{22}}{\sqrt{g_0}}\bar{v} - F_\xi + C_d\sqrt{U^2 + V^2}\,\bar{u} = 0 \tag{2-8}
$$

$$\frac{\partial \bar{v}}{\partial t} + g^{22}\frac{\partial \zeta}{\partial \eta} + \frac{g_{11}}{\sqrt{g_0}}\bar{u} + \frac{g_{21}}{\sqrt{g_0}}\bar{v} - F_\eta + C_d\sqrt{U^2 + V^2}\,\bar{v} = 0 \tag{2-9}$$

where

C_d is bottom friction coefficient;
$\bar{u}$, $\bar{v}$ are the contravariant depth-averaged velocities;
U, V are the depth-integrated contravariant velocities;
F_ξ and F_η are the remaining nonlinear, horizontal diffusion, wind stress, deficit atmospheric pressure, radiation stress, surface slope terms in the ξ and η direction, respectively.

The finite difference form of the simplified equations (2.7) to (2.9) can be written as:

$$\begin{aligned}
&\frac{\zeta_{i,j}^{n+1} - \zeta_{i,j}^{n}}{\Delta t} + \frac{\beta\theta_1}{\sqrt{g_{o,i,j,s}}\,\Delta\xi}\left(\sqrt{g_{0,u,i+1,j}}\,H_{u,i+1,j}^{n}\bar{u}_{i+1,j}^{n+1} - \sqrt{g_{0,u,i,j}}\,H_{u,i,j}^{n}\bar{u}_{i,j}^{n+1}\right) \\
&\quad + \frac{\beta\theta_1}{\sqrt{g_{o,i,j,s}}\,\Delta\eta}\left(\sqrt{g_{0,v,i,j+1}}\,H_{v,i,j+1}^{n}\bar{v}_{i,j+1}^{n+1} - \sqrt{g_{0,v,i,j}}\,H_{v,i,j}^{n}\bar{v}_{i,j}^{n+1}\right) \\
&\quad + \frac{\beta(1-\theta_1)}{\sqrt{g_{o,i,j,s}}\,\Delta\xi}\left(\sqrt{g_{0,u,i+1,j}}\,H_{u,i+1,j}^{n}\bar{u}_{i+1,j}^{n} - \sqrt{g_{0,u,i,j}}\,H_{u,i,j}^{n}\bar{u}_{i,j}^{n}\right) \\
&\quad + \frac{\beta(1-\theta_1)}{\sqrt{g_{o,i,j,s}}\,\Delta\eta}\left(\sqrt{g_{0,v,i,j+1}}\,H_{v,i,j+1}^{n}\bar{v}_{i,j+1}^{n} - \sqrt{g_{0,v,i,j}}\,H_{v,i,j}^{n}\bar{v}_{i,j}^{n}\right) = 0
\end{aligned} \tag{2-10}$$

$$\begin{aligned}
&\frac{\bar{u}_{i,j}^{n+1} - \bar{u}_{i,j}^{n}}{\Delta t} + \frac{g_{u,i,j}^{11}\theta_1}{\Delta\xi}\left(\zeta_{i,j}^{n+1} - \zeta_{i-1,j}^{n+1}\right) + \frac{g_{u,i,j}^{11}(1-\theta_1)}{\Delta\xi}\left(\zeta_{i,j}^{n} - \zeta_{i-1,j}^{n}\right) \\
&\quad - \frac{g_{12,u,i,j}}{\sqrt{g_{0,u,i,j}}}\bar{u}_{i,j}^{n} - \frac{g_{22,u,i,j}}{\sqrt{g_{0,u,i,j}}}\bar{v}_{u,i,j}^{n} + \frac{C_d\theta_2\sqrt{U_{i,j}^{n\,2} + V_{i,j}^{n\,2}}}{H_{u,i,j}^{n}}\bar{u}_{i,j}^{n+1} \\
&\quad + \frac{C_d(1-\theta_2)\sqrt{U_{i,j}^{n\,2} + V_{i,j}^{n\,2}}}{H_{u,i,j}^{n}}\bar{u}_{i,j}^{n} - F_{\xi,i,j}^{n} = 0
\end{aligned} \tag{2-11}$$

$$
\begin{aligned}
&\frac{\bar{v}_{i,j}^{n+1}-\bar{v}_{i,j}^{n}}{\Delta t}+\frac{g_{v,i,j}^{22}\theta_1}{\Delta\eta}(\zeta_{i,j}^{n+1}-\zeta_{i,j-1}^{n+1})+\frac{g_{v,i,j}^{22}(1-\theta_1)}{\Delta\eta}(\zeta_{i,j}^{n}-\zeta_{i,j-1}^{n}) \\
&\quad -\frac{g_{11,v,i,j}\theta_3}{\sqrt{g_{0,v,i,j}}}\bar{u}_{v,i,j}^{n+1}-\frac{g_{11,v,i,j}(1-\theta_3)}{\sqrt{g_{0,v,i,j}}}\bar{u}_{v,i,j}^{n} \\
&\quad -\frac{g_{21,v,i,j}\theta_3}{\sqrt{g_{0,v,i,j}}}\bar{v}_{i,j}^{n+1}-\frac{g_{21,v,i,j}(1-\theta_3)}{\sqrt{g_{0,v,i,j}}}\bar{v}_{i,j}^{n} \\
&\quad +\frac{C_d\theta_2\sqrt{U_{i,j}^{n\,2}+V_{i,j}^{n\,2}}}{H_{v,i,j}^{n}}\bar{v}_{i,j}^{n+1}+\frac{C_d(1-\theta_2)\sqrt{U_{i,j}^{n\,2}+V_{i,j}^{n\,2}}}{H_{v,i,j}^{n}}\bar{v}_{i,j}^{n}-F_{\eta,i,j}^{n}=0
\end{aligned}
\tag{2-12}
$$

where θ_1, θ_2, θ_3 are degrees of the implicitness of the surface slope, bottom friction and Coriolis terms, respectively. Substituting the finite difference equations (2.11) and (2.12) into the continuity equation (2.9) yields the equation for surface elevation:

$$
\begin{aligned}
&\Pi_{nw,i,j}^{n}\zeta_{i-1,j+1}^{n+1}+\Pi_{n,i,j}^{n}\zeta_{i,j+1}^{n+1}+\Pi_{ne,i,j}^{n}\zeta_{i+1,j+1}^{n+1} \\
&+\Pi_{w,i,j}^{n}\zeta_{i-1,j}^{n+1}+\Pi_{c,i,j}^{n}\zeta_{i,j}^{n+1}+\Pi_{e,i,j}^{n}\zeta_{i+1,j}^{n+1}=(\mathrm{RHS})_{\mathrm{i,j}}^{\mathrm{n}} \\
&+\Pi_{sw,i,j}^{n}\zeta_{i-1,j-1}^{n+1}+\Pi_{s,i,j}^{n}\zeta_{i,j-1}^{n+1}+\Pi_{sw,i,j}^{n}\zeta_{i+1,j-1}^{n+1}
\end{aligned}
\tag{2-13}
$$

where

$$\Pi_{nw,i,j}^{n}=-\frac{\Gamma_{i,j+1}}{4}\frac{\Delta t}{\Delta\xi}\theta_1\beta_{u,i,j+1}g_{u,i,j+1}^{11} \tag{2-14}$$

$$\Pi_{ne,i,j}^{n}=+\frac{\Gamma_{i,j+1}}{4}\frac{\Delta t}{\Delta\xi}\theta_1\beta_{u,i+1,j+1}g_{u,i+1,j+1}^{11} \tag{2-15}$$

$$\Pi_{n,i,j}^{n}=-\Pi_{nw,i,j}^{n}-\Pi_{ne,i,j}^{n}-\Phi_{v,i,j+1} \tag{2-16}$$

$$\Pi_{sw,i,j}^{n}=+\frac{\Gamma_{i,j}}{4}\frac{\Delta t}{\Delta\xi}\theta_1\beta_{u,i,j-1}g_{u,i,j-1}^{11} \tag{2-17}$$

$$\Pi_{se,i,j}^{n}=-\frac{\Gamma_{i,j}}{4}\frac{\Delta t}{\Delta\xi}\theta_1\beta_{u,i+1,j-1}g_{u,i+1,j-1}^{11} \tag{2-18}$$

$$\Pi_{w,i,j}^{n}=+\frac{\Gamma_{i,j}}{4}\frac{\Delta t}{\Delta\xi}\theta_1\beta_{u,i,j}g_{u,i,j}^{11}-\frac{\Gamma_{i,j+1}}{4}\frac{\Delta t}{\Delta\xi}\theta_1\beta_{u,i,j}g_{u,i,j}^{11}-\Phi_{u,i,j} \tag{2-19}$$

$$\Pi^n_{e,i,j} = -\frac{\Gamma_{i,j}}{4}\frac{\Delta t}{\Delta\xi}\theta_1\beta_{u,i+1,j}g^{11}_{u,i+1,j} + \frac{\Gamma_{i,j+1}}{4}\frac{\Delta t}{\Delta\xi}\theta_1\beta_{u,i+1,j}g^{11}_{u,i+1,j} - \Phi_{u,i+1,j} \tag{2-20}$$

$$\begin{aligned}\Pi^n_{c,i,j} = \sqrt{g_{0,s,i,j}} &- \Pi^n_{w,i,j} - \Pi^n_{e,i,j} - \Pi^n_{n,i,j} - \Pi^n_{s,i,j} \\ &- \Pi^n_{nw,i,j} - \Pi^n_{ne,i,j} - \Pi^n_{sw,i,j} - \Pi^n_{se,i,j}\end{aligned} \tag{2-21}$$

$$\begin{aligned}(RHS)^n_{i,j} = {} & \zeta^n_{i,j}\sqrt{g_{0,s,i,j}} + \frac{\Delta t}{\Delta\xi}H^n_{u,i,j}\alpha_{u,i,j}\beta_{u,i,j}\sqrt{g_{0,u,i,j}}\gamma\theta_1 \\ & - \frac{\Delta t}{\Delta\xi}H^n_{u,i+1,j}\alpha_{u,i+1,j}\beta_{u,i+1,j}\sqrt{g_{0,u,i+1,j}}\gamma\theta_1 \\ & + \frac{\Delta t}{\Delta\eta}H^n_{v,i,j}\alpha_{v,i,j}\beta_{v,i,j}\sqrt{g_{0,v,i,j}}\gamma\theta_1 - \frac{\Delta t}{\Delta\eta}H^n_{v,i,j+1}\alpha_{v,i,j+1}\beta_{v,i,j+1}\sqrt{g_{0,v,i,j+1}}\gamma\theta_1 \\ & + \frac{\Delta t(1-\theta_1)}{\Delta\xi}(\sqrt{g_{0,u,i,j}}H^n_{u,i,j}\bar{u}^n_{i,j} - \sqrt{g_{0,u,i+1,j}}H^n_{u,i+1,j}\bar{u}^n_{i+1,j})\gamma \\ & + \frac{\Delta t(1-\theta_1)}{\Delta\eta}(\sqrt{g_{0,v,i,j}}H^n_{v,i,j}\bar{v}^n_{i,j} - \sqrt{g_{0,u,i,j+1}}H^n_{v,i,j+1}\bar{v}^n_{i,j+1})\gamma \\ & - \frac{\Gamma_{i,j}}{4}(\alpha_{u,i,j}\beta_{u,i,j} + \alpha_{u,i+1,j}\beta_{u,i+1,j} + \alpha_{u,i,j-1}\beta_{u,i,j-1} + \alpha_{u,i+1,j+1}\beta_{u,i+1,j+1}) \\ & + \frac{\Gamma_{i,j+1}}{4}(\alpha_{u,i,j}\beta_{u,i,j} + \alpha_{u,i,j+1}\beta_{u,i,j+1} + \alpha_{u,i+1,j}\beta_{u,i+1,j} + \alpha_{u,i+1,j+1}\beta_{u,i+1,j+1})\end{aligned} \tag{2-22}$$

where

$$\begin{aligned}\alpha_{u,i,j} = {} & \Delta t F^n_{u,i,j} + \bar{u}^n_{i,j} + \bar{v}^n_{u,i,j}\Delta t\frac{g_{22,u,i,j}}{\sqrt{g_{0,u,i,j}}} \\ & - \frac{\Delta t}{\Delta\xi}(\zeta^n_{i,j} - \zeta^n_{i-1,j})(1-\theta_1)g^{11}_{u,i,j} - \frac{C_d\Delta t}{H^n_{u,i,j}}\left|\vec{U}\right|^n_{u,i,j}\bar{u}^n_{i,j}(1-\theta_2)\end{aligned} \tag{2-23}$$

$$\begin{aligned}\alpha_{v,i,j} = {} & \Delta t F^n_{v,i,j} + \bar{v}^n_{i,j} - \bar{v}^n_{i,j}\Delta t(1-\theta_3)\frac{g_{21,v,i,j}}{\sqrt{g_{0,v,i,j}}} - \bar{u}^n_{v,i,j}\Delta t(1-\theta_3)\frac{g_{11,v,i,j}}{\sqrt{g_{0,v,i,j}}} \\ & - \frac{\Delta t}{\Delta\eta}(\zeta^n_{i,j} - \zeta^n_{i,j-1})(1-\theta_1)g^{22}_{v,i,j} - \frac{C_d\Delta t}{H^n_{v,i,j}}\left|\vec{U}\right|^n_{v,i,j}\bar{v}^n_{i,j}(1-\theta_2)\end{aligned} \tag{2-24}$$

$$\beta_{u,i,j} = \frac{1}{1 + \frac{C_d\Delta t}{H^n_{u,i,j}}\left|\vec{U}\right|^n_{u,i,j}\theta_2} \tag{2-25}$$

$$\beta_{v,i,j} = \frac{1}{1 + \frac{C_d \Delta t}{H^n_{v,i,j}} \left|\vec{U}\right|^n_{v,i,j} \theta_2 + \Delta t \theta_3 \frac{g_{21,v,i,j}}{\sqrt{g_{0,v,i,j}}}} \tag{2-26}$$

$$\Gamma_{i,j} = \theta_1 \theta_3 \frac{\Delta t}{\Delta \eta} H^n_{v,i,j} \beta_{v,i,j} \Delta t g_{11,v,i,j} \gamma \tag{2-27}$$

$$\Phi_{u,i,j} = \frac{\Delta t}{\Delta \xi} \theta_1 H^n_{u,i,j} \frac{\Delta t}{\Delta \xi} \theta_1 \beta_{u,i,j} \sqrt{g_{0,u,i,j}} g^{11}_{u,i,j} \gamma \tag{2-28}$$

$$\Phi_{v,i,j} = \frac{\Delta t}{\Delta \eta} \theta_1 H^n_{v,i,j} \frac{\Delta t}{\Delta \eta} \theta_1 \beta_{v,i,j} \sqrt{g_{0,v,i,j}} g^{22}_{v,i,j} \gamma \tag{2-29}$$

Equation (2-13) can be solved using the conjugate gradient algorithm (Casulli and Cheng, 1992). The detailed procedures are described by Davis (1996). Once water level is available, the vertical-integrated velocities can be calculated from Equation (2.11) and (2.12).

2.2.2 Radiation Stress

As discussed by Alymov (2005), two kinds of radiation stresses are used in CH3D, vertically uniform and vertically varying. Following Dean and Dalrymple (1991), the vertically uniform radiation stresses S_{xx}, S_{yy}, S_{xy} can be written as:

$$S_{xx} = E[n(\cos^2 \theta + 1) - \frac{1}{2}] \tag{2-30}$$

$$S_{yy} = E[n(\sin^2 \theta + 1) - \frac{1}{2}] \tag{2-31}$$

$$S_{xy} = \frac{E}{2} n \sin 2\theta \tag{2-32}$$

Where E is wave energy, n is the ratio of group velocity to wave celerity, and θ is the angle wave propagating to the onshore direction.

The vertically varying radiation stress was derived by Mellor (2003) when surface waves was considered in three-dimensional ocean circulation modeling, which takes the following form:

$$S_{\alpha\beta} = kHE[\frac{k_\alpha k_\beta}{k^2} F_{CS} F_{CC} + \delta_{\alpha\beta}(F_{CS} F_{CC} - F_{SS} F_{CS})] \tag{2-33}$$

Where H is the total depth; $\sigma = (z\text{-}\zeta)/H$; k is the wave number whose x- and y- components are k_α and k_β, respectively; E is the total wave energy; $\delta_{\alpha\beta}$ is the Kronecker delta; and

$$F_{SS} = \frac{\sinh KH(1+\sigma)}{\sinh KH}$$
$$F_{CSS} = \frac{\cosh KH(1+\sigma)}{\sinh KH}$$
$$F_{SC} = \frac{\sinh KH(1+\sigma)}{\cosh KH}$$
$$F_{CC} = \frac{\cosh KH(1+\sigma)}{\cosh KH}$$

2.2.3 Boundary Conditions

Because of flooding and drying feature in CH3D, water is free to move over land if the water level is high enough. At the river boundary, water is introduced into the system by given fresh water discharge. At the open boundary, there are three kinds of conditions that can be applied: clamped boundary condition (water level specified), specified water mass flux specification and radiation condition. As water domain along the open boundary is very large, continuous measurement or estimation of water mass is normally very difficult to obtain, especially during a storm event, therefore the second boundary condition of specified water mass is not generally used. The most common open boundary condition for CH3D is the clamped boundary. This is mainly because of the fact that water levels are relatively easier to prescribe. For tidal simulation case, tidal constituents, predicted tide or tide from circulation models can all be applied depends on data availability. Deficit atmospheric pressure induced water level at the

open boundary can be estimated from analytical Holland model based on hurricane intensity and track. Surge induced water level is normally available from regional circulation model ADCIRC. Thus, the total water level at open boundary can be written as:

$$\varsigma = \varsigma_T + \varsigma_S + \varsigma_D \tag{2-34}$$

where ζ is water level along open boundary; ζ_T is the component from tide; ζ_S is surge provided by regional circulation model; and ζ_D is water level adjustment if different vertical datum is considered. The Flather radiation boundary condition (Flather, 1976) is also available in CH3D-SSMS. Comparing to clamped boundary condition, the Flather radiation boundary condition allow the disturbed water level inside domain to be transported outside. However, it requires both water level and current to be specified at the open boundary, which may not be easy to obtain and may introduce more uncertainties. The detailed explanation and validation of the Flather boundary condition is included in Appendix E.

At the free surface, wind stresses are applied as the boundary condition:

$$\begin{aligned} \tau_x^w &= \rho_a C_d u_w \sqrt{u_w^2 + v_w^2} \\ \tau_y^w &= \rho_a C_d v_w \sqrt{u_w^2 + v_w^2} \end{aligned} \tag{2-35}$$

where τ_x^w and τ_y^w are wind stresses in x and y directions; ρ_a is air density; u_w and v_w are wind speed in x and y directions; and C_d is the drag coefficient calculated from Garratt (1977) formulation:

$$C_d = 0.001(0.75+0.067\ W_s) \tag{2-36}$$

where W_s is speed of wind with unit m/s. When C_d is greater than 0.003, it will be set to constant of 0.003 instead of increasing with wind speed.

In two-dimensional cases, the bottom boundary condition is expressed using the Chezy formulation:

$$\tau_x^b = \frac{gu\sqrt{u^2+v^2}}{C_z^2}$$
$$\tau_x^b = \frac{gv\sqrt{u^2+v^2}}{C_z^2} \tag{2-37}$$

where τ_x^b and τ_y^b are bottom stresses in x and y directions; g is gravity; u and v are wind speed in x and y directions; and C_z^2 is the Chezy friction coefficient:

$$C_z = 4.64\frac{R^{1/6}}{n} \tag{2-38}$$

where R is the hydraulic radius (cm) which can be represented by the total water depth (cm) and n is the Manning's coefficient ($cm^{1/2}/s$). 4.64 has the unit of $cm^{1/3}/s$.

2.2.4 Model Validation

The atmospheric pressure, wind setup and flooding and drying sections in CH3D have been verified by Alymov (2005) in his dissertation. A tidal circulation test on a curvilinear annular grid was tested in this study and validated against an analytical solution. The details of the annular test are included in Appendix C.

2.3 Regional Wave Model

WaceWatch-III (Tolman, (1997, 1999)) is a third generation NOAA/NCEP operational wave model developed at NOAA/NCEP. It solves the spectral action density balance equation for wave number-direction spectra. The implicit assumption of this equation is that properties of medium water depth and current as well as the wave field itself vary on time and space scales that are much larger than the variation scales of a single wave. A further constraint is that the parameterizations of physical processes included in the model do not address conditions where the waves are strongly depth-limited. These two basic assumptions imply that the model can

generally by applied on spatial scales (grid increments) larger than 1 to 10 km and outside the surf zone (NOAA-C, 2006).

The governing equations of WaveWatch-III include refraction and straining of the wave field due to temporal and spatial variations of the mean water depth and of the mean current (tides, surges etc.), when applicable. Parameterizations of physical processes (source terms) include wave growth and decay due to the actions of wind, nonlinear resonant interactions, dissipation (`whitecapping'), and bottom friction. Wave propagation is considered to be linear. Relevant nonlinear effects, such as resonant interactions are therefore included in the source terms. The WaveWatch-III North Atlantic computational grid covers the western North Atlantic including the Gulf of Mexico and Caribbean with grid size of 0.25 degrees.

The 6-hour hindcast waves from WaveWatch-III are available for recent years. In this study, those wave parameters, including significant wave height, peak wave period and mean wave direction, are used to interpolate for waves along open boundaries for the local wave model, SWAN during the Hurricane Ivan and Hurricane Dennis simulations.

2.4 Regional Circulation Model

ADCIRC (Westerink and Luettich, 1991, 1992) solves the equations of fluid motion on a rotating earth. These equations are based on hydrostatic pressure and Boussinesq approximations and have been discretized in space using the finite element method and in time using the finite difference method. The EC2001 computational grid (ADCIRC, 2001) consists of 58369 elements and 31435 nodes and covers the western part of the North Atlantic including the Gulf of Mexico and the Caribbean. With input of wind field, ADCIRC can provide storm surge elevations and velocities corresponding to each node over a very large domain. The varying grid spacing ability allows it to use a very coarse grid in the open water and a relatively fine grid near coastal region. However, the resolution of the EC2001 grid inside the Escambia Bay area is insufficient (5-6

km) to resolve detailed surge evolution, not to mention that land is not included in the EC2001 grid. However, the development of storm surge in the open water could be simulated reasonably well with EC2001 grid due to its coverage of a very large domain. Therefore, ADCIRC is applied in the CH3D-SSMS integrated modeling system to provide water level along the CH3D grid open boundaries using this EC2001 grid.

2.5 Local Wave Model

When transported to near shore and coastal bay areas, these big waves will break and the associated radiation stresses will make wave setup which may significantly increase storm surge water level during hurricane storm events. At the same time, the rising water from the storm surge may also change the wave transport process by altering total water depth. Therefore, the circulation and waves interact with each other, and these coupling processes should not be neglected for storm surge simulations. Developed at the Delft University of Technology in the Netherlands, SWAN is a very well-validated third-generation wave model which computes random, short-crested wind-generated waves in coastal regions and inland waters (Holthuijsen et al., 2003). The model is based on the wave action balance equation (or energy balance in the absence of currents) with sources and sinks. The model predicts a 2D wave field on already specified grid points. SWAN accounts for the following physics: 1) wave propagation in time and space, shoaling, refraction due to current and depth, frequency shifting due to currents and nonstationary depth; 2) wave generation by wind; 3) three- and four-wave interactions; 4) whitecapping, bottom friction and depth-induced breaking; 5) wave induced setup; 6) propagation from laboratory up to global scales; and 7) transmission through and reflection from obstacles. In CH3D-SSMS, SWAN is dynamically coupled with CH3D to provide wave height, period, and directions at each CH3D grid cells. These wave parameters are used to estimate radiation stress in the water momentum transport equation to drive the flow.

2.6 Wind Model

The surface wind field associated with tropical cyclone is the key factor and the primary requirement for modeling storm surges. It not only generates a strong shear stress and atmospheric pressure gradient at air-sea interface to drive the surge, but also generates big waves that lead to further water setup near the coastline and inside the bay due to radiation stress. Therefore, it deserves a separate section on wind field and wind models

Considering the large domain and difficulty of open sea wind measurement, measured winds are always sparse. Modeled winds are often used for storm surge simulation. One of the best simulated winds is the Hurricane Research Division wind (HRD) of NOAA (HRD, 2006). HRD is formed to advance the understanding and prediction of hurricanes and other tropical weather. Its wind is based on a combination of computer models, theories, and observations, with particular emphasis on data obtained with research aircraft. With spatial resolution of 6 km over hurricane affect domain, the detailed wind structure can be accurately represented by HRD wind. There are two shortcomings of HRD wind. First, the background wind is not included. Secondly, there is rarely HRD wind after hurricanes make land fall.

WNA wind is simulated by National Centers for Environmental Prediction (NCEP/NOAA) for wave modeling. It has a coarser spatial resolution of 28 km over the Gulf of Mexico and most of the Atlantic Ocean. It is free to public and can be downloaded from the NOAA website. The WNA wind data is available as snapshots at three hours intervals. As land coverage is not included in WNA wind, it has difficulty resolving wind near the shore and inside the bay.

WINDGEN wind is an atmospheric model developed by University of Miami to predict the wind and pressure. The coverage of WINDGEN wind includes the Western Atlantic Ocean and the Gulf of Mexico. One advantage of WINDGEN is that it not only has wind over the ocean but also wind over the land, even though the land reduction effect is not considered. Compared to

HRD and WNA wind, WINDGEN wind has more frequent snapshots during hurricane event reporting wind speeds every hour. However, limited WINDGEN wind is available to Southeastern Universities Research Association (SURA) Coastal Ocean Observing and Prediction (SCOOP) Program partners only and cannot be accessed by the public (SCOOP, 2006).

The Planetary Boundary Layer (PBL) model is a complex wind model that calculates vertically averaged through the depth of the PBL velocities during a storm event. (Chow, 1971; Cardone et al., 1992). The interaction between the boundary layer and the free atmosphere is expressed in terms of the geotropic wind field (velocity at the top of the boundary layer) and the surface stress (frictional dissipation of the kinetic energy in the boundary layer). Further parameterization of the model includes vertical fluxes of momentum, heat and moisture. This parameterization is based on the matching of mean profiles of wind, temperature, and moisture by surface and outer layer similarity theories. The PBL model is a sophisticated wind model and has the potential to generate accurate wind field. However, in most real cases, the available storm parameters are limited to central pressure deficit, translation speed, direction, and radius to maximum winds. As the result, the PBL model is difficult to use because of the uncertainty in choosing the right parameters that are unknown.

The Holland wind model (Holland, 1980) is the most widely used "parametric" analytic wind model that requires fewer input parameters. The radial wind structure of the symmetric vortex is a function of the radius of maximum wind, maximum wind, and a measure of the width of the profile. The Holland model is used to provide wind input to the SLOSH storm surge model by FEMA to guide real-world financial and emergency response decisions. According to Holland (1980), the atmospheric pressure is assumed exponentially varying from the storm center:

$$P = P_0 + (P_\infty - P_0)e^{A/r^B} \tag{2-39}$$

where P_0 is the central atmospheric pressure, $P\infty$ is the atmospheric pressure far away from the center, r is the distance from the center of the storm, and A and B are scaling parameters. Following Wilson (1957), Davis (2001) further simplified the derivation by setting A is equal to the radius of maximum wind speed, R, and B is equal to 1 in his Hurricane Floyd and Hurricane Irene (1999) simulations:

$$P_a = \Delta P_0 (1 - e^{R/r}) \tag{2-40}$$

where P_a is the relative atmospheric pressure and $\Delta P_0 = P_0 - P\infty$ is the central pressure drop of the storm.

The cyclostrophic wind velocity, U_c, is

$$U_c = \sqrt{-\frac{\Delta P_0 R}{\rho_a r} e^{-R/r}} \tag{2-41}$$

The geotropic wind velocity, U_g, is

$$U_g = -\frac{\Delta P_0 R}{f \rho_a r^2} e^{-R/r} \tag{2-42}$$

The gradient wind velocity, U_G, is

$$U_G = U_c(\sqrt{\gamma^2 + 1} - \gamma) \tag{2-43}$$

Where

$$\gamma = \frac{1}{2}(\frac{V_s^*}{U_c} + \frac{V_c}{U_g}) \tag{2-44}$$

and the resolved part, V_s^*, of the translational velocity of the storm, V_s is

$$V_s^* = V_s \sin(\theta) \tag{2-45}$$

where θ is the angle from the direction of bearing of the storm, β, to any point inside the storm. The surface wind velocity, U_s, in the x- and y- directions is then written as

$$U_{sx} = KU_G \cos(90 + \theta + \beta + \phi) \tag{2-46}$$

$$U_{sy} = KU_G \sin(90 + \theta + \beta + \phi) \tag{2-47}$$

where ϕ is an inward rotation angle of 18° and K is the ratio of surface wind velocity to gradient wind velocity.

2.7 Simple Storm Surge Test

When hurricanes strike the continental shelf, one question is how the bathymetry and topography and their slopes affect the surge and wave along the coast? The relationship between the bathymetry, topography and their slopes and storm surge can be represented by simplified momentum equation. For steady state, the wind and bottom stress on the water and a hydrostatic force is balance by the water surface slope (Dean and Dalrymple, 1984):

$$\frac{\partial \varsigma}{\partial x} = \frac{\tau_w - \tau_B}{\rho g(h + \varsigma)} \tag{2-48}$$

Where ς is water level in x-coordinate directions; τ_w and τ_B are shear stress on water surface and bottom, respectively; ρ is water density; g is the acceleration of gravity; and h is water depth. By assuming zero water levels at deep water l with h_0 water depth, the solution for above equation for linearly increased bathymetry can be written as:

$$\frac{x}{l} = (1 - \frac{h + \varsigma}{h_0}) - A \ln(\frac{\frac{h + \varsigma}{h_0} - A}{1 - A}) \tag{2-49}$$

Where $A = n\tau_w l / \rho g h_0^2$; $n = 1 - \tau_B / \tau_w$. Thus for a given wind stress, the shallower the water depth, the smaller the slope, the higher storm surge can be obtained.

Numerical experiments are designed to further evaluate the relationship of bathymetry and storm surge using CH3D-SSMS. The test slopes are selected based on Florida coast bathymetry. As shown in Figure (2-2), five cross sections along east and west coast of Florida are chosen to represent the overall bathymetry slope. The cross shore slopes on the east coast of Florida (section 1 and 2) are steep with approximate ratio of 1:100 (Figure 2-3). Section 4 and 5 at the Florida Panhandle show similar but slightly milder slope compared to east coast. On the contrary, the section 3 located north of Tampa Bay on the west coast of Florida shows extreme mild slope. The water depth slowly increases to about 13m over 20km distance offshore. Based on sampled Florida coast cross shore bathymetry, four kinds of slope from 1:100, 1:200, 1:400 to 1:1000 are selected to represent steep to mild bathymetry (Figure 2-4). The open boundary is extended 15 km from shoreline with zero water levels. As wave energy will spread under an angle, the computational domain in the cross shore direction is set to 15 km to reduce the boundary effect on wave transport inside the computational domain. Constant wind speed of 30 m/s is applied over the entire domain to drive the surge. Rectangular grid with 20 m resolution is used in the simulation for steep case (1:100) and 50 m resolution is used for the other intermediate and mild slope cases.

The maximum surge obtained from the mild slope case is much bigger than that from the steep slope bathymetry case (Table 2-1) and is associated with severe flooding. In addition, the simulation results also imply the wind-driven surges vary approximately inversely with the bathymetry slope. In other words, a n-time milder slope would cause roughly n times higher surges. During the transient state in real storms, the water level may not be fully developed but the conclusion should still be valid as the rate of water level change is determined by surface stress and total water depth. When waves break in surf zone, it will cause water level to increase

due to wave setup. The tests are extended by including wave effect on storm surge. The same grid systems are used with zero water levels and waves with a 6 meter significant wave height and 10 second peak period at the open boundary. The net water level difference between simulations with wave effects and without wave effects are attributed to surge due to wave setup. The maximum wave setup is obtained from the steepest slope case (1:100) with magnitude of about 50 cm (Table 2-1). The setup decreases gradually as bathymetry slope becomes larger. For the extreme mild slope case (1:1000), the wave setup induced surge is only in the order of centimeter. This is possibly due to the stronger dissipation from nonlinear effect and bottom friction for the mild slope shallow water. The simulated setup from wave is lower than Dean & Dalrymple's (1991) estimation of 0.19 breaking wave height H_b, which is about 6.7 m. This may comes from the fact that their formulation is based on linear regular wave theory for small amplitude incident waves, which is not appropriate for this irregular strong storm waves.

The conducted tests suggest that Florida coastal bay areas are vulnerable to storm surge impact because of their gentle bottom slope and shallow water. In west Florida, the continental shelf in the Gulf of Mexico is relatively milder than the east coast of Florida in the Atlantic Ocean. Thus, higher storm surge is expected in the large shallow coastal area for same category hurricane. Waves are just the opposite. On the west Florida coast, the gentle bottom slope makes waves break earlier, resulting in smaller waves compared to the east Florida coast.

One advantage of 3D model over 2D model is that the bottom friction can be more accurately resolved. This is demonstrated using the simple wind case (a) as listed in Table 2-1. With same boundary and wind condition, 3D model generates maximum setup of 50 cm compared to 24 cm by 2D model. For this simplified case, zero vertical-averaged velocity is obtained from the 2D model, which implies that the bottom friction is zero. Therefore, wind

stress on the surface is the sole force that caused the setup. While for 3D model, the velocity at each layer is not zero even though the vertically-averaged velocity is. Near water bottom, the flow velocity from the stratified flow field is in the opposite direction of wind field. Therefore, this bottom stress provides addition force that caused higher setup together with wind stress. It has to be kept in mind that this is extreme case. In reality, the bottom flow is rarely in the exact opposite direction of wind field, thus the magnitude of bottom friction effect will be reduced.

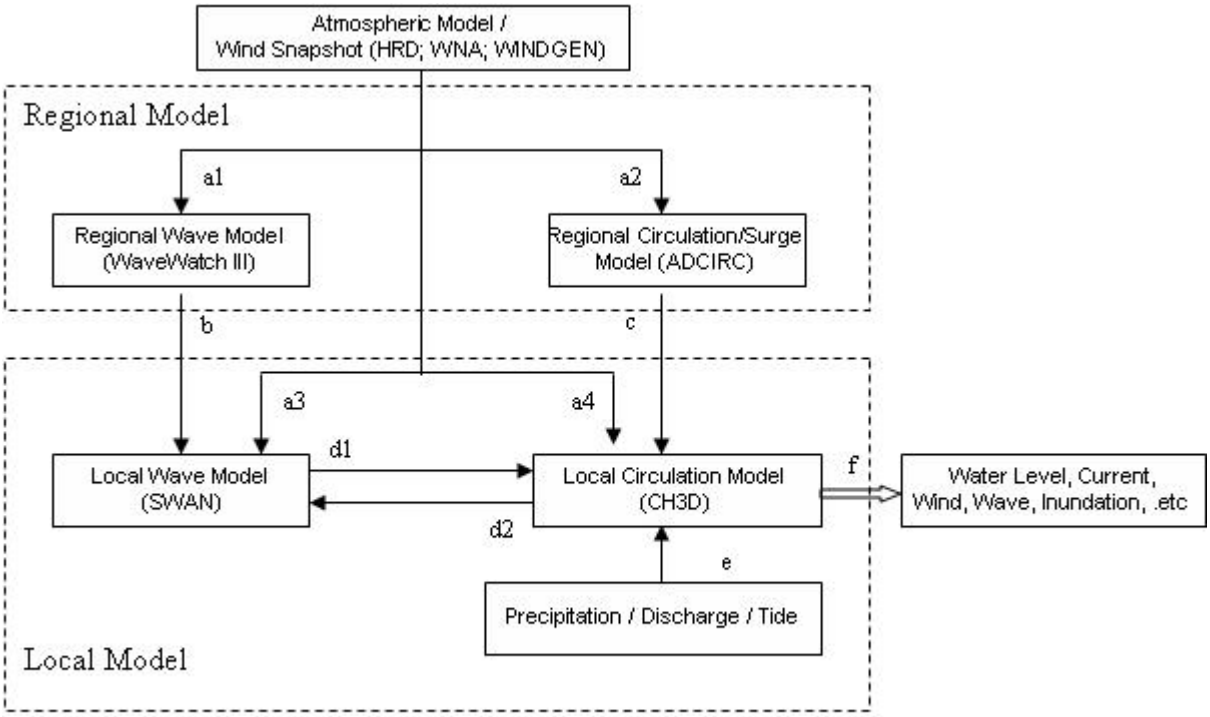

Figure 2-1. Description of Model coupling processes in CH3D-SSMS.

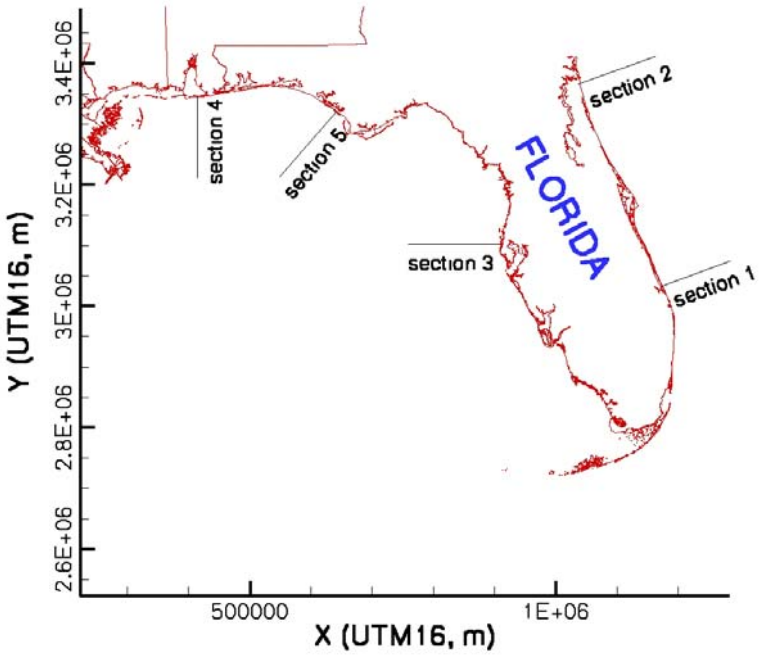

Figure 2-2. Cross section locations of bathymetry along Florida coast.

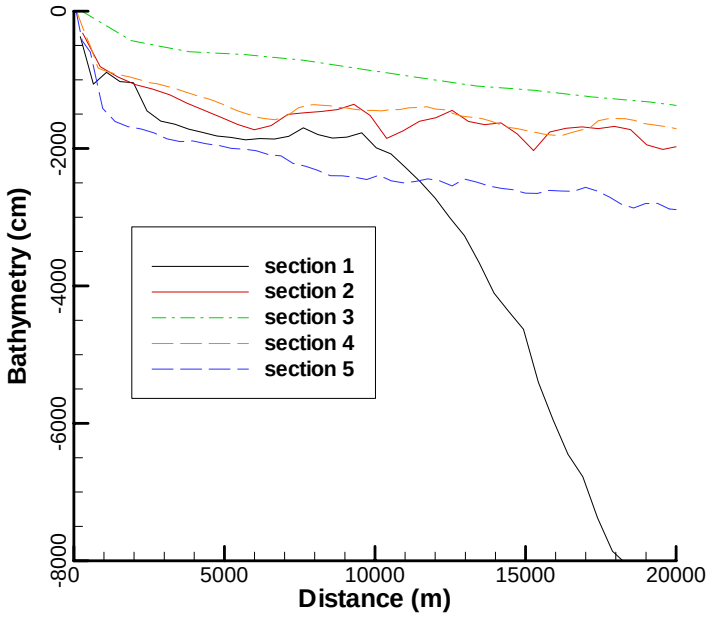

Figure 2-3. Bathymetry slopes at five cross sections along Florida coast.

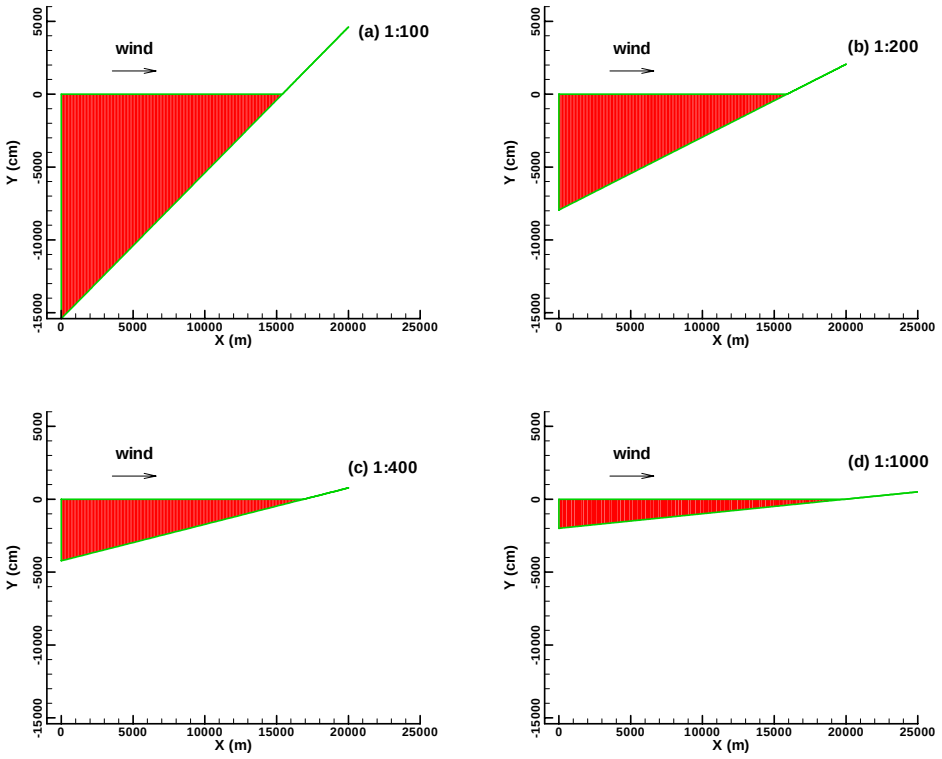

Figure 2-4. Bathymetry and topography slope used in wind and wave driven surge test.

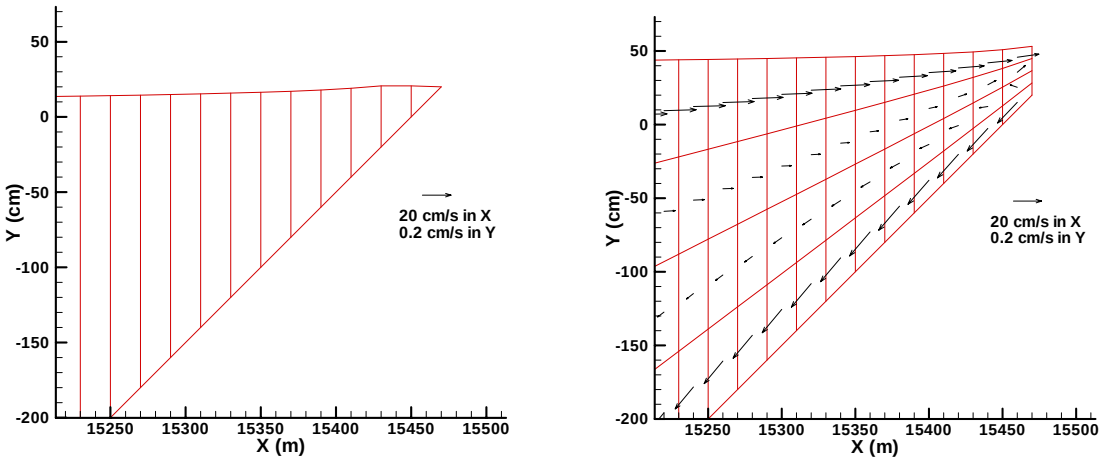

Figure 2-5. Wind setup test from 2D model (left panel) and 3D model (right panel).

Table 2-1. Wind and wave driven surge test using CH3D-SSMS

Case	Bathymetry Slope	Wind Speed (m/s)	Wave height (m)	Wave period (s)	Highest surge (cm)	Surge by wave setup (cm)
Wind (a)	1:100	30	-	-	23.5	-
Wind (b)	1:200	30	-	-	46.1	-
Wind (c)	1:400	30	-	-	93.6	-
Wind (d)	1:1000	30	-	-	201.7	-
Wind and wave (a)	1:100	30	6	10	74.3	50.8
Wind and wave (b)	1:200	30	6	10	91.2	45.1
Wind and wave (c)	1:400	30	6	10	108.6	15.0
Wind and wave (d)	1:1000	30	6	10	205.4	3.7

CHAPTER 3
HURRICANE IVAN SIMULATION

3.1 Introduction

Hurricane Ivan was a classical, long-lived Cape Verde hurricane that reached Category 5 strength on the Saffir-Simpson Hurricane Scale (SSHS, Figure A-1) three times. Ivan caused significant damage and loss of many lives as it passed through the Caribbean Sea and the southeastern United States (NHC, 2004). In this chapter, synoptic history of Hurricane Ivan is introduced. Then, a systematic modeling plan using CH3D-SSMS is presented. The CH3D-SSMS is calibrated and validated against available data. Using calculated storm surge and wave data, the I-10 Bridge (Escambia Bay, Florida) collapse event was analyzed by calculating the wave force on the bridge deck. Afterwards, extensive sensitivity tests were made to evaluate the key factors affecting storm surge simulation. The final part is the risk analysis for hurricane impacts based on different kinds of simulation scenarios.

3.2 Synoptic History

Hurricane Ivan developed from a large tropical wave that moved off the west coast of Africa on 31 August, 2004. It continued to develop to Tropical Storm Ivan at 0600 UTC 3 September and steadily strengthened to a hurricane at 0600 UTC 5 September. Ivan reached Category 5 strength three times in the Caribbean Sea before it entered the Gulf of Mexico on 14 September as a Category 4 hurricane. As Ivan moved to the northern Gulf of Mexico, it weakened slightly and made landfall as a Category 3 hurricane with 121 mph wind at 0650 UTC 16 September, just west of Gulf Shores, Alabama (SSEC, 2004) (Figure 3-1). By this time, the eye diameter had increased to 40-50 n mi, which resulted in some of the strongest winds occurring over a narrow area near the southern Alabama-western Florida Panhandle border. After Ivan moved across the barrier islands of Alabama, the hurricane turned north-

northeastward across eastern Mobile Bay and weakened into a tropical storm 12 h later over central Alabama (NHC, 2004).

The best track of hurricane is a subjectively-smoothed representation of a tropical cyclone's location and intensity over its lifetime. The best track contains the cyclone's latitude, longitude, maximum sustained surface winds, and minimum sea-level pressure at 6-hourly intervals (NOAA, 2004e). The best track central barometric pressure and wind speed history for Hurricane Ivan is depicted in Figure 3-2 (NHC, 2004). The details of best track for Hurricane Ivan are included in Appendix A. As Ivan grows to Category 5 hurricane, the maximum wind speed increased to 160 mile/hour. When Ivan moves closer to the continent it started to weaken. After landfall, central barometric pressure rose and wind speed dropped dramatically.

The forces of Ivan were directly responsible for 92 deaths, 25 of them were americans. Ivan also caused extensive damage to coastal and inland areas of the United States. Portions of the Interstate 10 bridge system across Pensacola Bay, Florida were severely damaged and as much as a quarter-mile of the bridge collapsed into the Bay. The U.S Highway 90 Causeway across the northern part of the bay was also heavily damaged. Thousands of homes and commercial buildings were damaged or destroyed. In addition, Ivan also destroyed millions of acres of woodlands and forests. The total estimated U.S. loss is approximately $14.2 billion.

3.3 Hurricane Ivan Simulation Using CH3D-SSMS

The measured data during Hurricane Ivan is explained followed by a discussion on Bathymetry/Topography and the grid system. Then, the calibrated CH3D-SSMS is applied to simulate Hurricane Ivan with consideration of astronomical tide, wind stress, barometric pressure, and dynamic wave setup. The simulated winds, atmospheric pressures, surges, waves, and high water marks are compared with observed measurement. Next, a series of sensitivity tests are designed to assess the importance of a few major parameters used in the Ivan

simulation. The validated water level and waves are used for I-10 Bridge over Escambia Bay to calculate wave force and to analyze the reasons that the bridge collapsed. The last section includes risk analysis tests to determine the vulnerabilities of coastal highways and bridges in severe storms like Hurricane Ivan.

3.3.1 Data Measured during Hurricane Ivan

During Hurricane Ivan, a large number of wind, atmospheric pressure, wave and water level data were collected by different agencies. These data are used to test the accuracy of storm surge and wave simulations. The station information of the available data used for the current Ivan simulation is summarized in Table 3-1. Figure 3-3 shows the track of Hurricane Ivan and the station locations.

3.3.2 Bathymetry, Topography and Grid System

The topography and bathymetry are downloaded from National Elevation Dataset (NED), USGS (2006) and GEOphysical Data System (GEODAS), Nation Geophysical Data Center (NGDC), NOAA (2006). The vertical datum is NAVD88 for both bathymetry and topography. NED data and GEODAS data are combined first and then interpolated into the CH3D grid system using an inverse distance interpolation technique. The generated grid and bathymetry/topography for Hurricane Ivan is shown in Figures 3-4 and Figure 3-5. The I-10 Bridge goes across the north part of Escambia Bay, where the average water depth is about 2-3 m. The grid size across the bridge is about 100 m (Figure 3-6).

Vertical datum

For storm surge model evaluation, simulated and measured water levels must be compared relative to a common vertical datum. Since the datum used in ADCIRC (Mean Sea Level (MSL)) is different from that used in CH3D Grid (North America Vertical Datum 88 (NAVD88)), water level simulated by ADCIRC must be adjusted before being imported to CH3D. The relationship

between NAVD88 and MSL is available at several NOAA stations (NOAA, 2006a) which was linearly interpolated into the entire domain. Detailed vertical datum translation can be found at Appendix A.

3.3.3 Wind Field

Wind field plays a very important role in storm surge modeling. It not only generates a strong shear stress and atmospheric pressure deficit at air-sea interface to drive the surge, but also generates big waves that lead to further water setup at the coast by radiation stress. Therefore, the accuracy of wind field fed into the surge model directly affects the accuracy of surge simulation. During a strong storm event, continuously measured wind is normally only available at limited stations. However, storm surge model requires complete wind information to cover the entire simulation domain before and after the hurricane makes landfall. As a result, simulated or data-assimilated wind field are normally used for storm surge simulation. The following are several representative wind data sets that are available to public and are used in this study.

3.3.3.1 HRD wind

The Hurricane Research Division (HRD) of NOAA was formed to advance the understanding and prediction of hurricanes and other tropical weather. Its wind is based on a combination of computer models, theories, and observations with particular emphasis on data obtained with research aircraft (HRD 2006). HRD wind has spatial resolution of 6 km over hurricane affect domain, normally ±4 degrees in both latitude and longitude. In general, HRD Ivan wind has snapshots every three hours until the hurricane made land fall. A representative HRD wind snapshot before Hurricane Ivan made landfall (0600 UTC 16 September, 2004) is depicted in Figure 3-7 (HRD, 2006).The wind is one-minute maximum sustained surface wind, valid for marine exposure over water and open terrain exposure over land.

3.3.3.2 WNA wind

WNA wind is simulated by the National Centers for Environmental Prediction (NCEP/NOAA) for wave modeling. It has a coarser spatial resolution of 28 km over the Gulf of Mexico and most of the Atlantic Ocean. For Hurricane Ivan, WNA wind coverage is available during the entire event with 3-hour intervals. However, wind over land is not included in WNA wind because it is primarily applied for wave simulation. Because of coarse resolution and no land-wind, WNA is not the best wind for storm surge simulation. It is a good substitute if there is no other wind available. Figure 3-8 shows the snapshot of WNA for Hurricane Ivan at 0600 UTC 16 September before it made landfall. It is obvious that there is no wind at either Escambia Bay, FL or Mobile Bay, AL.

3.3.3.3 WINDGEN wind

WINDGEN wind is an atmospheric model developed by Vincent Cardone at Ocean Weather to predict wind and pressures. WINDGEN wind for Hurricane Ivan is obtained from SCOOP Program Partner, University of Miami (SCOOP, 2006). The spatial resolution is 0.2 degrees in both latitude and longitude and wind snapshot data is available in hourly interval. The snapshot of WINDGEN wind at 0600 UTC 16 September is showed in Figure 3-9. Compared to WNA wind, WINDGEN wind has similar magnitude, direction, and additional wind over land. However, the wind over land is overestimated as it does not include any land reduction effect. The relatively coarse resolution, wind accuracy, and exclusion of land reduction effects are the major factors that are not favorable to the Hurricane Ivan storm surge simulation.

3.3.3.4 Land reduction effect on wind field

In storm surge modeling, wind is the most important factor as it generates large shear stresses over the water surface and reaction with flow field. As discussed above, numerous wind models are used to produce hurricane wind for storm surge simulation. Driven by wind stress,

wave setup, and shallow water effect, the highest surges are normally observed at shallow water zones, such as estuarine, lagoon, or coastal bays. Winds at these domains are very important for accurate storm surge simulation. Unfortunately, none of the wind models discussed above completely consider the land reduction effect when wind blows over land. WNA and WINDGEN do not have land reduction at all. HRD wind does add this effect by assuming land to be open terrain but it is not accurate enough to represent the true land. In order to incorporate the land roughness effect, the methods used by IPET (2006) for the Hurricane Katrina study are considered here. As an example, the following list the procedures to add land reduction effect to adjust HRD wind for use by CH3D-SSMS:

1. Remove open exposure effect in HRD wind.
2. Make continuous snapshots between three-hour snapshots using Lagrangian interpolation.
3. Convert one-minute wind to 10-minute wind.
4. Convert Land Cover to bottom roughness on land cells.
5. Calculate integrated bottom roughness at each individual grid cell, including water.
6. Reduce wind from open water to limited exposure; The conversion coefficient can be written as (Powell, M., 1996 & 1998):

$$f = \left(\frac{Z_{0s}}{Z_0}\right)^{0.0706}\left[\ln\left(\frac{Z}{Z_{0s}}\right)\ln^{-1}\left(\frac{Z}{Z_0}\right)\right]$$

Where Z_0 is open water roughness; Z_{0s} is integrated bottom roughness; Z is 10 m.

The land cover for Louisiana, Mississippi, Alabama, and Northwest Florida is available from The National Land Cover Database (NLCD), 2001, USGS (SEAMLESS, 2006). After downloading the high-resolution (30 m) land cover data and converting it from Albers projection to UTM16 projection, a map that includes detailed land cover over the northeast Gulf of Mexico

coastal regions is made (Figure 3-10). The bottom roughness of ocean and land converted from land cover for Hurricane Ivan is shown in Figure 3-11.

3.3.4 Wave

The WW3 model is an operational wave model of the NCEP/NOAA. The WNA wind is used to drive the model. The historical wave data from the WW3 model is downloadable from the NOAA website (NOAA-3). In this study, wave height, period and direction along the CH3D grid open boundary were abstracted from the WW3 data to feed local wave model SWAN along open boundary cells for Hurricane Ivan. At the grid resolution of WW3 (0.25 degree) is larger than the SWAN grid at open boundary (2 kms), an inverse-distance interpolation technique is used. Since the wave parameters from WW3 change gradually along the boundary, the interpolation should not introduce big errors. The WW3 model is also applied to simulate waves in open sea during Hurricane Ivan. The simulated wares are close to those downloaded from NCEP/NOAA. The details are described in Appendix F.

3.3.5 Water Level Boundary Conditions

There are two components of water level at open boundaries, astronomical tides and storm-induced surge. The surge component is generated by the regional surge model ADCIRC from the coupling process. As for tidal water level, it can be obtained from either tidal constituent database by ADCIRC or interpolation of predicted tide at available NOAA stations. Both were considered in this study.

3.3.6 Hurricane Ivan Storm Surge Simulation Results

Data collection is difficult during a storm event because of strong wind, big waves, and high surge. For Hurricane Ivan, only limited data of wind, atmospheric pressure, waves, water level, and high water marks are available at a few monitoring stations. In order to provide a comprehensive assessment of the accuracy of simulation results, model results are not only

compared with measurements at the stations but also presented as snapshot over the entire simulation domain. First, time series of water level, wind and wave are compared with data at available NOAA stations. Then the peak and phase of high water at several locations are compared with high water marks. Continuous snapshots of wind and water level are made before and after Ivan made landfall with three-hour intervals with hurricane track to describe the storm surge development process. The maximum of water elevation in each grid cell is saved to display the Envelope Of High Water (EOHW) for Hurricane Ivan. Inundation maps around Escambia Bay and other coastal regions are also made. The summary of model results comparison methods is listed in Table 3-2.

3.3.6.1 Wind and atmospheric pressure comparison

The wind field used in the Ivan simulation includes WNA wind and HRD wind. As discussed before, when Ivan moved close to the coast, the high resolution HRD wind is used in the model. Other times, WNA is applied as HRD wind cannot cover the computational domain. For both winds, land reduction effect by land use is considered to adjust the wind when the wind is blowing over land. As shown in Figure 3-12, the simulated wind compares well with the measurement at all stations. At FCMP station Tower 1 and Tower 2, the measurement was not made during the entire storm but long enough to capture the maximum wind as Ivan went by. Station Dauphin Island, Pensacola and T1 are located within the maximum wind radius range and the winds peak up to 35-40 m/s. T2 is also within the range, however the maximum wind speed is only about 30 m/s. The reason is that the station is located deep inland and wind is weakened by the surrounding rough land. Stations Panama City Beach and Waveland are located further away from hurricane center and have relatively weaker wind. It should be noticed that, even though Panama City Beach is located further from hurricane center than Waveland, it has much higher wind (25 m/s .vs . 15 m/s). Two reasons made the difference. First, it is on east side

of the hurricane which has stronger wind; secondly, wind at Panama City Beach always blow from water to land thus there is no land reduction effect, while Waveland is just the opposite. The time series of wind at these stations show that both magnitude and direction are also in good agreement of the measurement except at stations Waveland and Pensacola, but the differences of wind direction are simply caused by instrument error.

The atmospheric pressure for Ivan is calculated from the analytical Holland Model solution based on hurricane track, minimum deficit atmospheric pressure, and maximum wind radius. The time series comparisons at a few stations are shown in Figure 3-13. Since the Holland model assumes uniform atmospheric pressure structure, the spatial variation can not be fully resolved and sometimes may not give perfect results. As a result, the simulated pressure at stations close to the hurricane center shows better comparison than those from stations further away. For example, simulated atmospheric pressure at station Dauphin Island was much better than station Waveland and station Panama City Beach. The atmospheric pressure measurement at Station Pensacola is not complete because of instrument failure.

3.3.6.2 Water level and High Water Mark comparison

Hurricane Ivan is a very strong Category 3 storm that hit the northeast Gulf coast in 2004. The along shore current caused by the cyclonic wind generated a big storm surge up to 4 meters along the coast of Florida, Mississippi, and Alabaman. Continuous water levels were collected at a few NOAA stations along the Gulf coast during Hurricane Ivan. Located right next to Ivan's landfall location, large amounts of water were pushed into Pensacola Bay and Escambia Bay and causing significant storm surge. Unfortunately, the highest water level was unable to be measured at the Pensacola station because of instrument failure. At other stations, complete measurement was recorded. The time series of simulated water levels at these locations were

compared with observation (Figure 3-14). Overall, the comparisons are satisfactory. The storm surges were accurately simulated in both amplitude and phase.

Besides the water level collected from NOAA stations, the High Water Marks (HWMs) are the primary source of post hurricane high-water level data for the evaluation of storm surge models by individual site comparison. There are two kinds of high water marks, “inside high water marks”, which generally reflect the storm tide elevation without the effect of waves, and “outside high water marks”, which usually reflect the combined effect of storm tide and wave set up and run up, such as marks on buildings or other fixed structures (USACE, 2006). As a storm surge model does not include wind-generated surface gravity waves and wave run-up, only “inside high water marks” could be compared directly with model results. The US Army Corps of Engineers has collected some HWMs along the coast region during Hurricane Ivan. The comparison with simulation results are shown in Table 3-3. Some locations include not only the maximum water level but also the time when they are recorded; the others only have the maximum water level. At most stations the simulated maximum surge errors are within 10% of measured data.

3.3.6.3 Wave comparison

During Hurricane Ivan, the available measured wave is very limited. The only station is Mobile South, which is about 90 miles south of Mobile Bay. Because of instrument failure, wave parameters were recorded before peak wind occurred. By comparing available data, both significant wave height and peak wave period are accurately simulated by SWAN wave model (Figure 3-15). The maximum wave height went up to almost 20 m with 17 s peak wave period. As an important goal of this study is to determine the mechanisms that caused the I-10 Bridge collapse, the maximum wave heights and associated direction in Escambia Bay are shown in Figure 3-16 for Hurricane Ivan. Along the I-10 Bridge, the maximum wave is about 1.6 m.

3.3.6.4 Snapshot, EOHW, and inundation map

In order to capture the whole picture of the storm surge generated by Hurricane Ivan, multiple water level snapshots were shown before and after landfall every three hours (Figure 3-17). The strong wind from the Hurricane Ivan generated a strong longshore circulation, which propagated from the east coast to the west coast of the northeast Gulf of Mexico, pushing the water onshore producing storm surge at the coast. The current started from the Florida Panhandle, going through Alabama, reaching the western edge of Mississippi Delta, and Louisiana where Ivan's winds die down. The storm surge peaked at the point of landfall between Dauphin Island, AL and Pensacola, FL and generated high surge up to 4 meters. After the hurricane made landfall, the high water piled up in the bay and along the coast relaxed and receded back to open water shortly. The highest water level over the entire domain, known as EOHW, is shown in Figure 3-18. It described the overall highest surge distribution. Surge started increasing from Florida Panhandle with highest water level around 1.2 m. The surge maximized to 3-4 m near point of landfall and then slowly decreased to the west.

Hurricane Ivan caused significant flooding over the northeast Gulf coast, especially around Pensacola Bay and Escambia Bay. The inundation around the Pensacola Bay and Escambia Bay area is shown in Figure 3-19. According to simulation, a large amount of area east side of the I-10 Bridge and the barrier islands were flooded during Ivan.

3.3.7 Sensitivity Tests

Storm surge modeling is a complicated task that involves a lot of parameters. It is important to identify the roles of these parameters in storm surge simulation and how are model results to parameter variation. The parameters considered in this study include wind field, open boundary, bottom friction, atmospheric pressure, and wave effect. A detailed list of these sensitivity tests is given in Table 3-4.

Since wind is the main driving force during a storm event, it is of great importance to select the most realistic and accurate wind field for storm surge modeling. In this study, a total of 4 different wind sets are considered for the Hurricane Ivan simulation: HRD, WNA, WINDGEN and Holland analytical wind. When wind blows over land its strength is reduced by the land reduction effect. From Case 0 (base case) to Case 7, the sensitivity to wind field and the land reduction effect is determined for four selected wind sets. Case 8 uses ADCRIRC tidal constituents as a comparison to predict tide to study how model results vary with tidal open boundary. The bottom friction sensitivity is checked in Case 9 by applying a constant Manning's coefficient over the entire domain. In Case 10 and Case 11, the atmospheric pressure and wave effect are removed from the model to determine their influence on storm surge.

The base simulation uses Limited Land Exposure HRD wind, predicted tide, and ADCIRC surge along with the open boundary, special-varying bottom roughness, atmospheric pressure, and radiation stress effect from waves. The storm surge sensitivity on wind field is studied in Case 1 to Case 7 (Figure 3-20, a-f). When wind blows over land, wind strength weakens because of increased friction over land. The degree of weakening is determined by land roughness, which is related to land use, and the fetch over land. If land reduction is not considered in wind field, the model tends to over-predict water set down at station Biloxi and Waveland and over-predict storm surge at stations Dauphin Island and Pensacola. As for Panama City and Panama City Beach, the effect is minimized as wind comes from the open sea most of the time thus land reduction is no longer important. Since station Waveland is located far away from hurricane track, the relatively small wind magnitude leads to moderate surge change. When land reduction is considered, all four wind sets produce similar surge response for Hurricane Ivan except station Dauphin Island for WNA wind. This comes from two factors, first the low resolution WNA wind

does not have wind over land; secondly Dauphin Island is located very close to the hurricane center, so accurate wind field can not be obtained from limited wind over ocean before hurricane made landfall. Overall, the best simulation result is the base case simulation using Limited Land Exposure HRD wind.

When ADCIRC constituents are used along the open boundary, the highest storm surge is reduced slightly at all stations (a few cms) in Case 8 (Figure 3-21). This is simply because predicted tide is more accurate during this simulation period. If Hurricane Ivan made landfall during some other time, the predicted tide is not necessarily as good as ADCIRC constituents. In Case 9, a constant Manning's coefficient is applied in the model. Since the spatially-varying coefficient has modest variation, the constant one does not change the results much. The overall comparison is still relatively good. The atmospheric pressure effect is tested in Case 10. As the atmospheric pressure deficit decreases exponentially from the hurricane center, its effect on water level is limited to areas that are close to the hurricane eye. Therefore, station Dauphin Island and Pensacola experience bigger water level drops (approximate 20 cm) than other stations (several cms) because of their closeness to the hurricane track and the hurricane center. Case 11 implies that wave effect has a significant effect on storm surge (Figure 3-21). As big as approximately 70 cm water level drop is simulated at station Dauphin Island and Pensacola, where stronger wind and wave setup are prominent at other stations.

In order to determine what roles estuaries play in affecting the storm surge and inundation in coastal zones, the Pensacola Bay is removed from the grid system with cut off line starting from barrier islands (Figure 3-22). Then Hurricane Ivan is simulated once again with the test grid. Output stations for storm surge are selected both along coast and in open water within 50 km radius from Pensacola Inlet. The time series of storm surge at all stations are compared with

those from simulations with Pensacola Bay (Figure 3-23). Station 3, which locates right at the Pensacola Inlet, is the only one that shows obvious water level difference. The simulated storm surge for the grid without Pensacola is about 5 cm higher than the simulations with Pensacola Bay. This implies that the existence of estuaries do not have significant effect on the storm surge and inundation in continental shelf coastal zones. While within coastal bay or lagoon area, the effect from estuarine is much bigger. The shallow water induces larger surge and delayed the peak of the surge. For example, the maximum simulated storm surge at the north rim of Pensacola Bay is about 4.8 m during Hurricane Ivan, which is about 1.7 m higher than simulated surge at mouth of Pensacola Bay with 1.5 hour delay (Figure 3-18). As the storm surge advanced within the bay, water level gradually increased and maximized at the north end. The abnormally elevated water caused extensive flooding at the low-land areas along the bay coast zone. The inundation within Pensacola Bay is even worse than coastal barrier islands (Figure 3-19).

3.3.8 Hurricane Ivan 3D simulation

The above simulations have shown that the two dimensional CH3D-SSMS is a computationally efficient model which produces reasonable good water levels during the Hurricane Ivan. This is important for both storm surge forecast and hindcast when simulation time is a key factor and many calibration simulations have to be conducted. However, in a 2D model, as the vertical flow structure can not be obtained while the bottom friction, nonlinear, diffusion and Coriolis terms have to be calculated from vertical averaged velocity. In a 3D model, all these terms can be more accurately simulated and vertical flow structure can be obtained.

In CH3D-SSMS, there are three major differences between 3D mode and 2D mode for storm surge simulation. First, the equilibrium closure turbulence model is applied in 3D to calculate eddy viscosity, which is then used to solve for velocities at each vertical layer.

Secondly, a quadratic bottom friction formulation based on log law is used in 3D mode, which is the function of bottom flow velocity and bed roughness. This is superior to the Chezy formulation in 2D mode using vertically averaged velocity. The third difference is that the nonlinear, diffusion and Coriolis terms in 3D mode are calculated based on velocities at each vertical layer, which is more accurate than the 2D mode that uses the vertical averaged velocities.

As storm surge becomes more significant in shallow coastal waters, a modest number of vertical layers are needed. In this study, a total of four layers are used for Hurricane Ivan simulation. At bottom, a constant roughness of 0.4 cm is considered for bottom friction calculation. When coupling with local wave model SWAN, the wave-current induced bottom friction is included. In CH3D-SSMS, two methodologies for wave enhanced bottom stress are implemented. The first one applies the Grant and Madsen (1979) theory described in a simplified form by Signell et al. (1990). The second methodology makes use of a one-dimensional wave-current bottom boundary layer model (Sheng and Villaret, 1989) to generate a lookup table for wave enhanced bottom stress calculation. The detailed formulations are described by Alymov (2005). All the other model coefficients and the grid system are the same as those used in previous 2D simulation. The time series of water levels from the first set of 3D simulations are shown in Figure 3-24. Overall, the simulated storm surges from 3D models are similar to those from 2D models. There is no obvious difference of maximum surge between two models for stations located further away from hurricane center, such as Panama City and Panama City Beach. While for station Dauphin Island and station Pensacola, which are close to hurricane track, the 3D model simulated slightly higher surge than 2D model. The wave enhanced bottom friction has little effect on storm surge simulation for either method. In general, the maximum

surge is reduced by several centimeters when wave-current interaction effect on friction is considered. Because of higher simulated storm surge, the inundation area near Pensacola Bay is extended slightly (Figure 3-25). Using 3D velocities should have limited effect on coastal inundation.

One big advantage of 3D model is its ability to resolve vertical flow structures by including the turbulence model. During hurricane events, the strong wind-induced shear stresses on water surface may generate quite different flow structures in the vertical direction. In addition, it is also of interest to explore the flow development pattern for inundated land during flooding & drying process. Two stations are selected for velocity output. Station 1 is located at the middle of I-10 Bridge over Escambia Bay to represent a permanent water cell, while station 2 is located on the bank of east Pensacola Bay to represent a land cell (Figure 3-26). The time series of velocities at all layers for station 1 and station 2 are shown in Figure 3-27 and Figure 3-28, respectively. As hurricane approached, the current at water cell station 1 began to show noticeably stratified structure. Between Julian days 260.4 and 260.45, opposite flows were observed at surface and bottom layers. This is the ebb tide period when the high water in Escambia Bay began to retreat while the wind at surface kept pushing water into the bay. Because of lack of measured current, this phenomenon needs further validation. For land cell station 2, the original zero velocity jumped to almost 1 m/s when water level increased and flooded the land. Then the cell just behaved like a normal water cell until surge receded and became a dry cell again. The strong “west-to-east” flow and “south-to-north” at the I-10 Bridge represented by colored magnitude contour plot in Figure 3-29 shown more clear flow stratification during the peak of Hurricane Ivan.

Even though 3D model has better estimation of bottom friction and vertical turbulence, its expensive simulation time prohibits it from extensive application. Because the mode splitting technique used in 3D mode, the bottom friction has to be calculated in explicit mode, which requires significantly reduced time step to maintain numerical stability. In Hurricane Ivan simulation, as small as 10 second is used in 3D model compared to 60 second in 2D model. In addition, solving for velocities in each vertical layers also need addition computing time. Therefore, the selection of 2D or 3D simulation mode is dependent on the interests of the user. When accuracy of the storm surge estimation is the primary concern and there is enough computer resource, the 3D model is the choice. On the contrary, when both simulation time and accuracy are equally important, the 2D model should be used as it can produce reasonably good water level simulations within a short period of time. 2D model have been widely used for storm surge forecast simulation for its efficiency and accuracy.

3.3.9 Risk Analysis Tests

Hurricane Ivan caused significant damage by wind, waves, and flooding along the coasts of Florida, Mississippi, and Alabama. Successful field and model studies would help to recognize how storm surges evolve and to enable analysis of flooding risk potentials. However, for a particular coastal domain, one single storm is never enough to identify the vulnerability to storm surge because of its uniqueness. Storm surge is sensitive to hurricane intensity, direction, size (maximum of wind radius), speed of approach, and location of landfall. In this study, twelve hurricane scenarios are designed to assess the extensive water level and flooding response along northeast coast of Gulf of Mexico by varying each of those parameters (Table 3-5). For all the tests, wind and atmospheric pressure fields are driven by the analytical Holland model. At the open boundary, water level is determined by ADCIRC regional surge model, which is also

driven by the analytical Holland wind and tidal constituents. The effect of waves is not considered for risk analysis tests.

Base case, which uses direction, track, and intensity of Ivan at landfall, is selected as reference and compared with other scenarios. The other eleven risk analysis simulations are separated into five groups, each investigating one hurricane characteristic corresponding to reference base. Case 1 to 3 are designed to test hurricane intensity by downgrading to Category two and upgrading to Category four and five scales. Cases 4 and 5 refer to changing hurricane translate direction by ±45 degrees from original direction. The size of hurricane is adjusted by ±50% in Case 6 and 7 and the speed of approach is changed by one time slower/faster in Case 8 and 9. In Case 10 and 11, landfall location is shifted to west and east by 50 kms. For these scenarios, the storm specifications are held constant and the growth and weakness of the storm are not considered in the open water. The illustration of hurricane tracks for risk analysis is shown in Figure 3-30. Cases 1, 2, 3, 6, 7, 8 and 9 share the same track with the base case and each of the other cases has its own track.

The first group of risk analysis is designed to test storm surge response to hurricane intensity. Keeping other parameters unchanged, the strength of the test hurricane is set to Category 2, 3 (base case), 4, and 5, respectively. The time series at four stations are selected to compare water level along the west coast to the east coast of northeast GOM, which are Waveland, Dauphin Island, Pensacola, and Panama City Beach. As shown in Figure 3-31, a similar pattern of surge development was observed at all stations. More intensive wind results in higher water level as the hurricane translate closer to coastline. Located about 30 miles east of landfall location, Pensacola experiences the maximum wind and storm surge. Highest water level almost tripled when hurricane intensity increases from Category 2 to Category 5, jumping from

1.5 m to 3.9 m. With the additional effect from waves, the maximum surge would be even higher, especially in the upper Escambia Bay. If this should happen in reality, the damage from wind, wave, and flooding would be catastrophic. Many houses will be blown down, large area will be under water and many coastal structures, including highway bridges, may be totally destroyed. To describe the flooding problem clearly, the inundation around Pensacola is made for the Category 5 hurricane case (Figure 3-36). In this worst case scenario, most of the barrier islands outside of Pensacola Bay were submerged pushing more water into the bay. The high surge caused significant flooding to the east of Escambia Bay and Blackwater Bay. Considering the additional effect from wave, the flooding potential will be even greater.

The effect of the hurricane approach direction is tested by varying ±45 degrees from original track as Case 4 and Case 5. The effect is quite obvious. When the hurricane track is turned 45 degrees clockwise, wind is blowing from inland to offshore for west coastal domain before the hurricane makes landfall (Figure 3-32). As a result, only a small storm surge is generated along the coast. After landfall, the wind continuously blows offshore on the west of the track and pushes water away causing set down at both Waveland and Dauphin Island. On the east of the hurricane track, the stronger wind swifts from east to southeast when the hurricane moves close to landfall, pushing water onshore and generating significant storm surge over the Florida Panhandle. The highest water level at Panama City Beach is much larger than the base case simulation. Because of its closeness to hurricane eye, the wind field at station Pensacola does not change much, neither does the highest water level. For Case 5 when the hurricane direction of approach is turned 45 degrees counterclockwise, the wind field is just the opposite. The long-term continuous southeastly offshore wind keeps pushing water into the bays between Louisianan and Alabama causing high storm surge and serious flooding. The storm water goes

up to 2.5 m at station Waveland. The water level is comparable to the base simulation at Dauphin Island and gradually decreased from Pensacola to Panama City Beach.

The storm surge sensitivity to hurricane size is studied in group 3 by doubling maximum wind radius (Case 6) and reducing maximum wind radius to half size (Case 7). Similar to test of hurricane intensity, higher surge is generated for larger scale storm and lower surge for smaller scale storm at selected stations (Figure 3-33). This qualitatively agrees with the distribution of wind field. By extending maximum wind radius, the average magnitude of wind is increased while maximum wind is kept the same, resulting in an overall rising of high water along the northeast Gulf coast. The increased wind magnitude is bigger for domains far away from Maximum Wind Radius (MWR) and those near MWR comparing to the base case, as a result the higher surges are predicted at stations further away from the hurricane track, such as Waveland and Panama City Beach (about 50 cm). Station Dauphin Island is located within the range of MWR so the change of wind field is very small leaving almost no change of the highest water level compared to the base case. Similar analysis applies to test Case 7 for the half-sized hurricane. The reduced size weakens the wind field extensively over the whole domain. The highest surges at all stations are much lower than the base case. Even though it is still a Category 3 hurricane, the compact size limits its influence of wind to a substantially reduced area. The intensity of the hurricane is mitigated by its size.

The effect of the hurricane's speed of approach is studied in group 4 (Case 8 and Case 9). The one-time slower speed allows a longer time to redistribute water mass. Due to the slow moving speed, the wind change is small. A relatively more static balance is obtained between wind-induced shear stress and water level slope. At station Waveland, the wind magnitude is relatively greater than the base case at a particular time before landfall and the wind direction is

favorable to storm surge, thus water level rises earlier with bigger height. At other stations, water levels also rise earlier, but the maximum water level is comparable to what in the base case (Figure 3-34). When the hurricane speed of approach is increased by two times in Case 9, the faster moving hurricane does not fully respond to wind stress. The water level is more controlled by local wind. Similar high water levels are generated at Dauphin Island and Pensacola, but with much shorter developing period. At Waveland, the highest surge is much lower than base case as there is not enough time for water to be transported to the station.

Storm surge is also sensitive to point of landfall. In Case 10, the landfall location is shifted by 50 km to the west from the base case, redistributing hurricane strength to the west with the same hurricane structure. The shift results in higher wind on the west and lower wind on the east, generating higher surge at Waveland and Dauphin Island and lower surge at Pensacola and Panama City Beach, respectively (Figure 3-35). Exactly the opposite results are obtained for case 11 when the landfall location is shifted by 50 km to the east. For both cases, the change of surge magnitude is significant.

3.4 Wave Loadings On Highway Bridges

During a storm event, wind waves are a big threat to coastal structures such as jetties, pipelines, piers, and coastal highway bridges. They may cause severe property damage, interruption of transportation, and seriously deteriorate the economy. As the waves impact a structure, the flow properties become more complex and cannot be completely solved by principle of fluid mechanics. Field measurement of flow kinematics and forces are very difficult to obtain. Researchers have to rely on both theoretical and laboratory analysis to develop simplified methods to calculate wave force for engineering applications. Wang (1970) performed physical model tests to investigate wave loads on horizontal decks subject to wave attacks. A simple formula was proposed to estimate uplift pressure on horizontal decks. He found out that

the slowly-varying pressure was about one to two times that of the hydrostatic pressure at the plate bottom. Similar relationships were also obtained by French (1970) on an experimental wave uplift study on flat horizontal platforms, Overbeek and Klabeers (2001) on Jetty deck design, and McConnell, et al. (2004) on hydraulic loading on piers and jetties. Douglass, et al. (2006) extended the formulation by considering highway bridge deck characteristics and applied wave loads calculation on the U.S. 90 Bridge across Biloxi Bay during Hurricane Katrina. The recommended method only considers maximum wave height and does not include wave period effect. The method may not be appropriate if waves do not fully impact the bridge decks. A series of laboratory tests on highway bridges decks were made by Denson (1978, 1980) to measure wave loads. Dimensionless charts were provided to calculate wave force from highway bridge decks. However, as pointed out by Douglass, et al. (2006), the unrealistic wave parameters and poor lab conditions made the results unreliable. Cuoto et al. (2003, 2007) proposed new guidelines for dynamic wave loads on jetties and platforms by analyzing impulsive wave loads. The more complex quasi-static force is obtained from best regression fit of data based on basic wave force. Because of different scales and shapes, these formulas may not be appropriate for bridge decks. Based on hydrostatic pressure assumption, Douglass et al. (2006) proposed a simplified formula to estimate wave load based on wave height. When waves are not able to fully attack the bridge deck, the wave force could be overestimated. In studying wave forces on offshore platforms, Kaplan et al. (1995) and Bea et al. (1999) proposed the method of total wave forces calculation by dividing into vertical buoyancy, velocity dependent drag and lift, acceleration dependent inertial force, and dynamic slamming force. The slamming force is the momentum transferred from water to structure when wave crest encounters the bridge deck. Its magnitude depends on the characteristic of the deck. The review discussed above

is summarized in Table 3-6. In this study, the wave load model by Bea et al. (1999) is adopted for the I-10 Bridge wave load calculation during Hurricane Ivan for the following reasons. First, both static and dynamic loads are considered in the individual forms. Second, the total force is derived from the flow field based on wave conditions, thus it can be applied to various coastal structures including bridge decks. The empirical coefficients are directly applied in this study without modification.

According to Bea et al. (1999), the total force imposed on the bridge deck can be formulated as slamming force and inundation force. As waves inundate the deck, buoyancy, drag, lift, and inertial force are developed together with slamming force. The common method is to split the forces in inline (horizontal) and vertical forces then calculate them separately. Following Kerenyi (2005), the detailed formulations of wave force on bridge decks are discussed next. A diagram of wave force on bridge decks is shown in Figure 3-37.

3.4.1 In-line Forces

The forces in line with oscillating flow are generally derived from the Morison (1950) approach, which is the sum of inertial force, drag force and slamming force.

The inertial force acts in phase with the water particle accelerations:

$$F_{I-X} = \rho V a_x + \alpha \rho \pi \left(\frac{b_h}{2}\right)^2 b_w a_x \tag{3-1}$$

where ρ is density of water
V is volume of the bridge deck.
a_x is horizontal particle acceleration
$\alpha = 2.23$ for $b_h/b_l<0.1$ (Kerenyi, 2005)
b_h is depth or height of the bridge deck
b_w is width of the bridge deck
b_l is length of the bridge deck

The drag force on a stationary structure acts in phase with the water particle velocity:

$$F_{D-X} = 0.5 C_D \rho b_w b_h u^2 \tag{3-2}$$

where C_D is drag coefficient $C_D = 2.0$ (Kerenyi, 2005) and u is horizontal particle velocity.

As the wave crest encounters the bridge deck, there is a transfer of momentum to the structure that is reflected as the initial slamming force:

$$F_{S-X} = 0.5 C_S \rho b_w b_h u^2 \tag{3-3}$$

where C_S is slamming coefficient 1.5π, which varies from $C_S = \pi$ to 2π.

When the bridge deck is tied down, a dynamic loading factor should be considered to reflect the deck response characteristics. In summary, the total in-line force can be written as:

$$F_{TOT-X} = F_{I-X} + F_{D-X} + F_{S-X} \tag{3-4}$$

3.4.2 Vertical Forces

The vertical forces on the bridge deck include inertial force, which act in phase with the vertical water particle accelerations, drag force, buoyancy and slamming force, which act in phase with the vertical water velocity. The formulations for each force are listed next.

The vertical inertial force on a stationary structure is:

$$F_{I-Z} = \rho V a_Z + \alpha \rho \pi \left(\frac{b_w}{2} \right)^2 b_1 a_z \tag{3-5}$$

where a_z is vertical water particle acceleration

$\alpha = 1.0$ for $b_h/b_w < 0.1$ (Kerenyi, 2005)

The vertical drag force component on a stationary structure is:

$$F_{L-X} = 0.5 C_L \rho b_w b_l w^2 \tag{3-6}$$

where C_L is lift coefficient $C_L = 2.0$ (Kerenyi, 2005)
w is vertical water particle velocity

The vertical slamming force is also a function of vertical water particle velocity:

$$F_{S-Z} = 0.5 C_S \rho b_w b_l w^2 \tag{3-7}$$

where C_S is slamming coefficient $C_S = 1.5\,\pi$, which varies from $C_S = \pi$ to 2π.

The buoyancy force can be formulated as:

$$F_B = \rho g V \tag{3-8}$$

Adding each component together leads to the total vertical force on bridge deck:

$$F_{TOT-Z} = F_{I-Z} + F_{L-Z} + F_{S-Z} + F_B \tag{3-9}$$

The above total wave loading calculation does not include phase difference. However, as the only out of phase force, inertial force, is normally small compared to other components, the method presented here is only slightly conservative.

3.4.2 Wave Loading On I-10 Bridge During Hurricane Ivan

During Hurricane Ivan, the I-10 Bridge over Escambia Bay was significantly damaged. On both east and west bounds of the bridge, many bridge spans were lifted and pushed into water by big storm waves (Figure 3-38 and Figure 3-39) (OEA, 2005). The middle bound of the bridge survived because the surge was not high enough to reach the elevated bridge deck. As for the mechanism, the storm surge raised the water level to an elevation that allowed individual waves to hit the bridge spans. The spans were progressively "bumped" off the pile caps by larger waves during the peak of the storm. Inspection indicates that the surge and wave forces were just barely sufficient to damage the spans (Douglass et al., 2006). The movement and damage was more severe on the southern lanes. This was likely because the high surge/wave event was relatively short and the southern lanes provided breakwater sheltering effect before the bridge decks were pushed into water. After the storm, debits were observed on some of the remaining bridge decks, indicating that the highest water reached the bridge surface about 16 feet above still water level.

The I-10 Bridge deck dimensions and wave parameters during Hurricane Ivan are summarized in Table 3-7 (FDOT, 1998). The wave height $H_{1\%}$ is used in wave loading calculation, which approximately corresponds to the maximum wave height during the several

hours high surge period. The length and width of the bridge deck is about 18 m and 10.5 m, respectively. The estimation of the deck's natural frequency is about 0.2 s (Narendra, 1998), which is far away from the peak wave period. As a result, the dynamic resonance effect is not considered in this study. The span weight is about 105 tons and a reasonable estimation of the resistance of the bolted connections is about 90 to 180 tons. Thus, a total of 195 to 285 tons force is needed to overcome the bridge weight and connection and push it into water. Based on simulated surge and waves, the wave force on the I-10 Bridge deck is calculated following previous wave force discussions (Table 3-8). The maximum total vertical force is 334 tons, which is slightly larger than the threshold limit to break the connection force and drive the bridge deck into the water. Considering the uncertainty in surge/wave estimation and coefficients used in wave force calculation, the total force may vary around 20%. Without the dynamic slamming force, the maximum wave force in this study is about 160 tons, which is similar to the estimation of static loading of 120 tons by Douglass et al. (2006). Sensitivity tests were made by reducing simulated surge 0.3 m and 0.6 m to determine how wave forces react (Table 3-8). It is found that slightly lower surges may significantly reduce total wave force as the mean water level is not high enough to allow wave fully attack bridge deck. A reduction of 0.6 m of the high surge would allow only limited wave force acting on the bridge and keep the bridge safe.

3.4.2 Wave Loading For Risk Analysis Simulations

Based on the simulated surge from above risk analysis, several bridges are selected to determine the vulnerability of coastal Highway and bridges to strong storms around Florida panhandle. These bridges include I-10 Bridge over Escambia Bay, I-10 Bridge over Blackwater Bay, I-10 Bridge over north Mobile Bay, U.S. 98 over Pensacola Bay, U.S. 90 over Biloxi Bay and SR281 over Pensacola Bay (Figure 3-40). As there are no detailed bridge dimensions in this study, similar bridge characteristics to I-10 Bridge are assumed for this study. The analysis on I-

10 Bridge over Escambia Bay during Hurricane Ivan indicates that wave force is very sensitive to surge level. Only when surge is high enough that waves can attack bridge deck with full capacity. Thus the surge level is used here as the degree of bridge vulnerability. The wave conditions are assumed similar for similar storm surge. As bridge deck is normally 3.5 m to 4 m above mean water level, surge of 3 m and above is selected as the threshold for worst scenario (Degree 3), or red alarm, considering the uncertainty of wind in simulation and wave effect not being included. For surge between 2 m to 3 m, the possibility of strong wave attack is significantly reduced but it still possesses moderate threat, which is considered as orange alarm or Degree 2. When surge is below 2m, the threat from wave can be neglected and the bridge should be safe (green alarm or Degree 1). The highest surge and associated risk degrees for all above risk analysis scenarios are summarized in Table 3-9. In general, I-10 Bridge over Escambia Bay and Blackwater Bay are most vulnerable to storms like Ivan, 4 and 3 out 12 total cases the surges reach red alarm. This is consistent with their geophysical locations characteristics. Being close to north end of the bay is favorable to large surge. The storm surges at bridges of US 98 and SR281 over Pensacola Bay are slightly lower comparing to north Escambia Bay, but 2 out of 12 cases they are high enough to allow wave damage the bridge deck when storm is strong. The I-10 Bridge over north Mobile Bay is safe unless for one case when the Ivan track is shifted 50 kms to west, in which the strong southeast wind push large amount of water into Mobile Bay and caused significant storm surge at north end of the bay. For all the 12 cases considered, no red alarm is issued to the I-10 Bridge over Choctawhatchee Bay in Florida and US90 Bridge over Biloxi Bay, Alabama. Because the assumption of similar bridge characteristics and similar wave conditions for similar storm surge, the above study should be considered rather as qualitatively analysis instead of quantitative conclusions.

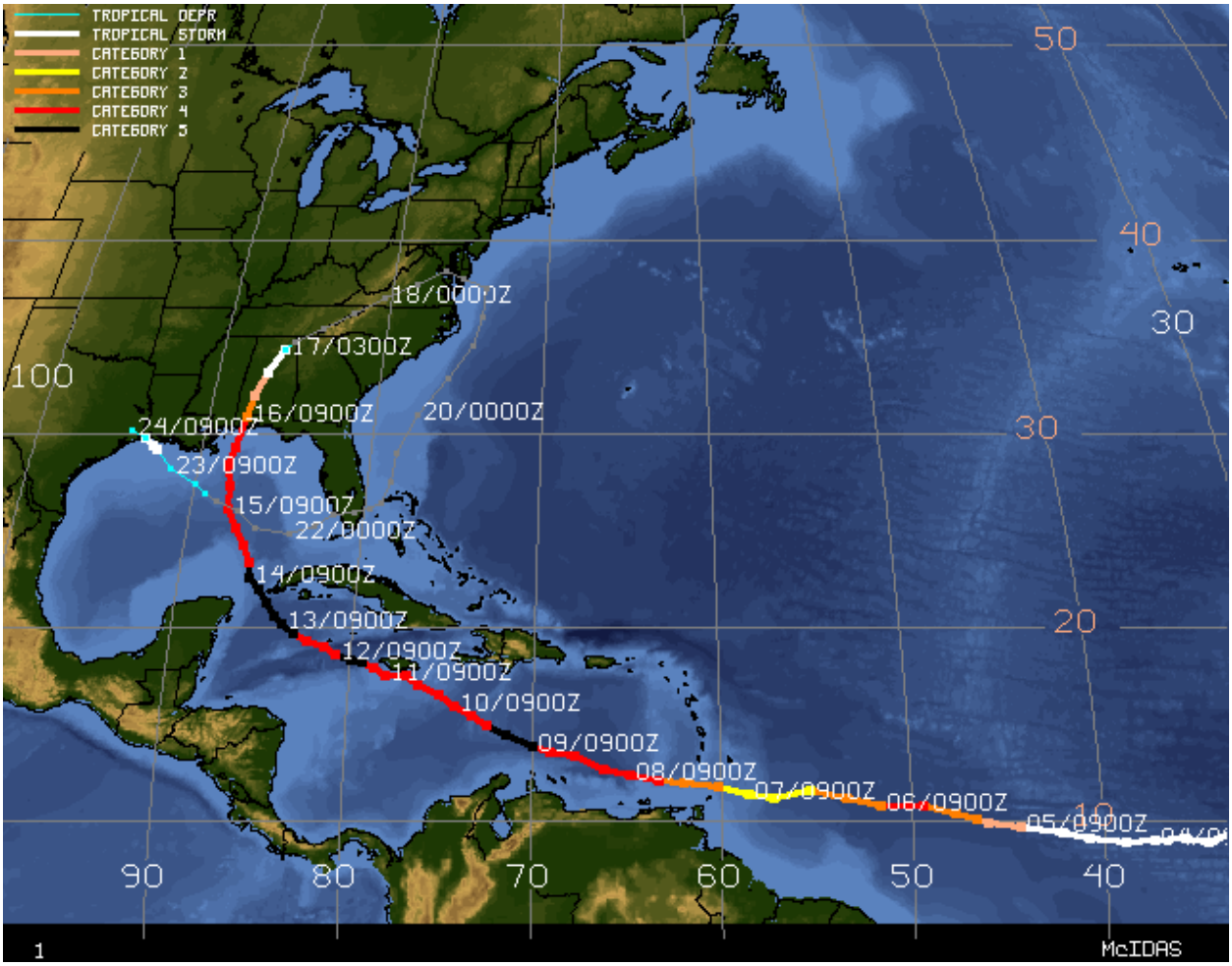

Figure 3-1. Hurricane Ivan Track

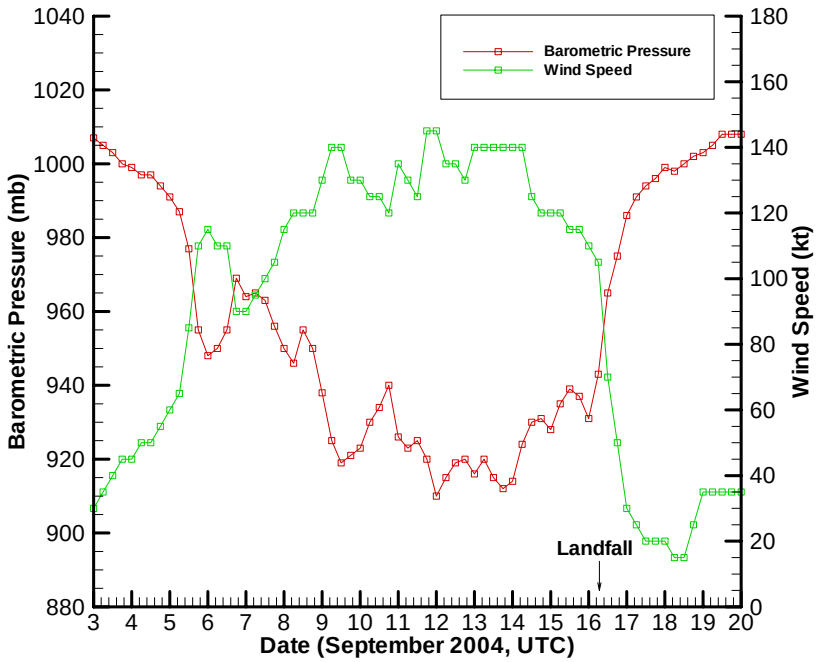

Figure 3-2. The best track central barometric pressure and wind speed history for Hurricane Ivan.

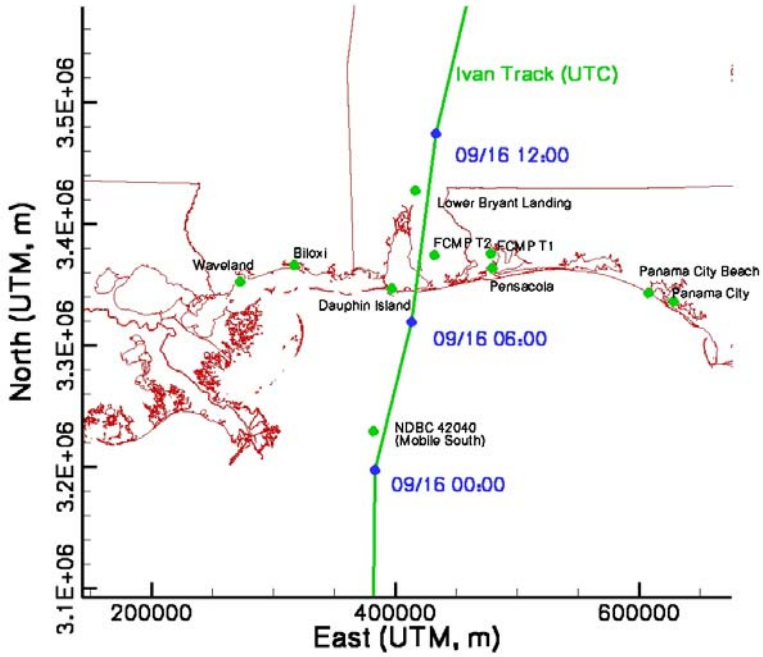

Figure 3-3. The NOAA Hurricane Ivan best track and locations of data collection stations.

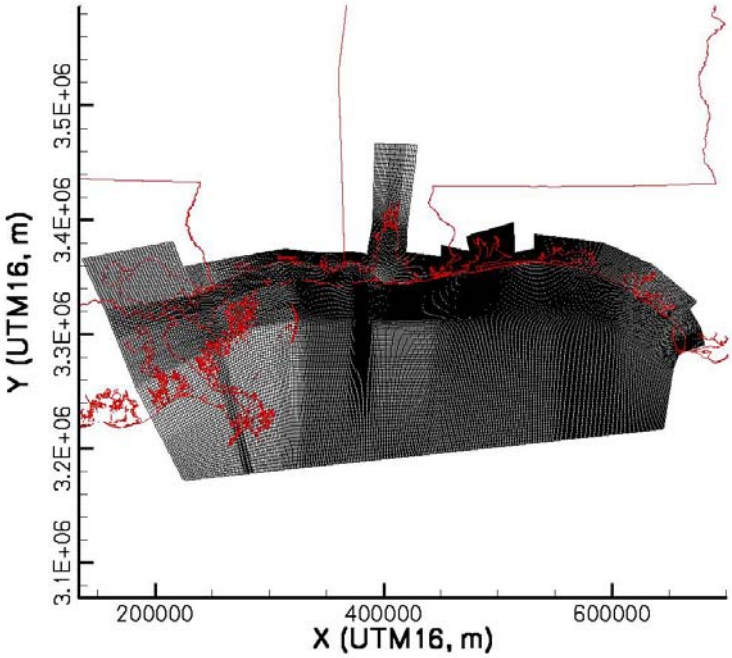

Figure 3-4. The grid system for Hurricane Ivan.

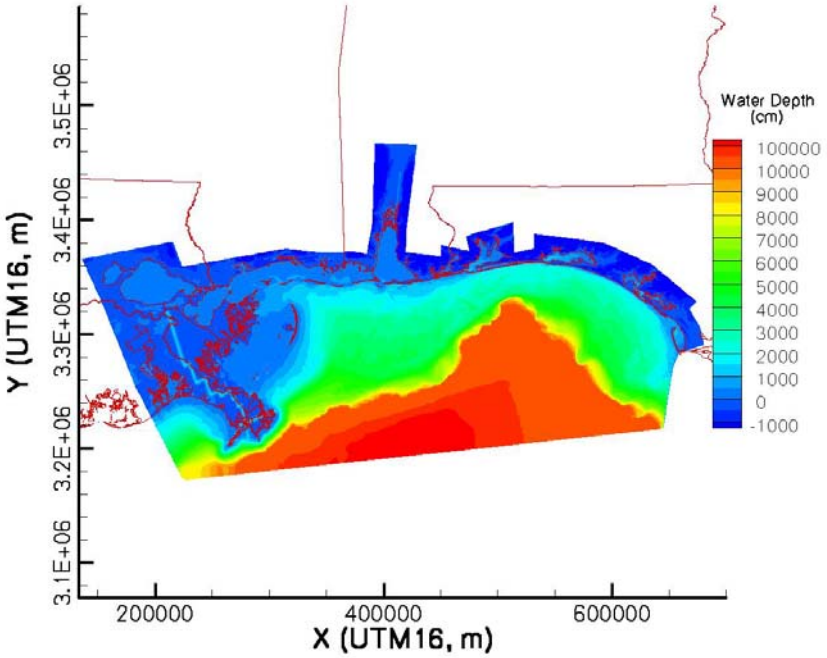

Figure 3-5. The bathymetry and topography in grid system for Hurricane Ivan.

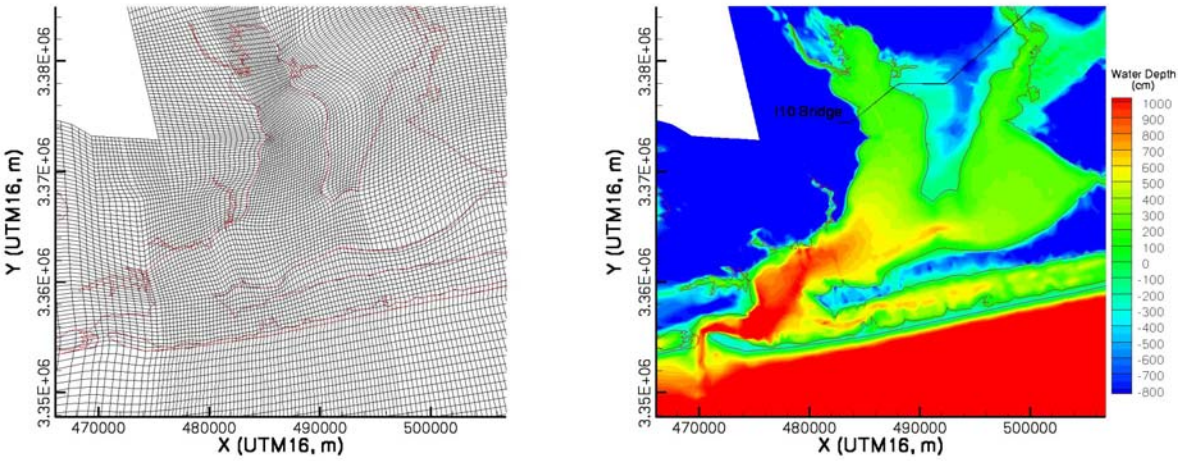

Figure 3-6. The grid and bathymetry and topography in Escambia Bay, Florida for Hurricane Ivan.

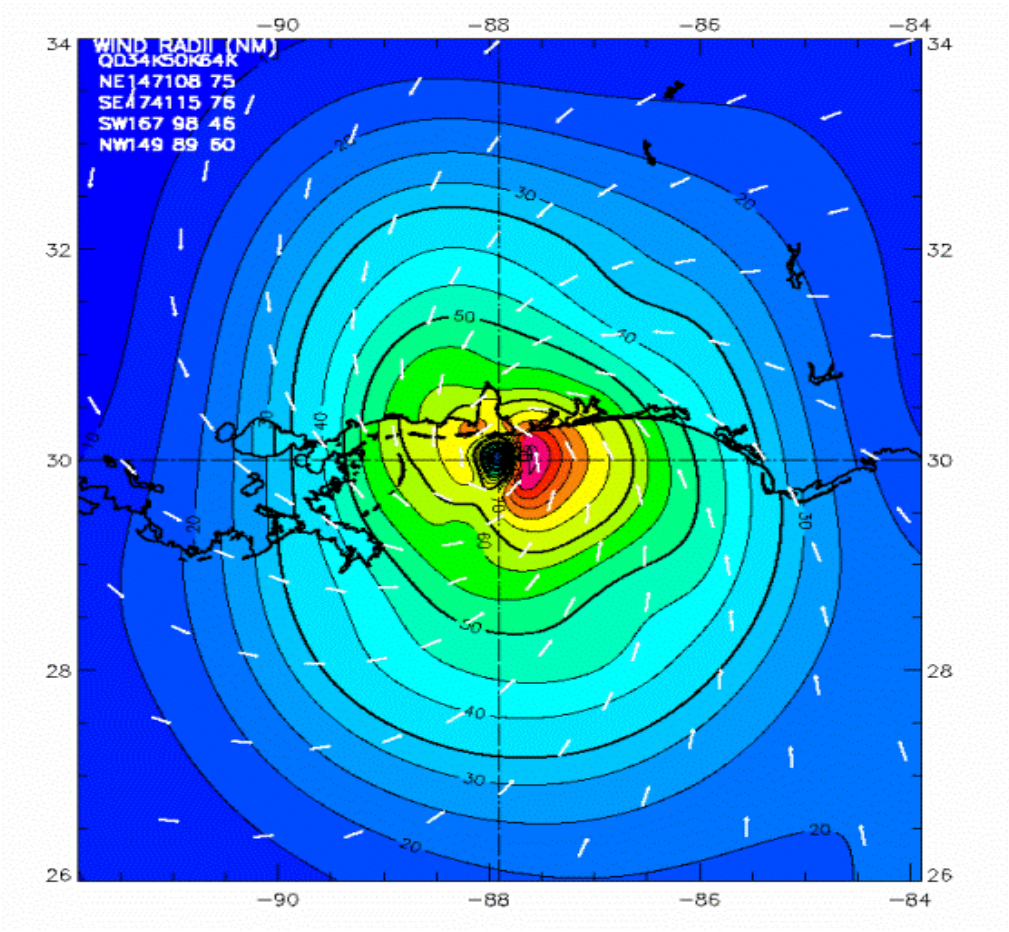

Figure 3-7. HRD wind snapshot for Hurricane Ivan at 0600 UTC 16 September, 2004

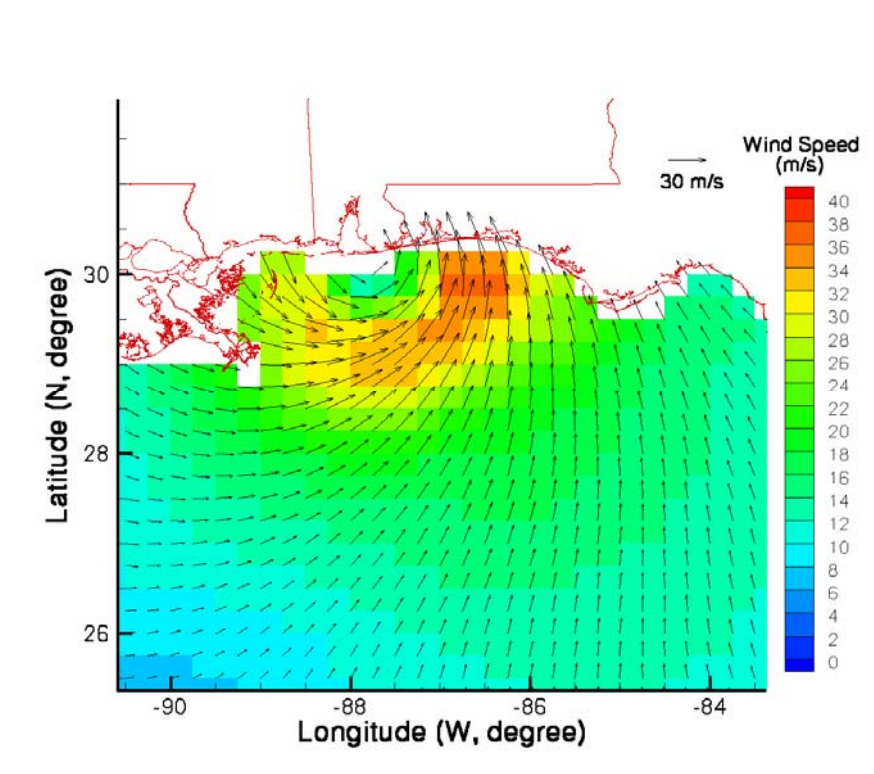

Figure 3-8. WNA wind snapshot for Hurricane Ivan at 0600 UTC 16 September, 2004.

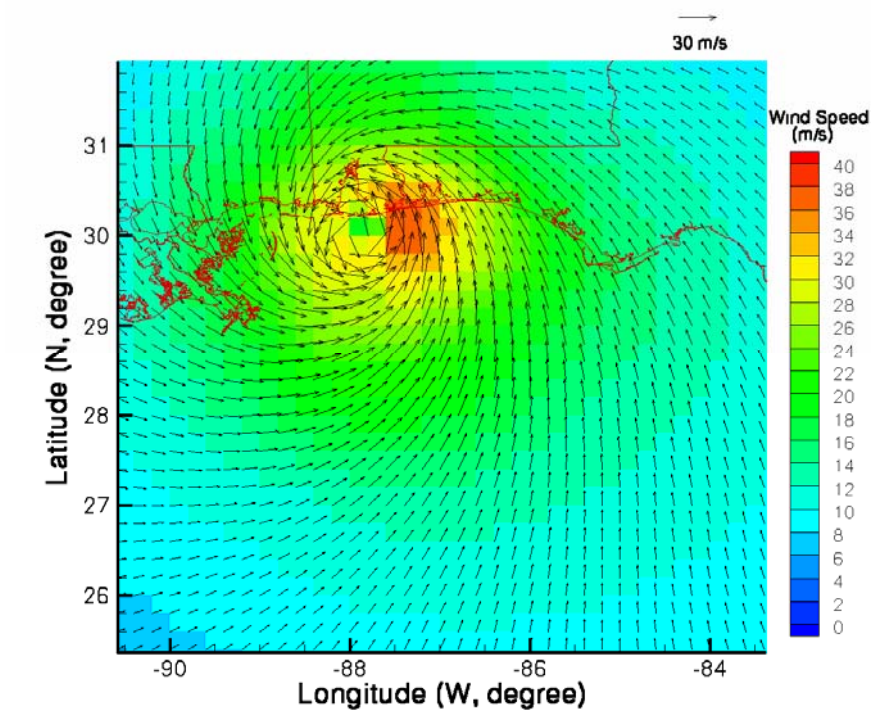

Figure 3-9. WINDGEN wind snapshot for Hurricane Ivan at 0600 UTC 16 September, 2004

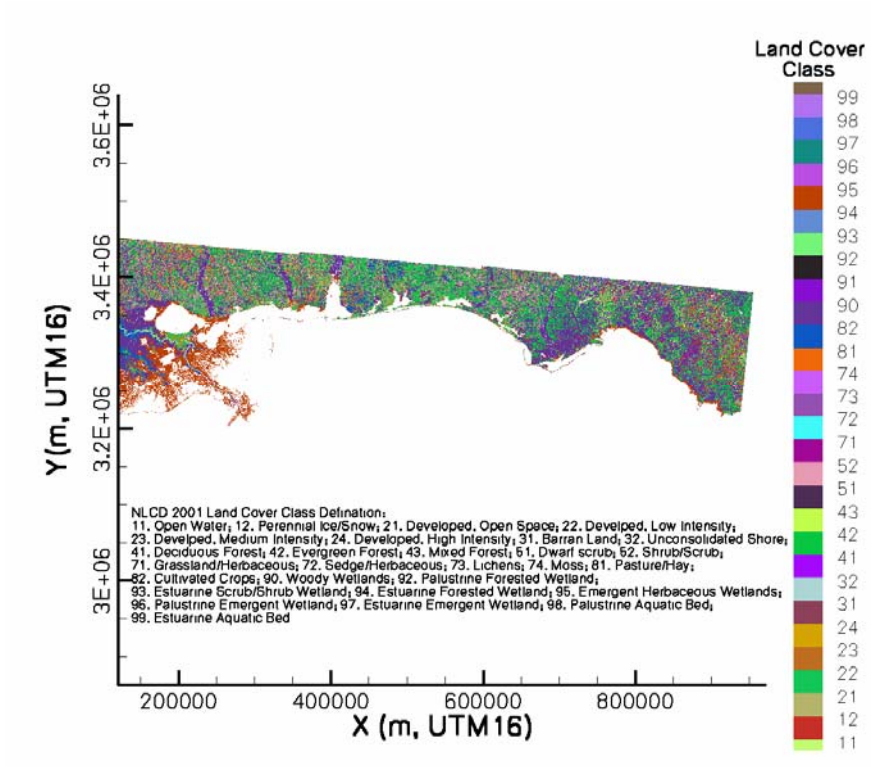

Figure 3-10. Land Cover over south Louisiana, Mississippi, Alabama and Northwest Florida.

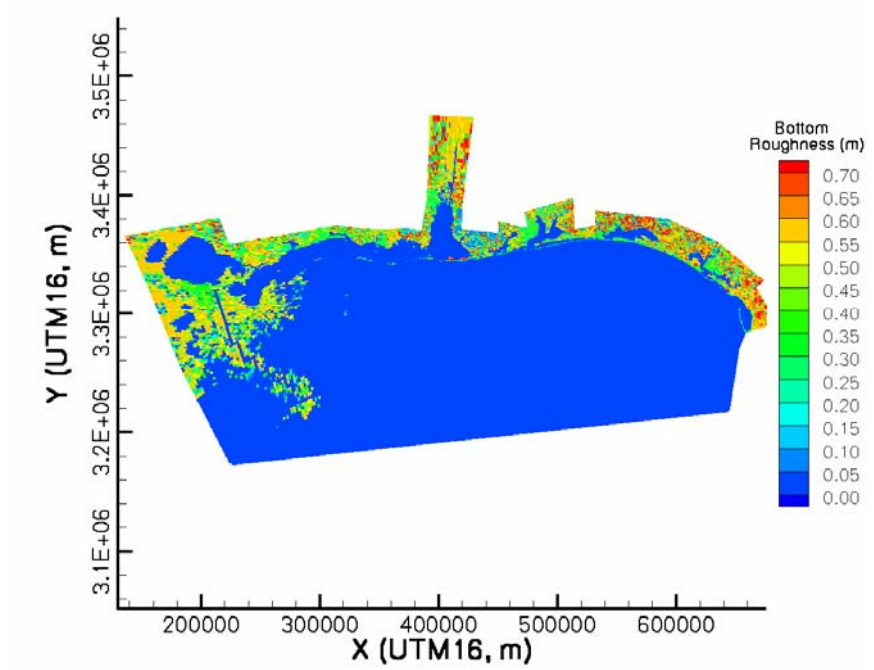

Figure 3-11. Bottom roughness map of water and land for Hurricane Ivan.

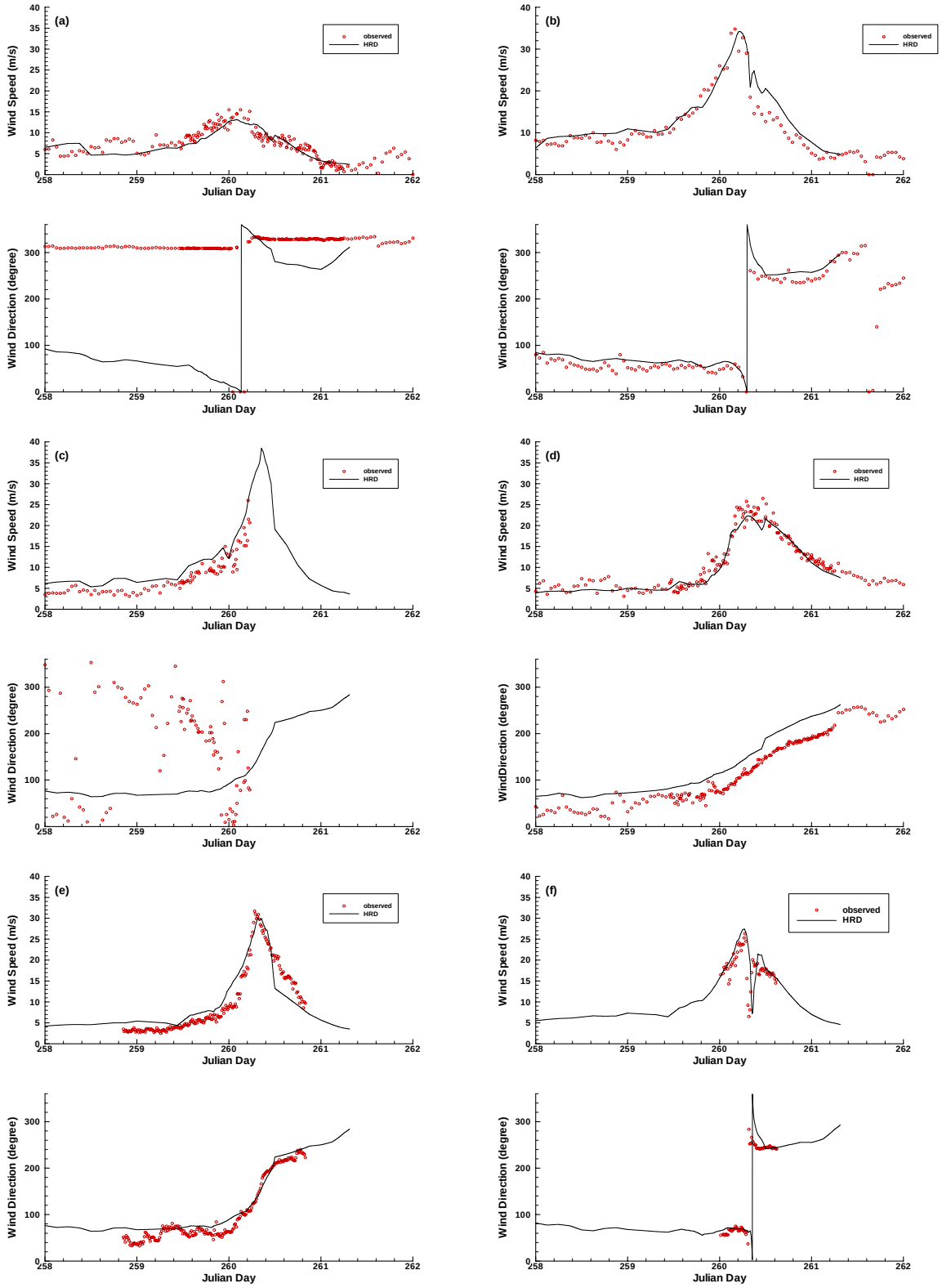

Figure 3-12. Wind comparison for Hurricane Ivan at (a). Waveland; (b). Dauphin Island; (c). Pensacola; (d). Panama City Beach; (e). FCMP Tower 1; (f). FCMP Tower 2.

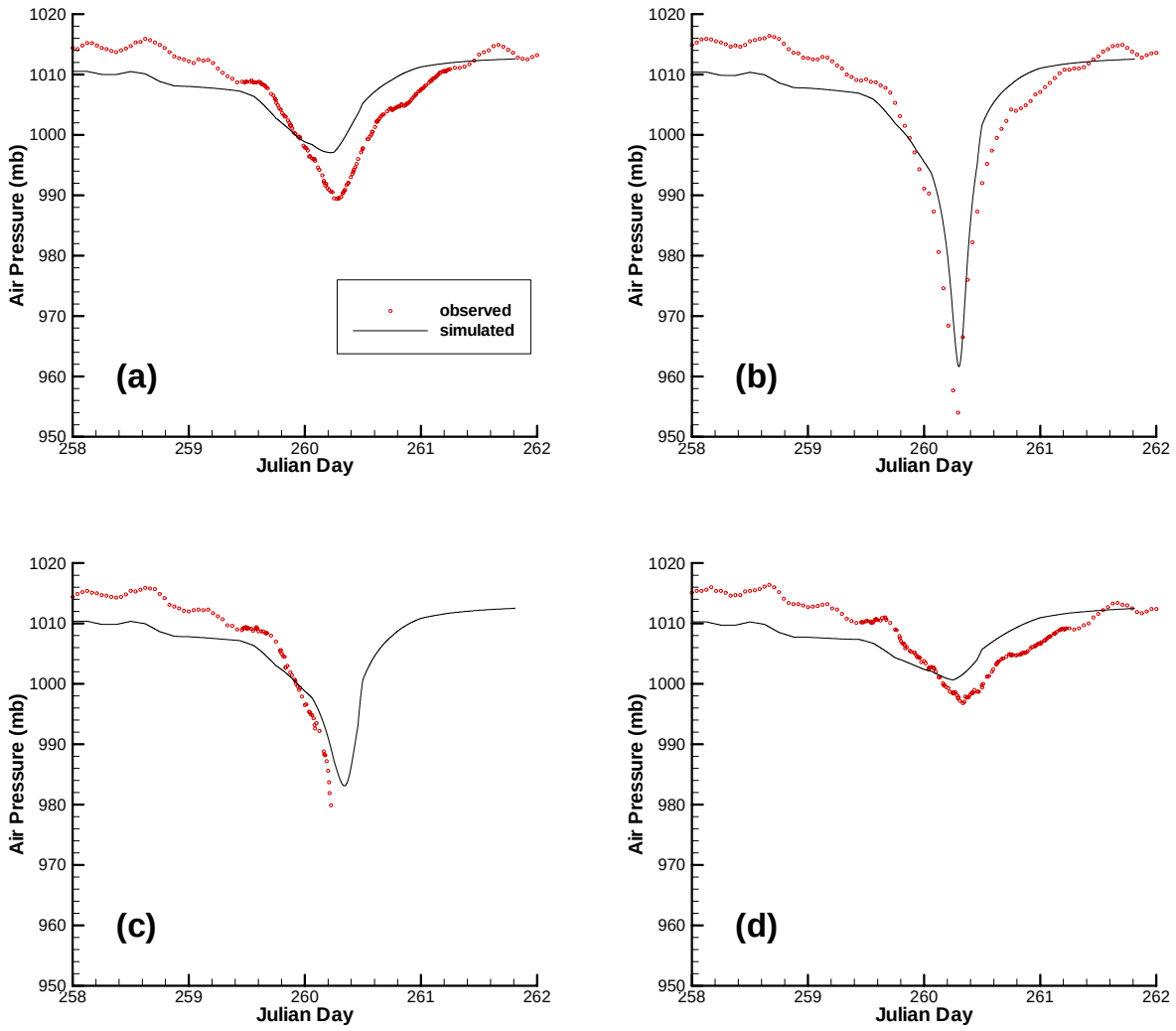

Figure 3-13. Atmospheric pressure comparison for Hurricane Ivan at (a). Waveland; (b). Dauphin Island; (c). Pensacola; (d). Panama City Beach.

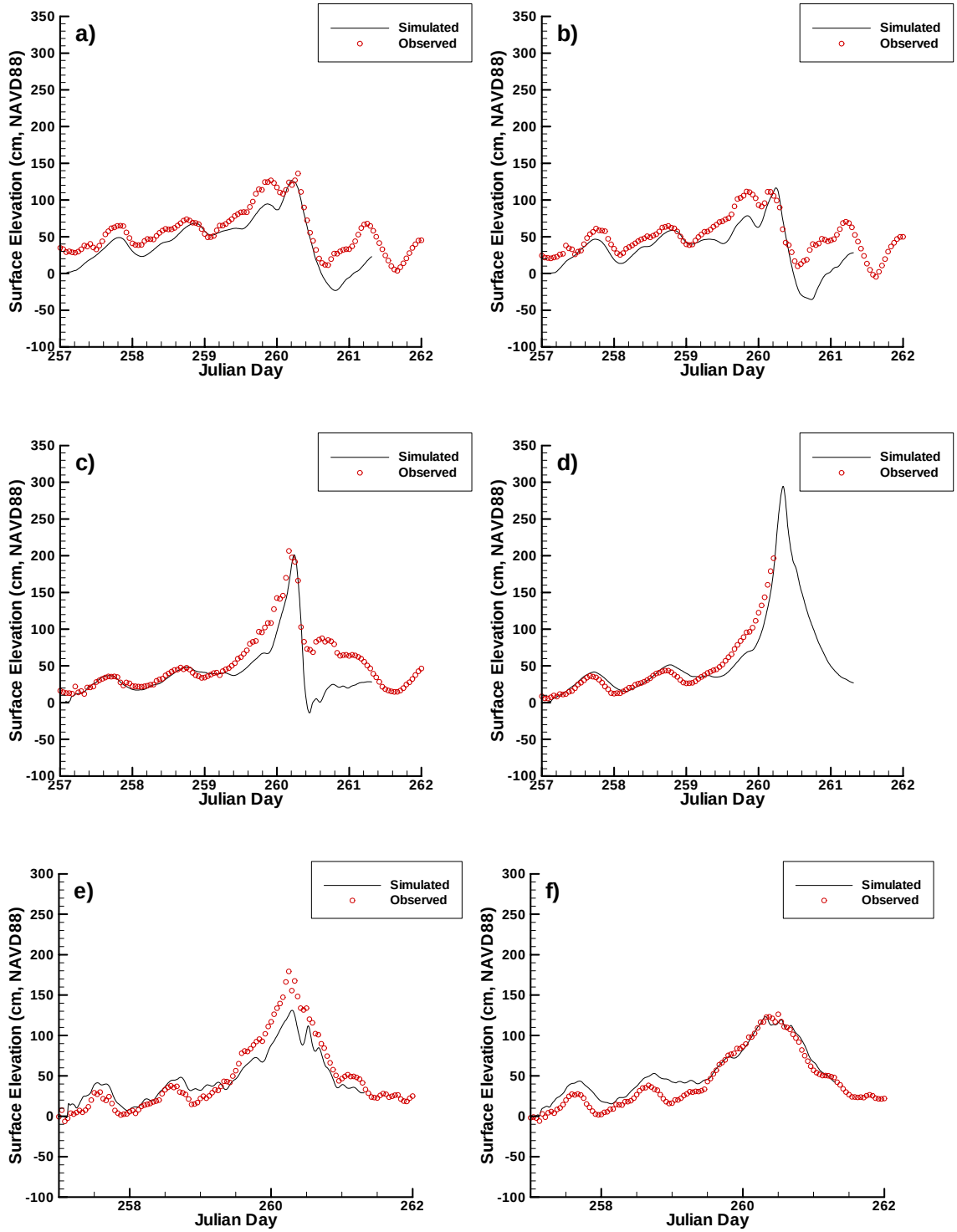

Figure 3-14. Water level comparison for Hurricane Ivan at (a). Biloxi; (b). Waveland; (c). Dauphin Island; (d). Pensacola; (e). Panama City Beach; (f). Panama City.

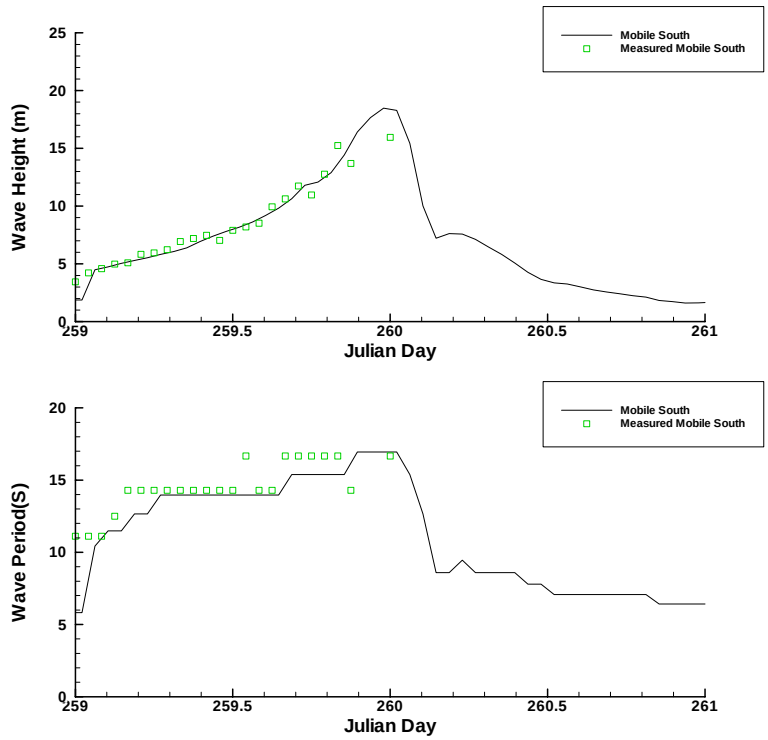

Figure 3-15. Wave comparison for Hurricane Ivan at station Mobile South.

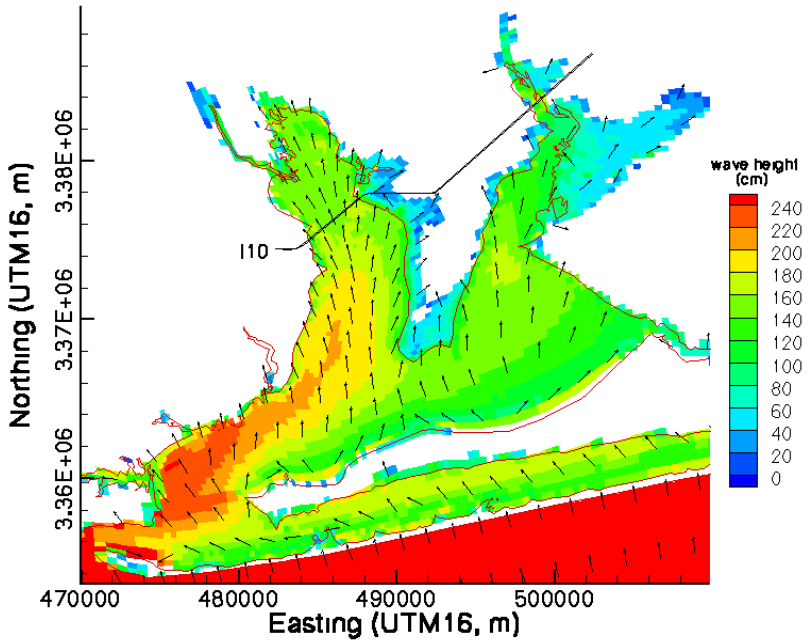

Figure 3-16. Maximum wave height and associated peak wave period in Escambia Bay during Hurricane Ivan.

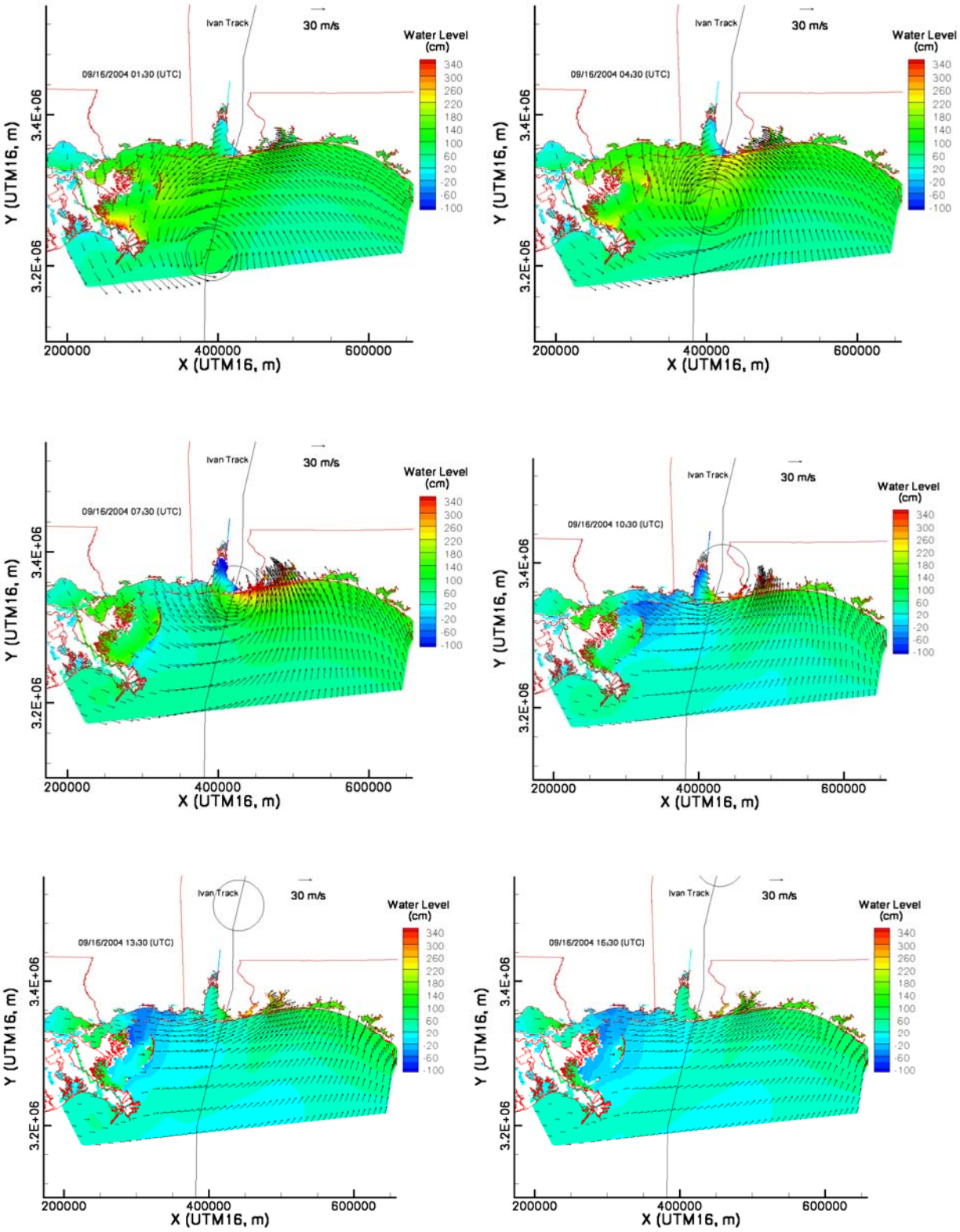

Figure 3-17. Snapshots of water level for Hurricane Ivan before and after landfall.

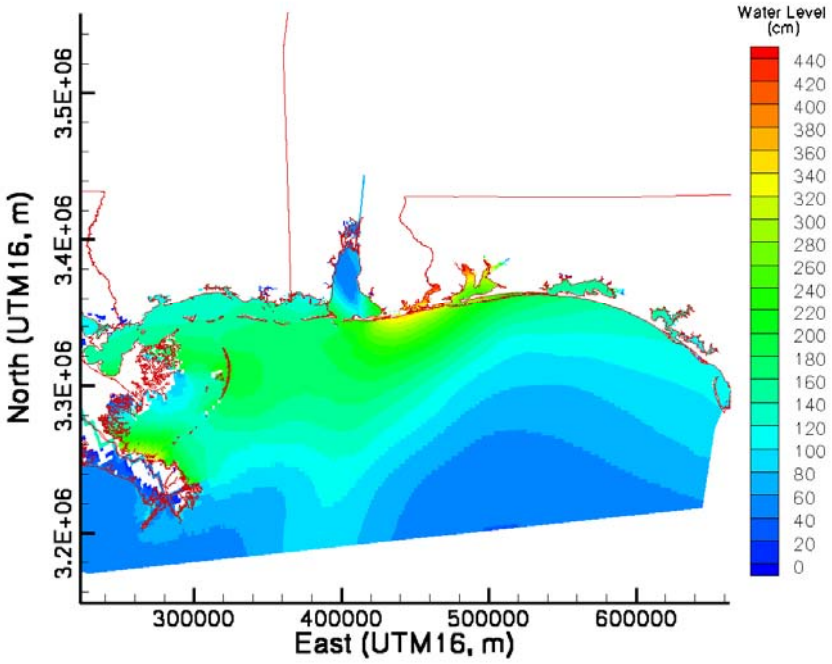

Figure 3-18. Envelop of High Water from Hurricane Ivan simulation using CH3D-SSMS.

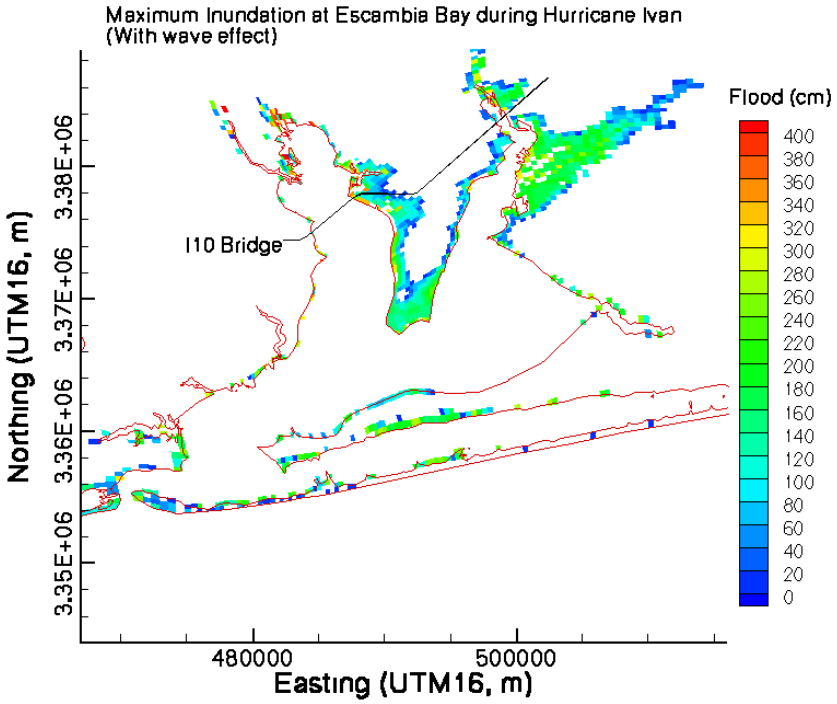

Figure 3-19. Maximum Inundation around Pensacola Bay and Escambia Bay by Hurricane Ivan.

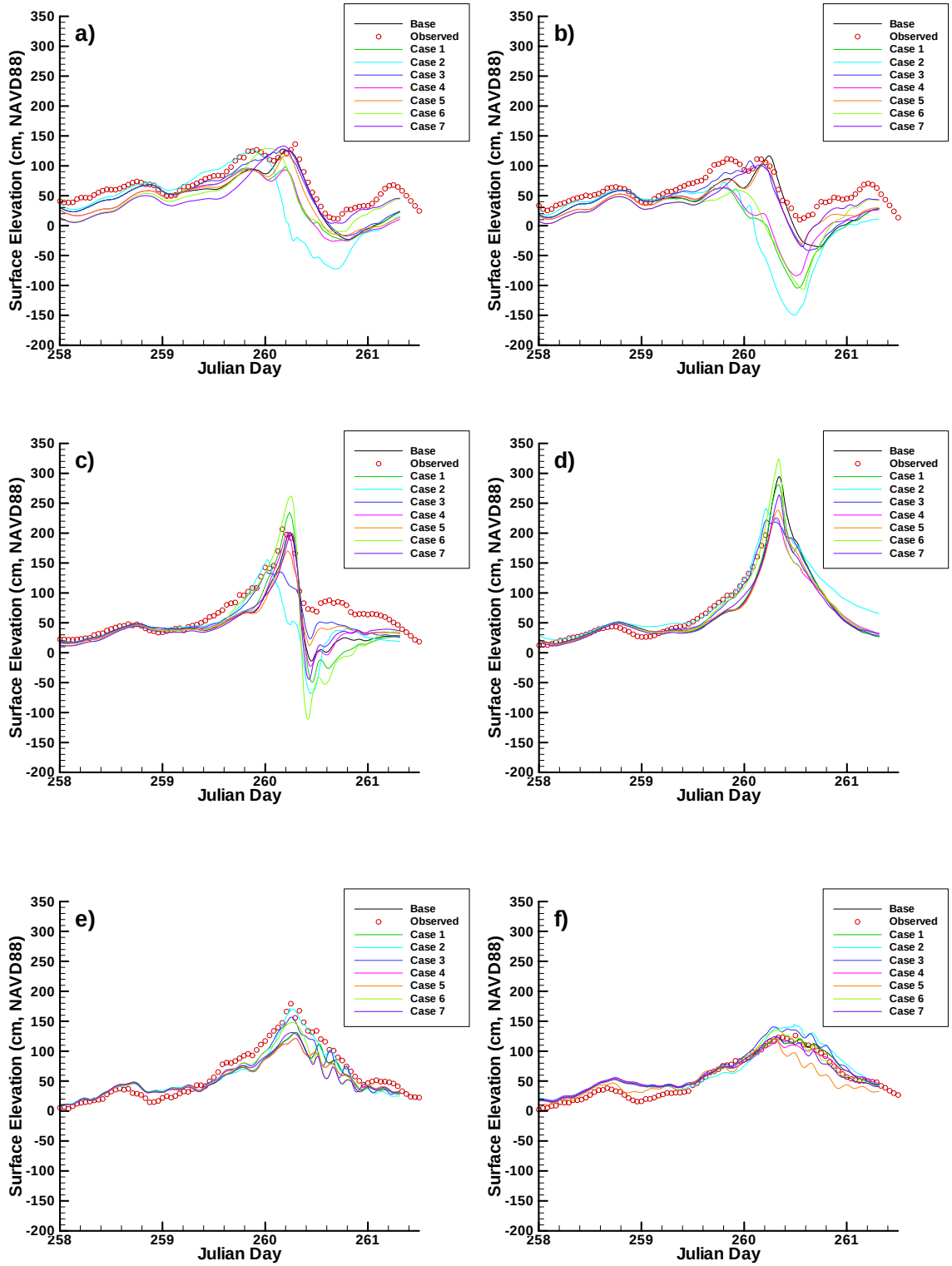

Figure 3-20. Water level comparison for Hurricane Ivan sensitivity test case 1 to case 7 at (a). Waveland; (b). Biloxi; (c). Dauphin Island; (d). Pensacola; (e). Panama City Beach; (f). Panama City.

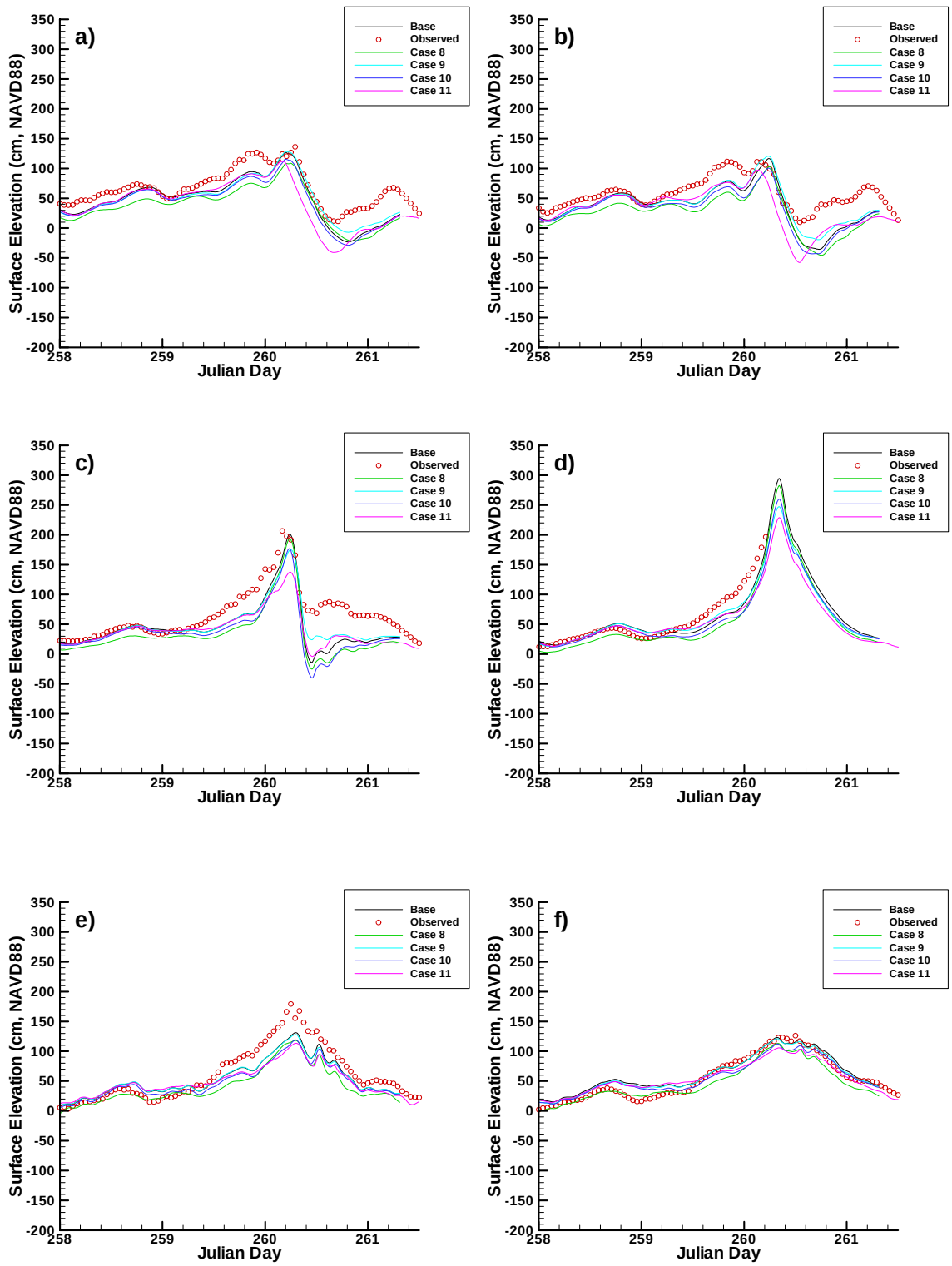

Figure 3-21. Water level comparison for Hurricane Ivan sensitivity test case 8 to case 11 at (a). Biloxi; (b). Waveland; (c). Dauphin Island; (d). Pensacola; (e). Panama City Beach; (f). Panama City.

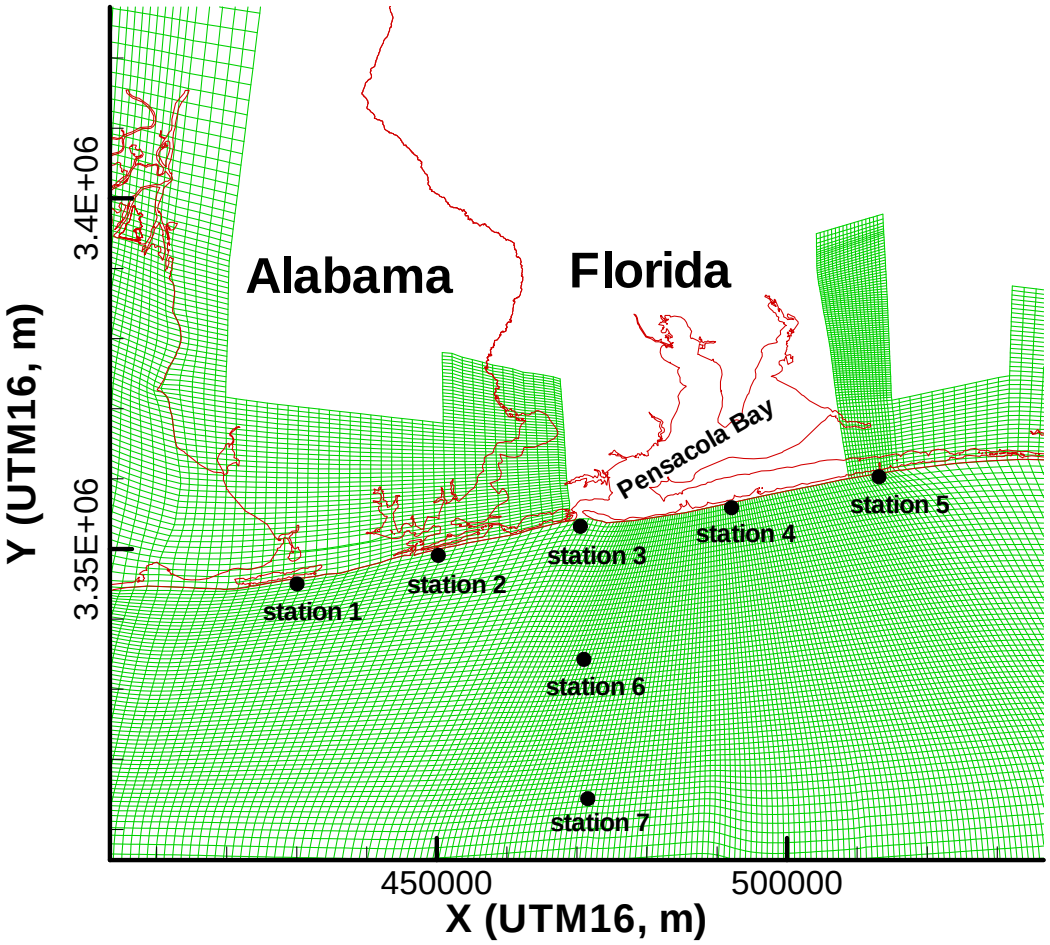

Figure 3-22. The grid system and water level output station for Hurricane Ivan simulation without Pensacola Bay.

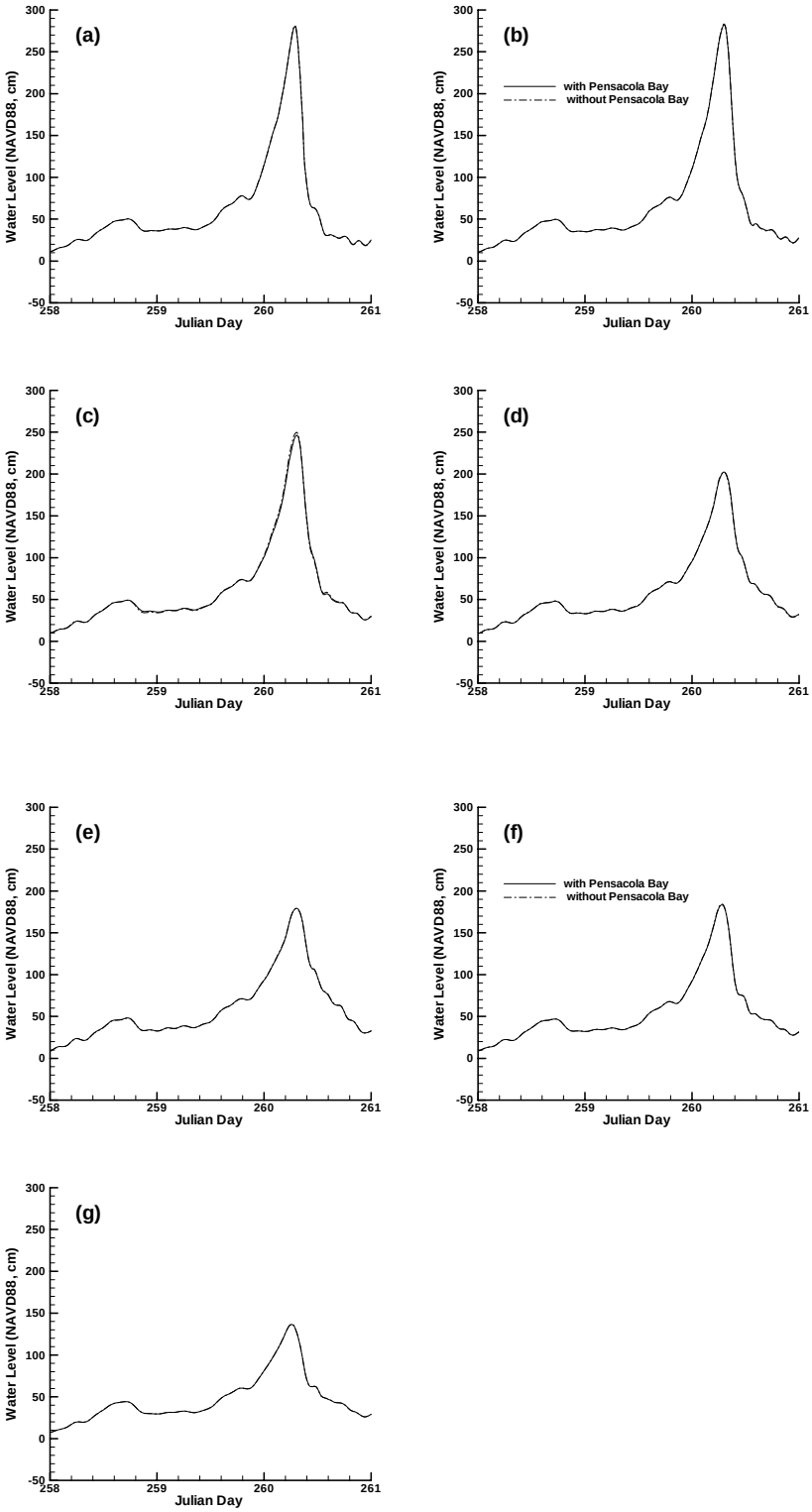

Figure 3-23. Water level comparison for Hurricane Ivan simulation w/o Pensacola Bay. (a). Station 1; (b). Station 2; (c). Station 3; (d). Station 4; (e). Station 5; (f). Station 6; (g). Station 7.

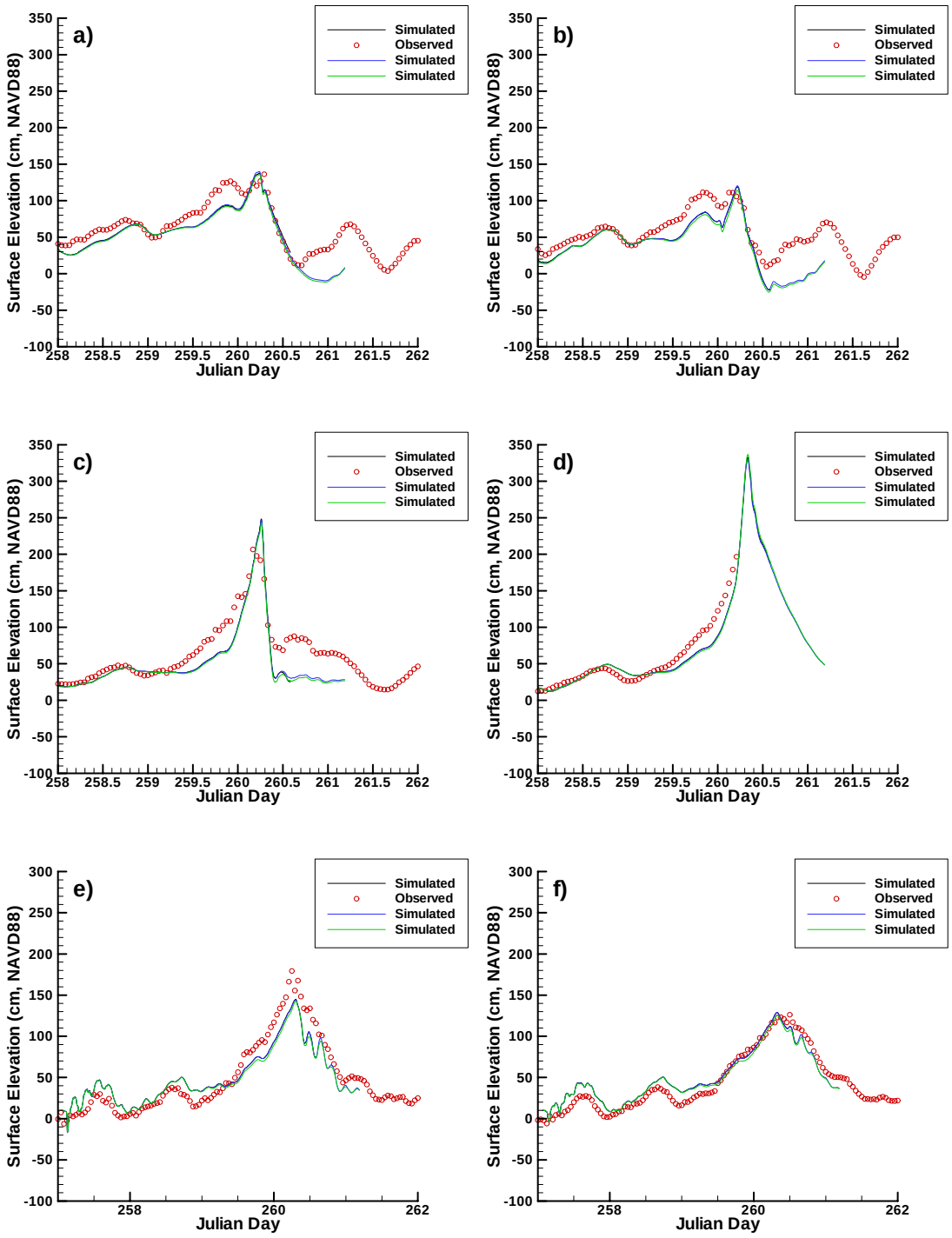

Figure 3-24. Water level comparison for Hurricane Ivan from 3D simulations at (a). Biloxi; (b). Waveland; (c). Dauphin Island; (d). Pensacola; (e). Panama City Beach; (f). Panama City. The blue line represents simulations without wave-current interaction. The black line represents simulations with wave-current interaction using table. The green line represents simulations with wave-current interaction using Grand Madsen method.

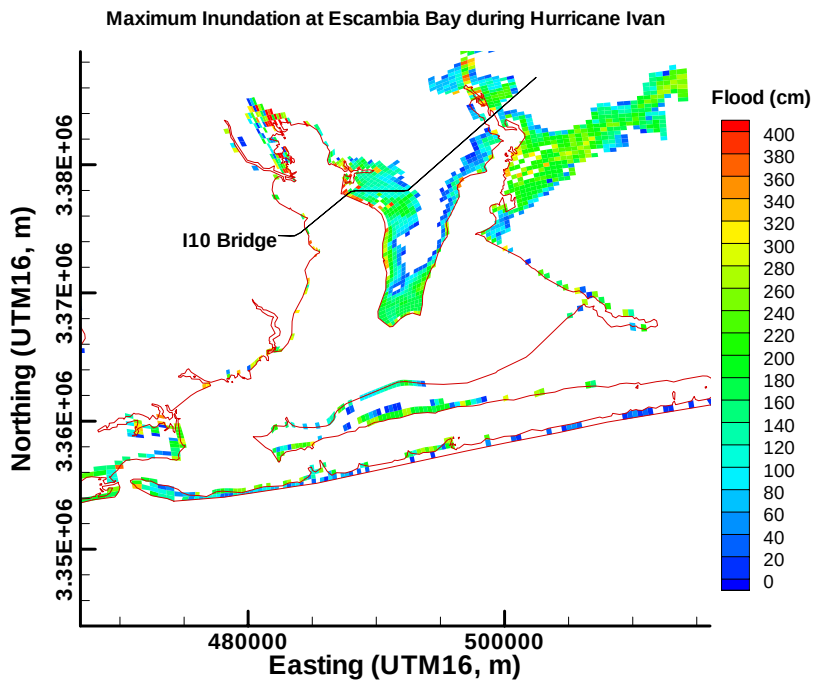

Figure 3-25. Maximum Inundation around Pensacola Bay and Escambia Bay by Hurricane Ivan using 3D model.

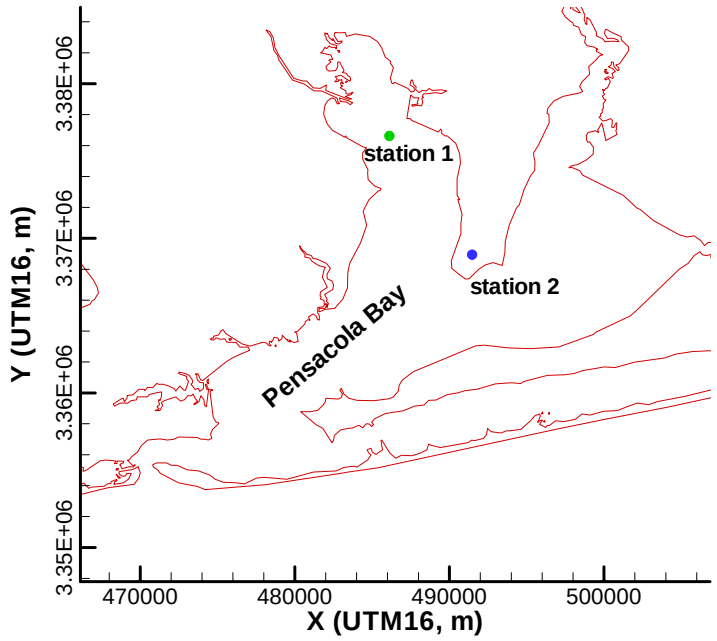

Figure 3-26. Velocity output stations in Pensacola Bay from 3D model simulations.

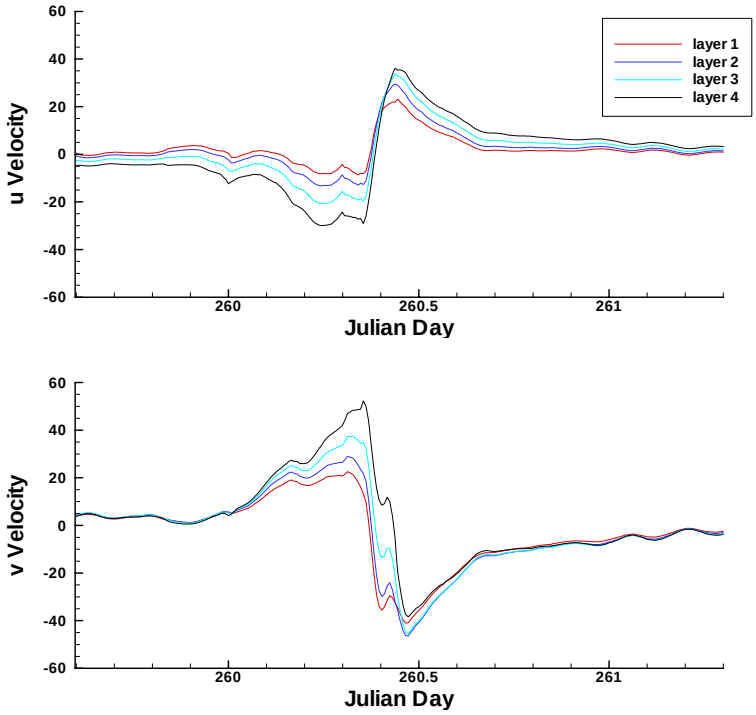

Figure 3-27. Time series of velocity at all vertical layers from 3D model simulations at station 1.

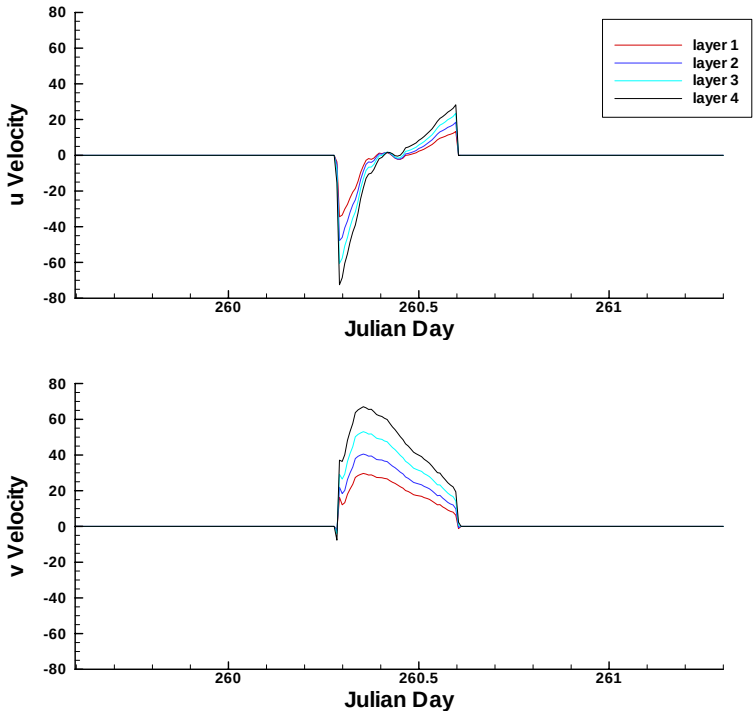

Figure 3-28. Time series of velocity at all vertical layers from 3D model simulations at station 2.

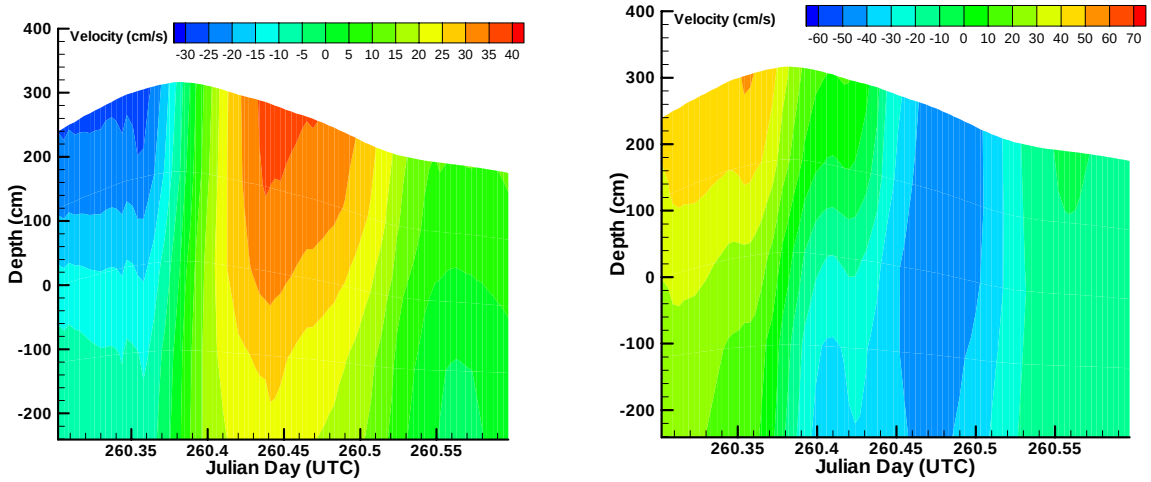

Figure 3-29. Simulated west to east current (left panel) and south to north current (right panel) at I-10 Bridge during Hurricane Ivan from 3D model.

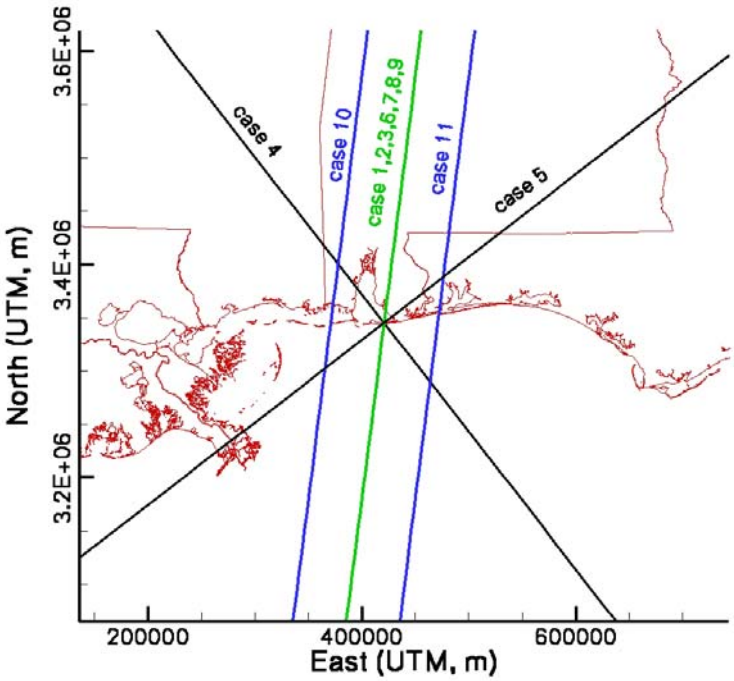

Figure 3-30. Hurricane tracks used for risk analysis test.

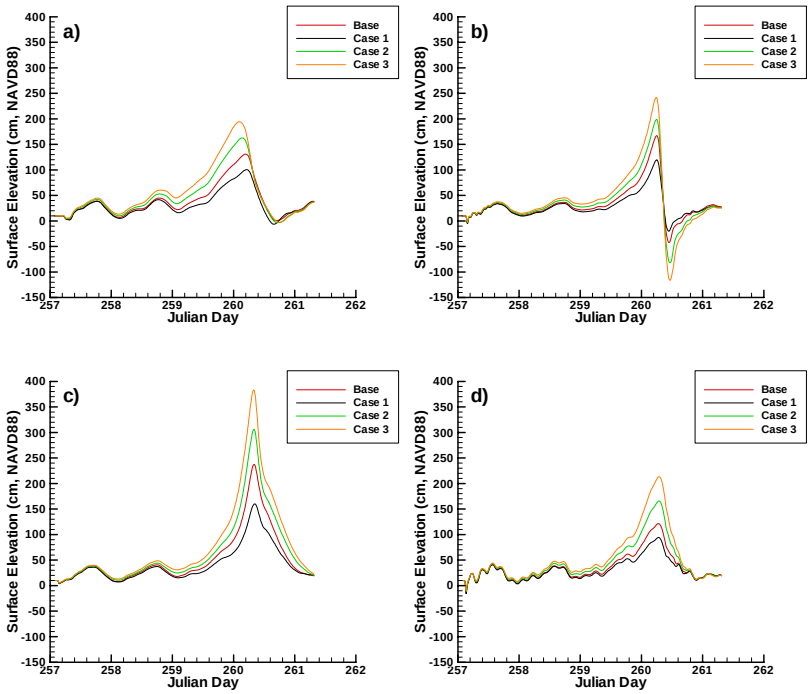

Figure 3-31. Water level comparison for risk analysis test on hurricane intensity: case 1, 2 and 3. (a). Waveland; (b). Dauphin Island; (c). Pensacola; (d). Panama City Beach;

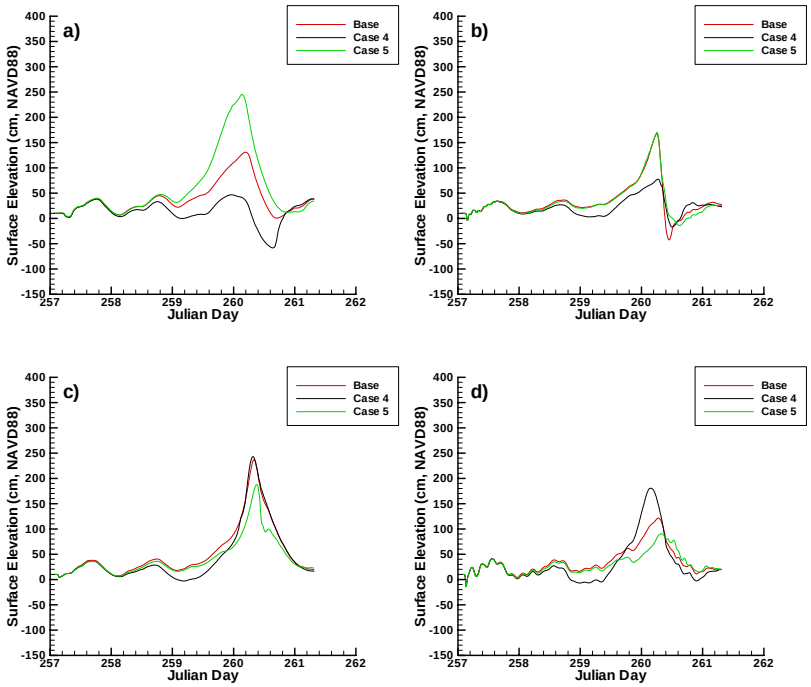

Figure 3-32. Water level comparison for risk analysis test on hurricane landfall direction: case 4 and 5. (a). Waveland; (b). Dauphin Island; (c). Pensacola; (d). Panama City Beach

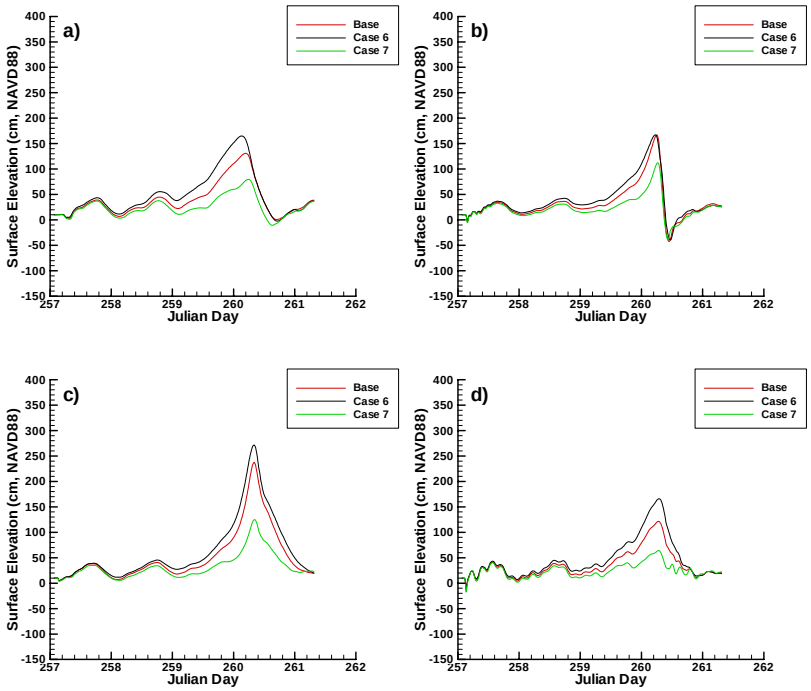

Figure 3-33. Water level comparison for risk analysis test on hurricane size: case 6 and 7. (a). Waveland; (b). Dauphin Island; (c). Pensacola; (d). Panama City Beach;

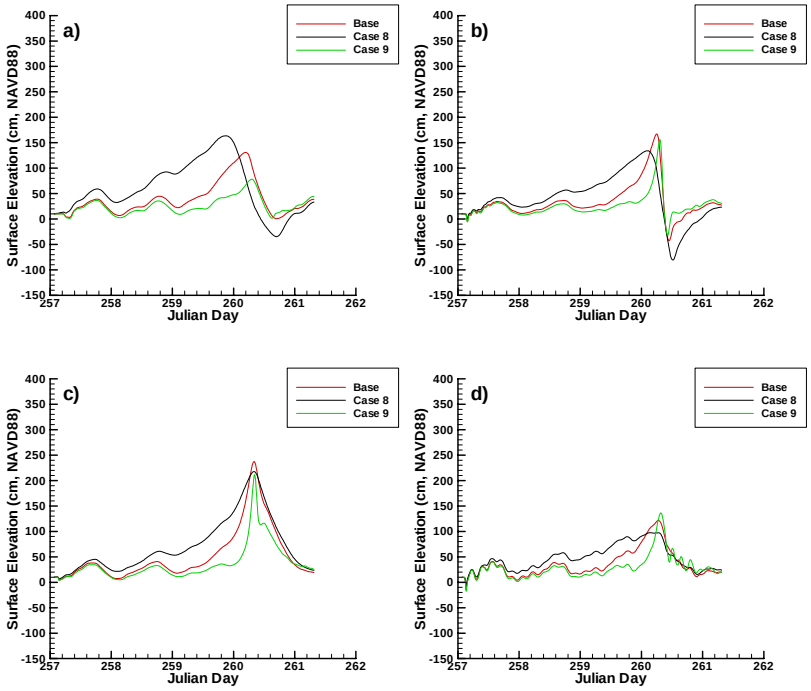

Figure 3-34. Water level comparison for risk analysis test on hurricane speed of approach: case 8 and 9. (a). Waveland; (b). Dauphin Island; (c). Pensacola; (d). Panama City Beach.

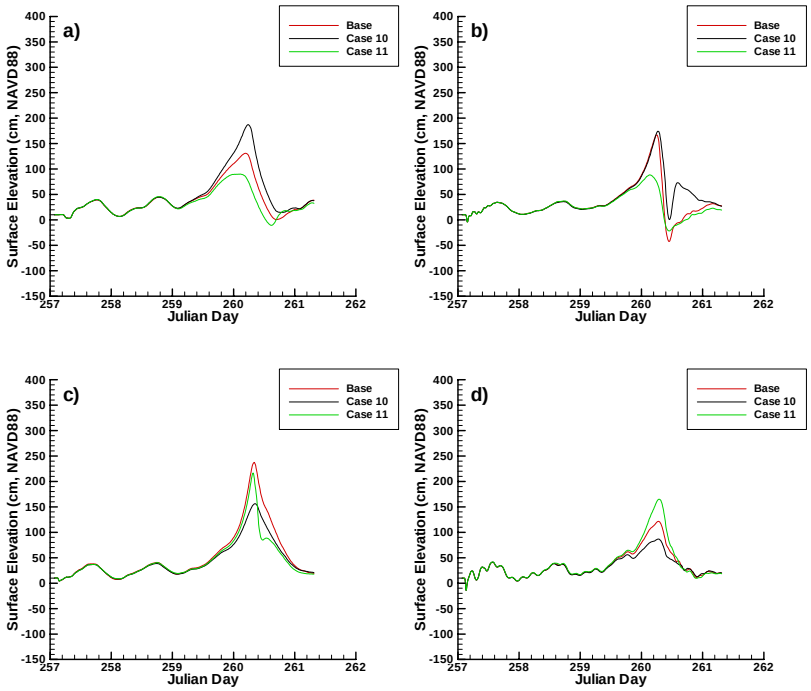

Figure 3-35. Water level comparison for risk analysis test on hurricane landfall locations: case 10 and 11: (a). Waveland; (b). Dauphin Island; (c). Pensacola; (d). Panama City Beach.

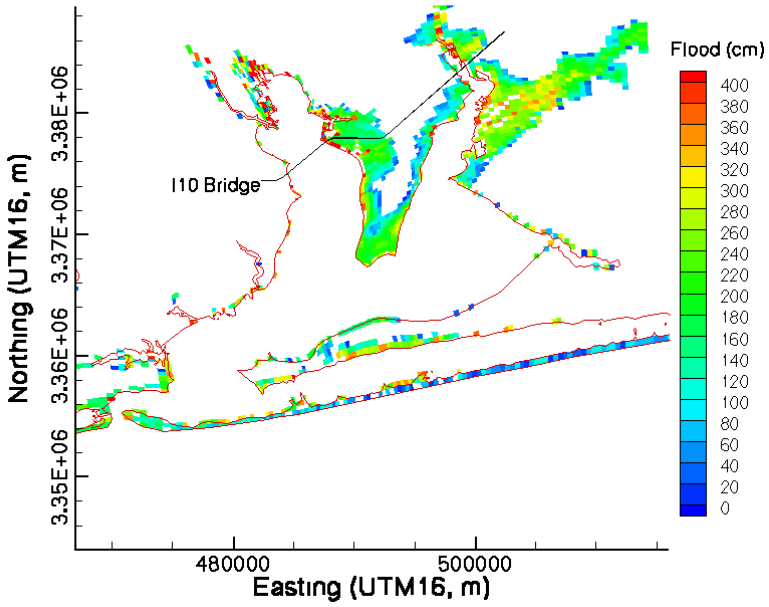

Figure 3-36. Maximum Inundation around Pensacola Bay and Escambia Bay from a Category 5 hurricane.

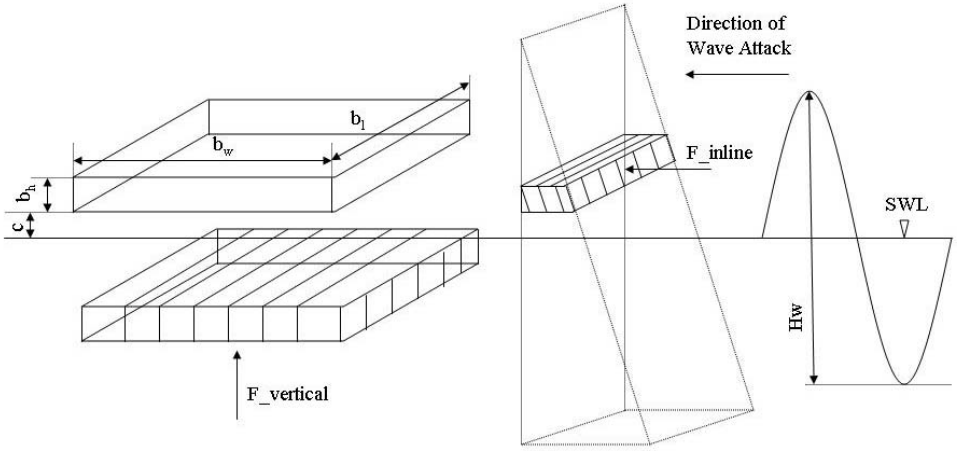

Figure 3-37. Diagram of wave force on bridge deck.

Figure 3-38. Missing spans on the East Bound I-10 Bridge during Hurricane Ivan.

Figure 3-39. Damaged pile group on West Bound I-10 Bridge during Hurricane Ivan.

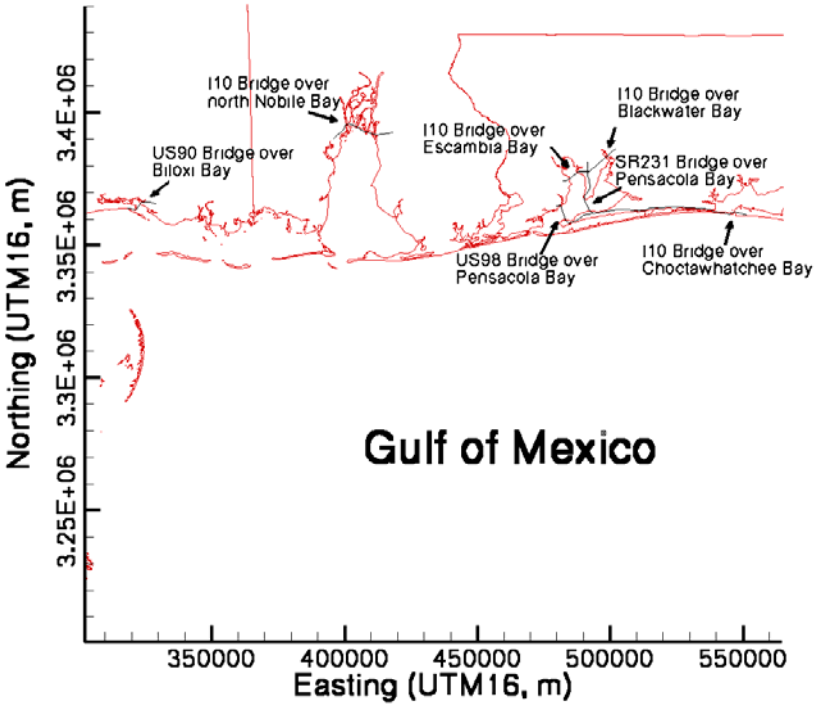

Figure 3-40. Bridge locations for risk analysis tests.

Table 3-1. Observe Data Stations of Hurricane Ivan

Data Source	Station Name	Station ID	Station Location (Long/Lat)	Data Type			
				Wind	Water Level	Wave	Atmospheric pressure
NOAA	Pensacola	8729840	-88.2117/30.4033		x		x
	Dauphin Island	8735180	-88.0733/30.2483	x	x		x
	Panama City	8729108	-85.6667/30.1517		x		x
	Panama City Beach	8729210	-85.8800/30.2133	x	x		x
	Biloxi	8744117	-88.9033/30.4117		x		
	Waveland	8747766	-89.3667/30.2817	x	x		x
	Pilot Station East, SW Pass	8760922	-89.4067/28.9317	x	x		x
	Grand Isle	8761724	-89.9567/29.2633	x	x		x
	Port Fourchon	8762075	-89.4067/28.9317	x	x		
NDBC	Mobile South	42040	-88.2133/29.1842	x		x	
FCMP	Pensacola	T1	-87.1869/30.4793	x			x
	Firehope	T2	-87.8750/30.4725	x			x

Table 3-2. Model results comparison methods

	Time Series	Tide Statistics	Peak	Phase	Snapshot (every 3 hours)
Wind	x				
Tide	x	x			
Water Level (Tide and Surge)	x		x	x	x
HWM			x		
Inundation					x
Hurricane Track/Size					x
Wave	x				

Table 3-3. High Water Mark comparison for Hurricane Ivan simulation

Station Name	Observed High Water Level (cm)	Time of Observed High Water Level (hr)	High Water Mark (cm)	Simulated High Water Level (cm)	Time of Simulated High Water Level (hr)	High Water Level Difference(cm)	Relative High Water Level Difference (%)	Time Difference of High Water Level (hr)
Waveland	136.20	7.0	-	126.72	5.13	-9.48	-6.96	-1.87
Biloxi	111.10	3.0	-	116.46	5.83	+5.36	+4.82	+2.83
Dauphin Island	206.60	4.0	-	201.42	5.66	-5.18	-2.51	+1.66
Pensacola	-	-	-	294.68	8.17	-	-	-
Panama City Beach	179.30	6.0	-	131.16	7.17	-48.14	-26.84	+1.17
Panama City	126.20	12.0	-	123.18	7.67	-3.02	-2.39	-4.33
Perdido Pass Orange Beach	-	-	264.72	356.00	-	+91.28	+34.48	-
GIWW at Pensacola Gulf Beach	-	-	290.86	330.20	-	+39.34	+13.53	-
Pensacola Bay at Ft. McRee	-	-	291.47	297.80	-	+6.33	+2.17	-
Pensacola Bay at Pensacola	-	-	306.49	298.70	-	-7.79	-2.54	-
Escambia Bay West Bank at Hwy 90	-	-	388.22	354.90	-	-33.22	-8.58	-
Escambia Bay West Bank at North of I-10	-	-	364.18	379.50	-	+15.32	+4.21	-
GIWW at Gulf Breeze	-	-	309.49	295.80	-	-13.69	-4.42	-

Table 3-4. Hurricane Ivan sensitivity test simulation

	Wind								Open Boundary			Bottom Friction		Atmospheric pressure		Wave Effect	
Case	HRD		WNA		WINGEN		Analytical		Tide		Surge	uniform 0.020	spatial varying	No	Holland model	No	Radiation Stress
	LLE	OLE	OWE	LLE	OWE	LLE	OWE	LLE	Predict Tide	AC	AC						
Base 0	x								x		x		x		x		x
1		x							x		x		x		x		x
2			x						x		x		x		x		x
3				x					x		x		x		x		x
4					x				x		x		x		x		x
5						x			x		x		x		x		x
6							x		x		x		x		x		x
7								x	x		x		x		x		x
8	x									x	x		x		x		x
9	x								x		x	x			x		x
10	x								x		x		x	x			x
11	x								x		x		x		x	x	

LLE: Limited Land Exposure; OLE: Open Land Exposure; OWE: Open Water Exposure;
AC: ADCIRC Constituents;

Table 3-5. Risk analysis test for Hurricane Ivan simulation

	Hurricane Intensity				Land Fall Direction			Hurricane Size			Speed of Approach			Analytical Wind	Land Fall Location		
Case	2	3	4	5	+ 45°	original	- 45°	- 50%	original	+ 50%	one time slower	origin al	one time faster	with land reduction	move west 50 km	origin al	move east 50 km
Base		x				x			x			x		x		x	
1	x					x			x			x		x		x	
2			x			x			x			x		x		x	
3				x		x			x			x		x		x	
4		x			x				x			x		x		x	
5		x					x		x			x		x		x	
6		x				x		x				x		x		x	
7		x				x				x		x		x		x	
8		x				x			x		x			x		x	
9		x				x			x				x	x		x	
10		x				x			x			x		x	x		
11		x				x			x			x		x			x

Table 3-6. Literature reviews on wave force calculation

Authors (Year)	Nature of Study	Nature of Model	Major Feature	Model Strength	Model Weakness	Model Verification
Wang (1970)	Wave pressure on plate	Lab experiment	Function of static pressure	Simple; Derived from lab test;	Idealized structure (plate); Rough coefficient estimation	Lab data
French (1970)	Wave load on platform	Lab experiment	Function of hydraulic static pressure	Simple; Derived from lab test;	Regular wave; Simplified platform;	Lab data
Overbeek & Klabeers (2001)	Wave load on Jetty	Empirical formulation	Impact and slow-varying pressure; Function of wave height;	Easy to implement; Less parameters;	Not related to structure shape; Rough coefficient Estimation	Platform in Hurricane Lenny
McConnell, et al. (2004)	Wave load on Jetty	Physical model	Dimensionless equations for quasi-static and impact force	Combination of theoretical analysis and lab experiment	Simplified experiment structure; Application limited;	Lab data
Denson (1978, 1980)	Wave load on bridge deck	Lab experiment	Dimensionless charts derived from experiments	Designed for bridge deck from lab	Unrealistic wave parameters; Poor lab conditions	Lab data
Kaplan, et al. (1995)	Wave force on platform	Analytical Solution with experiment	Extension of Morison's equation	Adjusted coefficient from experiment	Limited application for platform;	Lab data
Bea, et al. (1999)	Wave force on platform	Analytical solution with adjustable coefficient	Total force is combination of individual force components	Theoretic sound; Application beyond platform;	Difficulty to determine coefficients;	Platform in Gulf of Mexico during Hurricane Camille
Cuoto, et al. (2003, 2007)	Wave load on Jetty	Physical model	Dimensionless equations from regression of lab tests	Obtained from comprehensive lab tests;	Equations designed only for jetty	Lab data
Douglass, et al. (2006)	Wave load on coastal bridge	Theoretical Equation	Equations obtained from static hydraulic pressure	Simplified equations;	No wave length consideration;	I-10 Mobile Bay; I-10 Escambia Bay; US90 Biloxi;

Table 3-7. I-10 Bridge deck dimensions and extreme wave parameters during Hurricane Ivan

	Bridge Deck Length (m)	Bridge Deck Width (m)	Bridge Deck Height (m)	Bridge Deck Weight (tons)	Significant Wave Height (m)	Peak Wave Period (s)	Wave Direction (degree)
I-10 Bridge	18.03	10.52	1.05	105.0	1.6	4.4	153.0

Table 3-8. Wave Loads on I-10 Bridge during Hurricane Ivan

Study case		Inertial Force (tons)	Drag/Lift Force (tons)	Buoyancy (tons)	Slamming Force (tons)	Total force (tons)	Bridge deck weight (tons)	Bridge deck connection force (tons)	Bridge deck force (tons)
Ivan Surge (3.7 m)	In-Line Force	88.6	18.6		30.8	137.8			
	Vertical Force	24.6	80.0	66.3	163.7	334.6	105.0	90.7-181.4	195.7-286.4
Ivan Surge -0.3 m (3.4 m)	In-Line Force	78.3	17.5		29.5	125.2			
	Vertical Force	10.5	50.7	26.5	107.8	195.5	105.0	90.7-181.4	195.7-286.4
Ivan Surge -0.6 m (3.1 m)	In-Line Force	52.1	12.6		21.5	86.3			
	Vertical Force	1.0	12.9	1.5	29.7	44.7	105.0	90.7-181.4	195.7-286.4

Table 3-9. High surge (cm) and risk degree index for risk analysis simulations

Case	I-10 Bridge over Escambia Bay	I-10 Bridge over Blackwater Bay	I-10 Bridge over Mobile Bay	I-10 Bridge over Choctawhatchee Bay	US98 over Pensacola Bay	US90 over Biloxi Bay	SR281 over Pensacola Bay
Base	304.9 / 3	295.8 / 2	36.9 / 1	105.9 / 1	223.0 / 2	107.1 / 1	214.1 / 2
1	212.7 / 2	215.1 / 2	35.2 / 1	78.0 / 1	152.1 / 1	81.4 / 1	150.4 / 1
2	376.8 / 3	346.6 / 3	40.0 / 1	145.4 / 1	283.6 / 2	115.7 / 1	252.6 / 2
3	453.3 / 3	420.0 / 3	43.4 / 1	194.3 / 1	351.5 / 3	132.4 / 1	302.3 / 3
4	288.2 / 2	248.0 / 2	80.2 / 1	121.7 / 1	227.2 / 2	42.2 / 1	209.5 / 2
5	278.0 / 2	274.9 / 2	97.8 / 1	77.0 / 1	175.2 / 1	170.1 / 1	163.7 / 1
6	336.5 / 3	323.7 / 3	41.1 / 1	144.9 / 1	255.5 / 2	117.6 / 1	237.9 / 2
7	173.2 / 1	174.2 / 1	33.7 / 1	57.0 / 1	118.2 / 1	67.4 / 1	113.8 / 2
8	267.6 / 2	251.5 / 2	46.0 / 1	112.3 / 1	207.3 / 2	127.6 / 1	194.2 / 1
9	285.8 / 2	223.0 / 2	39.5 / 1	83.2 / 1	189.5 / 1	58.9 / 1	160.8 / 1
10	202.1 / 2	202.1 / 2	336.9 / 3	77.9 / 1	151.2 / 1	147.3 / 1	151.1 / 1
11	224.2 / 2	254.3 / 2	37.3 / 1	138.7 / 1	205.9 / 2	71.4 / 1	146.3 / 1
Worst scenario	453.3 / 3	420.0 / 3	336.9 / 3	194.3 / 1	351.5 / 3	170.1 / 1	302.3 / 3
Average Risk Degree	2.3	2.2	1.2	1.0	1.7	1.0	1.5

CHAPTER 4
HURRICANE DENNIS SIMULATION

4.1 Introduction

Hurricane Dennis was an unusually strong major hurricane that left a trail of destruction from the Caribbean Sea to the northern coast of the Gulf of Mexico. Dennis made landfall at about 1930 UTC 10 July, 2005, as Category 3 hurricane on Santa Rosa Island, Florida, approximately 30 miles to the east of where Hurricane Ivan had made landfall 10 months before. Even though it had a relatively weaker wind, Dennis still caused considerable damage (NHC, 2005). Surprisingly, the highest storm surge (2-3 m) was found in Apalachee Bay, Florida, about 150 miles away from landfall location. In this chapter, a systematic storm surge modeling for Hurricane Dennis was made using CH3D-SSMS. The high surge in Apalachee Bay is successfully simulated with in-depth analysis.

4.2 Synoptic History

Dennis formed from a tropical wave that moved westward from the coast of Africa on 29 June, 2005. The system became a tropical storm on 5 July as it turned west-northwestward. Dennis reached hurricane strength early on 7 July, then rapidly intensified into a Category 4 hurricane with winds of 120 kt before making landfall near Punta del Ingles in southeastern Cuba near 0245 UTC 8 July. Dennis weakened significantly over Cuba, with the maximum sustained winds decreasing to 75 kt by the time the center left the island.

Dennis gradually intensified for the next 6-12 h over the Gulf of Mexico before beginning another cycle of rapid intensification near 1800 UTC 9 July accompanied by a turn toward the north-northwest. During this intensification, the central pressure fell 37 mb in 24 h, including 20 mb in 6 h and 11 mb in 1 h 35 min. Maximum sustained winds reached a third peak of 125 kt near 1200 UTC 10 July. Thereafter, weakening occurred and the maximum sustained winds

decreased to 105 kt and the central pressure rose to 946 mb before Dennis made landfall on Santa Rosa Island, Florida, about 1930 UTC 10 July, which is approximately 30 miles to the east of where Hurricane Ivan had made landfall 10 months before (Wikipedia, 2006) (Figure 4-1). Dennis continued north-northwestward after landfall, with the center moving across the western Florida Panhandle into southwestern Alabama before it weakened into a tropical storm. It became a depression as it moved into east-central Mississippi on 11 July.

Dennis did not cause as much damage as Ivan. Dennis moved about 7 mph faster than Ivan at landfall and had hurricane-force winds that only extended 40 miles from its center, compared to Ivan's 105 miles. During the height of the storm, Dennis produced storm surges as high as 9 ft in the Apalachee region and as high as 7 ft on the Florida Panhandle leaving 680,000 customers without electricity in four southern states. Hurricane Dennis directly caused 3 deaths in the United States and an estimated total U. S. damage of $2.23 billion.

The best track central barometric pressure and wind speed history for Hurricane Dennis is shown in Figure 4-2 (NHC, 2005). Dennis once strengthened to Category 4 hurricane with the maximum wind speed increasing to 130 kt/s in the Caribbean, but weakening dramatically after making landfall in Cuba. After leaving Cuba, Dennis gained strength again and moved northwest to the Florida Panhandle at about 15 miles/h. Dennis started to weaken again about 6 hours before making landfall on the U.S. continent and losing its strength significantly.

4.3 Hurricane Dennis Simulation Using CH3D-SSMS

As Hurricane Dennis has a similar track and landfall location to Hurricane Ivan so the model setup procedures in Chapter 3 are also applied in this section. The grid system for Ivan was extended to cover the entire northeast Gulf of Mexico, Florida Panhandle and Northwest Florida coast. With the new grid system, storm surge of Hurricane Dennis was successfully simulated using CH3D-SSMS. The comparisons between simulated water levels and

observations at NOAA stations are very good. Both high water peak and time of peak agree well with data. The highest simulated surge during Hurricane Dennis was about 8 ft in Apalachee Bay, Florida.

4.3.1 Data Measurement during Hurricane Dennis

Similar to Hurricane Ivan, the wind, atmospheric pressure, wave, and water level data collected during Hurricane Dennis are mainly obtained from NOAA and NBDC. Table 4-1 summarizes the data type and station information. The best track of Hurricane Dennis from the National Hurricane Center and station locations are shown in Figure 4-3.

4.3.2 Bathymetry, Topography and Grid System

As shown in Figure 3-1 and Figure 4-1, the landfall locations for Hurricane Dennis and Ivan are only approximately 30 miles away, the grid originally developed for the Ivan simulation is used again for Dennis. However, the grid is not sufficient to cover Apalachee Bay and the west coast of Florida, where the highest surge were observed. Therefore the old grid is expanded extensively to west Florida, including both water cells and land cells (Figure 4-4). The additional topography and bathymetry for the extended grid are also downloaded from NED, USGS (2006) and NGDC, NOAA (2006) and then interpolated to the new grid system (Figure 4-5). The dimension of the grid system is 572x230.

4.3.3 Wind Field

The wind fields considered for the Hurricane Dennis simulation include WNA wind and HRD wind. The procedures to download and process wind for Hurricane Ivan are implemented again for Dennis. For the extended grid, additional land cover data are used to provide bottom roughness when land reduction effect is considered for hurricane wind (Figure 4-6). As land cover is not available between Tamp Bay and Cedar Kay, FL, an estimated averaged bottom roughness of 0.5 m is used. Since that region is far away from the Dennis track, the estimation

should not significantly affect the overall wind field. When the hurricane is long time before and right after landfall, only WNA wind is used to generate wind field for storm surge simulation as HRD wind is not available. During the time in between, both WNA wind and HRD wind are used because the grid system for Hurricane Dennis is so large that HRD wind alone can not cover the west coast of Florida. Linear interpolation is used at the wind interfering domain to keep smooth transition in the wind combination process. An example is shown in Figure 4-7 on the combination of HRD and WNA wind at west coast of Florida at 16:30, July 10th, 2005, UTC. At domains where HRD does not have coverage, extrapolation was used to generate wind field, which introduced error. In this case, wind was underestimated. By combining with WNA wind, it is able to reconstruct wind field to keep both accurate HRD wind near hurricane center and good WNA wind far away from the hurricane center. The transit zone is determined at locations where both HRD and WNA have approximately the same wind amplitude.

4.3.4 Boundary Conditions

The historical wave height, period, and direction from WWIII model is downloaded from NOAA website (NOAA, 2006c) and then abstracted to the west and south open boundaries of the extended Northeast Gulf Grid System. Tidal constituents downloaded from ADCIRC database are used for Dennis simulation. Storm surge at the open boundary is obtained by dynamically coupling with regional surge model ADCIRC.

4.3.5 Hurricane Dennis Storm Surge Simulation Results

First, time series of water levels, winds, and waves are compared with measured data at available NOAA stations. Then, the peak of storm surge along the coastline of Gulf of Mexico is compared with observation. Inundation maps of Hurricane Dennis are presented at the Pensacola area and the Northwest coast of Florida.

4.3.5.1 Wind and atmospheric pressure comparison

The wind used in the Dennis simulation includes WNA wind and HRD wind. In general, the simulated wind compared well with measured data for both amplitude and direction at most stations (Figure 4-8). Since Dennis is a relatively compact hurricane, the maximum wind does not extend to a large domain and only blows with maximum speed of approximately 25 m/s. The relative error for wind magnitude is on the order of 10%. The direction is also in good agreement of measurement.

The atmospheric pressure for Dennis is calculated from the analytical Holland Model solution based on hurricane track, minimum deficit atmospheric pressure, and maximum wind radius. The comparison of atmospheric pressure time series for Hurricane Dennis between simulation and observation at a few stations are shown in Figure 4-9. Since the Holland model assumes uniform atmospheric pressure structure, the spatial variation can not be fully resolved and sometimes may not give perfect results. Therefore, the simulated pressure at stations close to the hurricane center shows better comparison than stations that far away from the hurricane center. For example, simulated atmospheric pressure at station Waveland is not quite good. However, this should have much less effect on simulated water level as the deficit atmospheric pressure error is approximately equal to only a few centimeters difference in water level.

4.3.5.2 Water level and high water marks comparison

Because Hurricane Dennis had relatively weaker wind and was smaller in size, the generated storm surges are not as significant as those produced by Hurricane Ivan. Dennis made landfall east of Pensacola as a Category three hurricane and generated surge around 5-6 feet along the Florida panhandle. However, the highest water level was observed at 8-9 feet inside Apalachee Bay, about 180 miles away from the landfall location. The time series of simulated water levels at multiple NOAA stations from fully-coupled CH3D-SSMS were shown in Figure

4-10. These representative stations cover a very large domain, from Waveland, 140 miles west of landfall, to Cedar Key, 240 miles east of land fall. Station Pensacola in Pensacola Bay is only a few thousands meters away from landfall. As Hurricane Dennis approached the Gulf Coast, the cyclonic wind induced an along shore current and produced storm surge along the coast. When Dennis made landfall, the raised water receded with weakened wind. The physical process was successfully simulated with very good comparison with observation.

Apalachicola, which is located west of Apalachee Bay, has the complete time series of water levels with maximum observed surge among those NOAA stations. The rise of water at that station was accurately simulated by CH3D-SSMS, both in amplitude and phase. The model slightly overestimated highest water level but in good agreement of trend.

At station Pensacola, the closeness to the hurricane center made it undergo significant wind direction change within short period of time. The water level change inside semi-closed Pensacola Bay is largely affected by local wind. When Dennis was moving from south to north in Gulf of Mexico, the generated long shore current pushed water into Pensacola Bay and caused the water level rise. When Dennis got close to shoreline and made landfall, the wind in the bay started to blow offshore and pushed water out of the bay. After the landfall, the wind direction kept changing from south to west to northwest. Again water was pushed back into the bay and then receded after Dennis weakened and moved further inland. This rise-drop-rise-drop process was simulated very well (Figure 4-10 (b)). At other stations, the comparisons are also fairly well. The simulated high surge is within 10% error compared to measurement.

4.3.5.3 Wave comparison

There are two buoys that recorded complete wave parameters during Hurricane Dennis. The simulated waves by SWAN show good agreement with observation (Figure 4-11). Both the high waves and peak period are captured as well as the wave development over time. The

absolute difference of significant wave height between measurement and simulation is about 0.5 m for station 42037 and 0.7 m for station 42007, respectively.

4.3.5.4 Snapshot, EOHW and inundation map

In order to capture the whole picture of storm surge generated by Hurricane Dennis over the entire northeast Gulf of Mexico coast, several water level snapshots were provided before/after landfall every three hours to describe the surge evolution during the storm event (Figure 4-12). Hurricane Dennis generates a similar flow pattern to Hurricane Ivan, but with a smaller scale because of hurricane intensity and scale. Another big difference is high surge was generated inside Apalachee Bay as Dennis moves along west coast of Florida and induced shelf wave transported along the hurricane (Morey et al., 2005). The high surge is further displayed in the plot of Envelope Of High Water (EOHW) for Hurricane Dennis in Figure 4-13. Due to a relatively weak storm, the inundation caused by Hurricane Dennis is not as significant as Ivan at point of landfall (Figure 4-14). However, large domain of Northwest Florida is flooded because of the big shelf wave (Figure 4-15).

For a complete storm surge simulation, coupling with wave model SWAN is the most time-consuming process to include wave effect. The total simulation time is totally determined by SWAN simulation time. Theoretically, SWAN should have the same time step as surge model. However, it is not practical to do so. First, the significantly long simulation time makes it unrealistic to simulate waves at every surge model time step, which is about 1 minute. Secondly, the wave boundary conditions for SWAN are obtained from the WW3 model with three hour frequency. The wave conditions interpolated from WW3 may not be very accurate if a small time step used. Therefore, longer time step has to be considered for SWAN during storm surge simulation. In order to evaluate how often it is necessary to run SWAN to get the correct surge-wave interaction and how sensitive the surge result is to frequency of running SWAN relative to

CH3D, multiple runs were made on Hurricane Dennis. As the development of wave is relatively a slow process, the change of wave parameters is normally not big within one hour. The sensitivity tests imply that storm surge are very close for SWAN simulations every 30 min and 1 hour. In the mean time, the total simulation time is approximately 10 times more if a one hour time step is used for SWAN and 20 times more if a 30 time step used. Considering both accuracy and efficiency, it is reasonable to use big time step for SWAN simulation, which is 1 hour as used for the Hurricane Ivan and Dennis simulations.

At the open boundary, clamped condition is used in the model using water level from tidal constituents and simulated surge from ADCIRC. In order to check the open boundary effect on simulated surge along coast, a Flather radiation boundary condition is introduced in CH3D-SSMS (Flather, 1976, 1993). The simulated water levels at NOAA stations during Hurricane Dennis vary slightly from the results from the clamped boundary condition. The differences of highest surges are in the order of centimeters. This implied that the open boundary condition did not have a significant effect on model results for this particular case and location of open boundaries seem to be sufficient. The detailed explanation of Flather radiation boundary condition and its application in Hurricane Dennis simulation is included in Append E.

Hurricane Dennis is further investigated by two more sensitivity tests by removing wave effect (case 1) and removing large scale wind field (WNA) during landfall (case 2). Because the weakness of the hurricane and its compact size, the waves are overall not strong and only cause moderate wave setup on top of wind stress generated surge. The averaged simulated surge reduced by up to 20 cm at NOAA stations (Figure 4-16). If large scale wind of WNA is removed at the west coast of Florida, the simulated surges there are obviously reduced at stations Apalachicola and Cedar Key (Figure 4-16). But its effect on other stations, where HRD wind in

control, is very limited. The inundation at the Pensacola area from simulation without wave effect (case 1) is shown in Figure 4-17. Due to slightly smaller surge, the flooded area is reduced accordingly. However the total extension of the flooding zone is kept almost the same.

4.3.5.5 High surge in Apalachee Bay

The damage by Hurricane Dennis is not limited to the Pensacola region where it made landfall. At about 275 km east of the landfall location, Shell Point and other coastal communities of Apalachee Bay experienced a devastating storm surge locally to 2 to 3 m above normal tide levels. The high surge caused extensive local property damage and isolated several communities. However, only 4 to 6 feet surge was predicted from the last Public Advisory issued by the National Hurricane Center before Dennis made landfall. The approximately 1 m surge difference cannot be explained by the weak hurricane wind far east from hurricane center.

The additional sea level rise of approximately one meter is explained by a remotely forced shelf wave, according to Morey et al. (2006). Hurricane Dennis traveled from Cuba to the western Florida Panhandle over the course of 34 hours, during which along-shore winds forced Ekman transport towards the Florida Peninsula coast building a high sea level anomaly that propagated northward as a topographic Rossby wave. The storm traveled nearly parallel to the shelf in the same direction of the waves, resulting in amplification of the sea level signal along the coast. This high sea level anomaly reached its maximum amplitude at the northernmost bounds within Apalachee Bay and combined with the surge to form the high water rise during the storm. In this study, a numerical experiment is set up to further discuss Morey's theory.

In order to isolate the effect of local wind and remote surge signal from shelf wave, the southern open water domain in the grid used previously for the Dennis simulation was removed (Figure 4-18). The left domain has similar coverage of Apalachee Bay comparing to the SLOSH model used by NOAA and Morey's test using Navy Coastal Ocean Model. Two separate tests

are conducted to analyze the unusual high surge observed in Apaalachee Bay. At first, the model is simulated driven only by surge signal from shelf wave which is calculated by ADCIRC regional surge model. The tidal signal, local hurricane wind, and deficit atmospheric pressure are not considered. In this way the contribution of shelf wave to total water rise can be approximately estimated. The second set of simulations are just the opposite. All other local forcings but the surge signals from shelf wave are used to drive the surge model and simulate the surge development within Apalachee Bay. At the open boundary, the tidal constituents are interpolated from ADCIRC tidal base. The comparison of these two simulations explicitly provides the contribution of surge signal from shelf wave and its effect on the total maximum surge.

Two nearby NOAA stations (Apalachicola and Cedar Key) have complete time series of water level measurement during Hurricane Dennis. At Shell Point, the maximum recorded surge is 2.19 m. As shown in Figure 4-19, the water level generated solely by surge signal from shelf wave is about 1 m at these stations as Hurricane Dennis moves closer to the Gulf coast. The other driving components produce another 1.2 to 1.3 m water level rise at station Apalachicola and Shell Point and 0.6 m at Cedar Key. The linearly combined water level at Apalachicola is about 2.1 m, which is very close to previous modeled highest surge from large-domain model result. This implies that simplifying the storm surge model using separate forcing has small effect on the final total surge in this case. Similar analysis is made by Morey et al. (2006) using the Naval Coastal Ocean Model (NCOM) (Martin, 2000). The maximum surge in Apalachee Bay is about 1.4 m from both local wind forcing and remote forcing. However, the deficit atmospheric pressure, tides and wave setup are not considered in the simulation. The maximum storm surges around Apalachee Bay for both test cases are shown in Figure 4-20 and Figure 4-

21. The isolated remote forcing from shelf wave by Hurricane Dennis contributes about 40% of the total high surge observed in upper Apalachee Bay depending on locations.

The above analysis further demonstrates Morey' s theory (2006) that when storm traveled nearly parallel to the shelf, it could generate surge signal from shelf wave which could significantly add additional water level rise on top of surge from local wind and deficit atmospheric pressure. The current domain for storm surge prediction by NOAA using SLOSH on the northwest coast of Florida is not enough to consider this shelf wave effect which may result in serous underestimation of storm surge and property loss. To fully incorporate this component, either the local storm surge model has to be coupled with a larger regional storm model, as was done in this study, or a larger domain has be to used directly to include enough computational area by single model simulation.

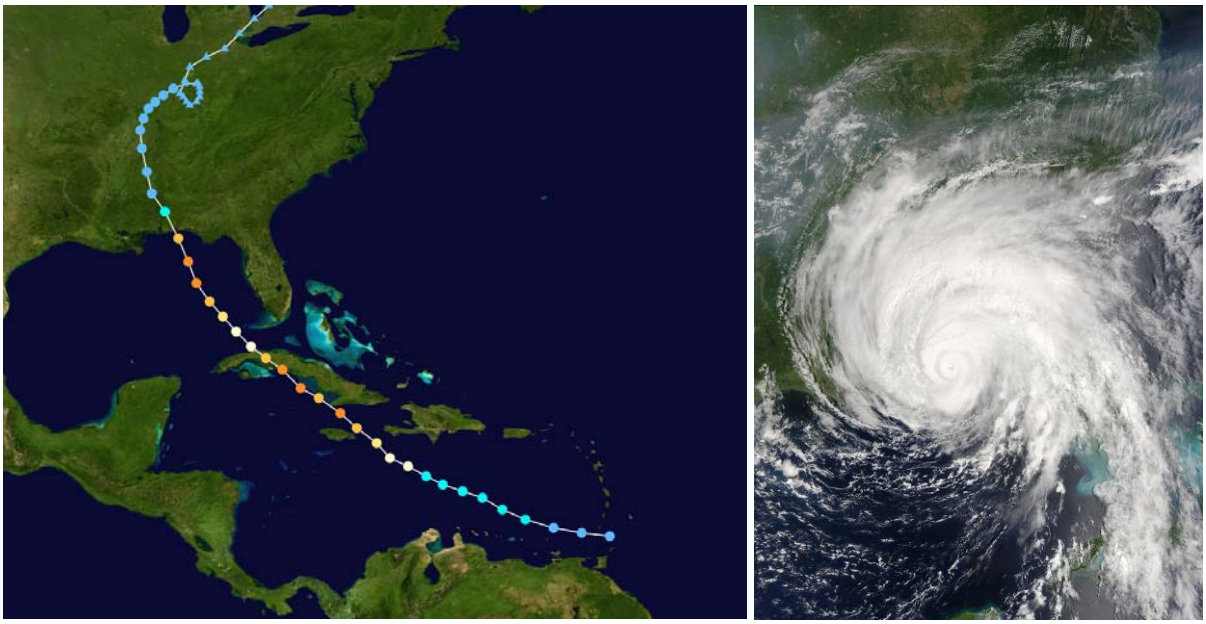

Figure 4-1. Hurricane Dennis Track (left panel) and aero photo at landfall.

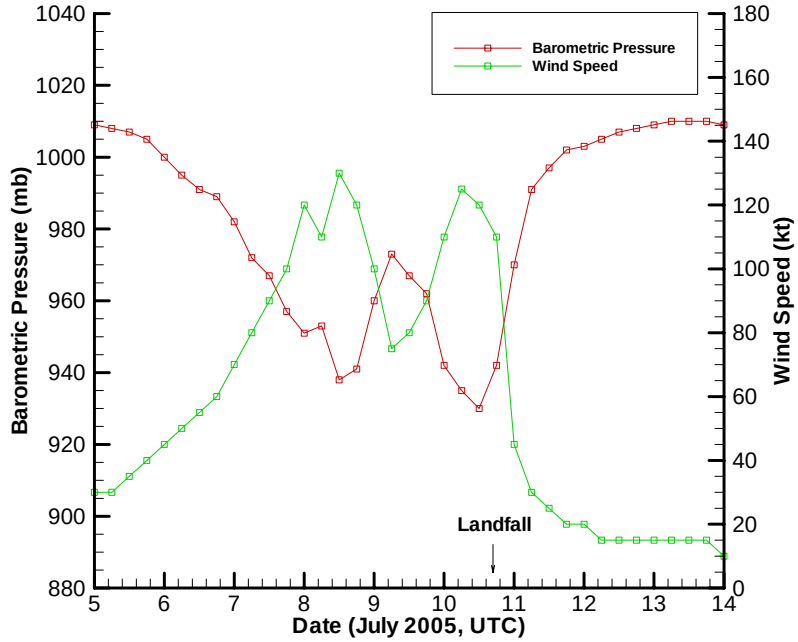

Figure 4-2. The best track central barometric pressure and wind speed history for Hurricane Dennis.

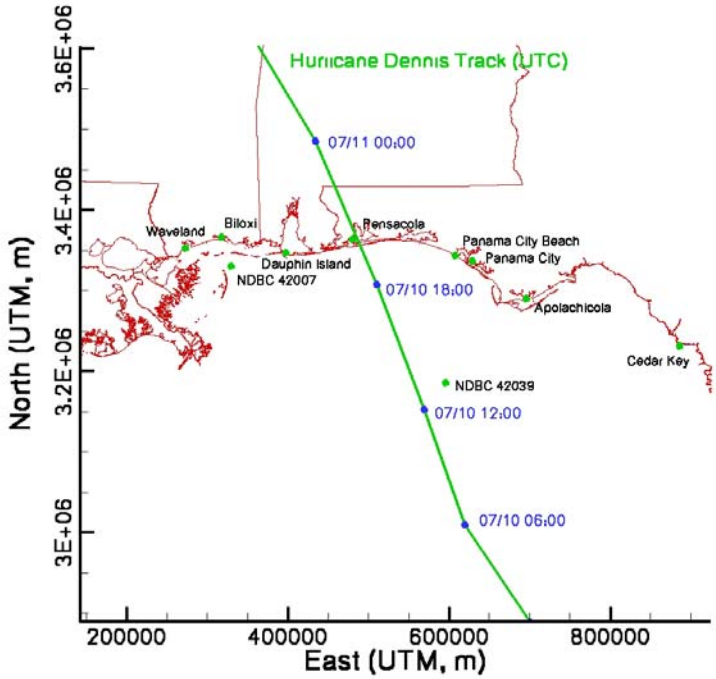

Figure 4-3. The NOAA Hurricane Dennis best track and locations of data collection stations.

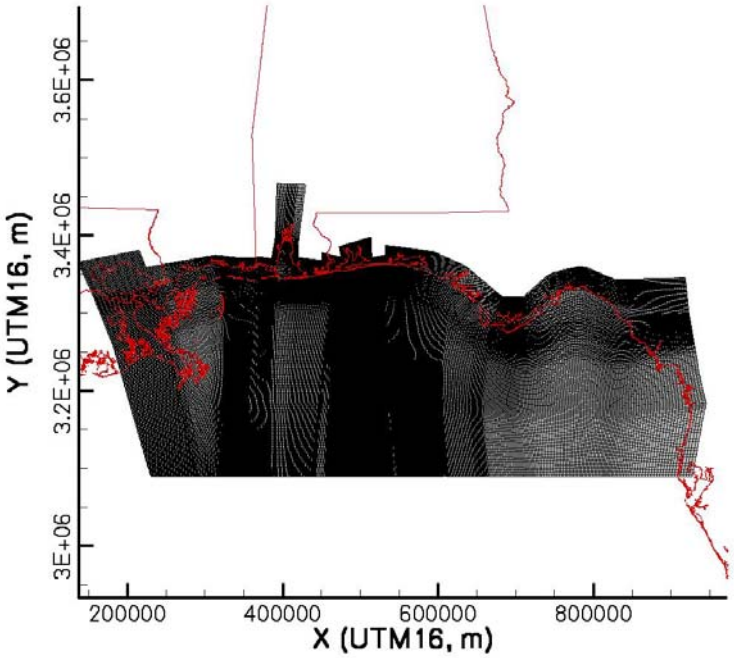

Figure 4-4. The grid system for Hurricane Dennis.

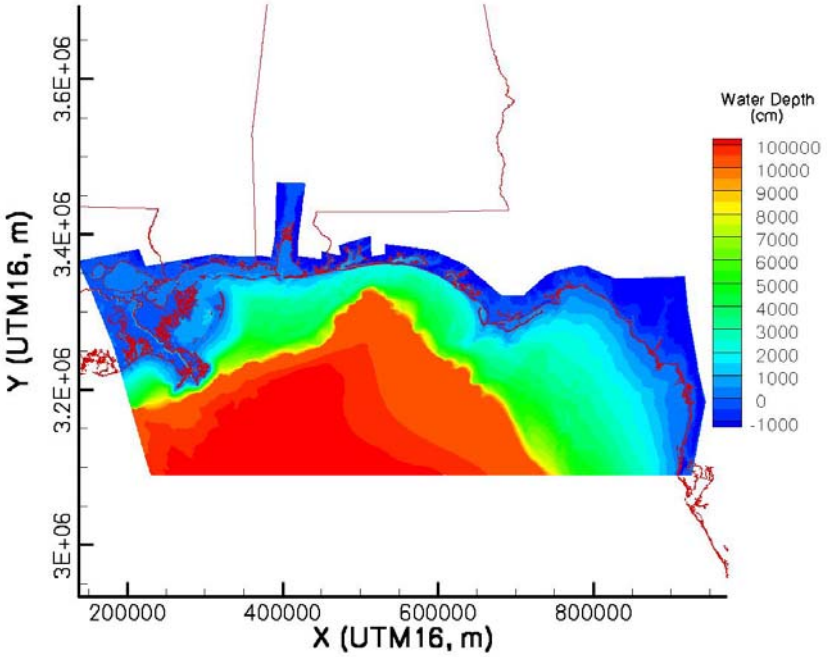

Figure 4-5. The bathymetry and topography in grid system for Hurricane Dennis.

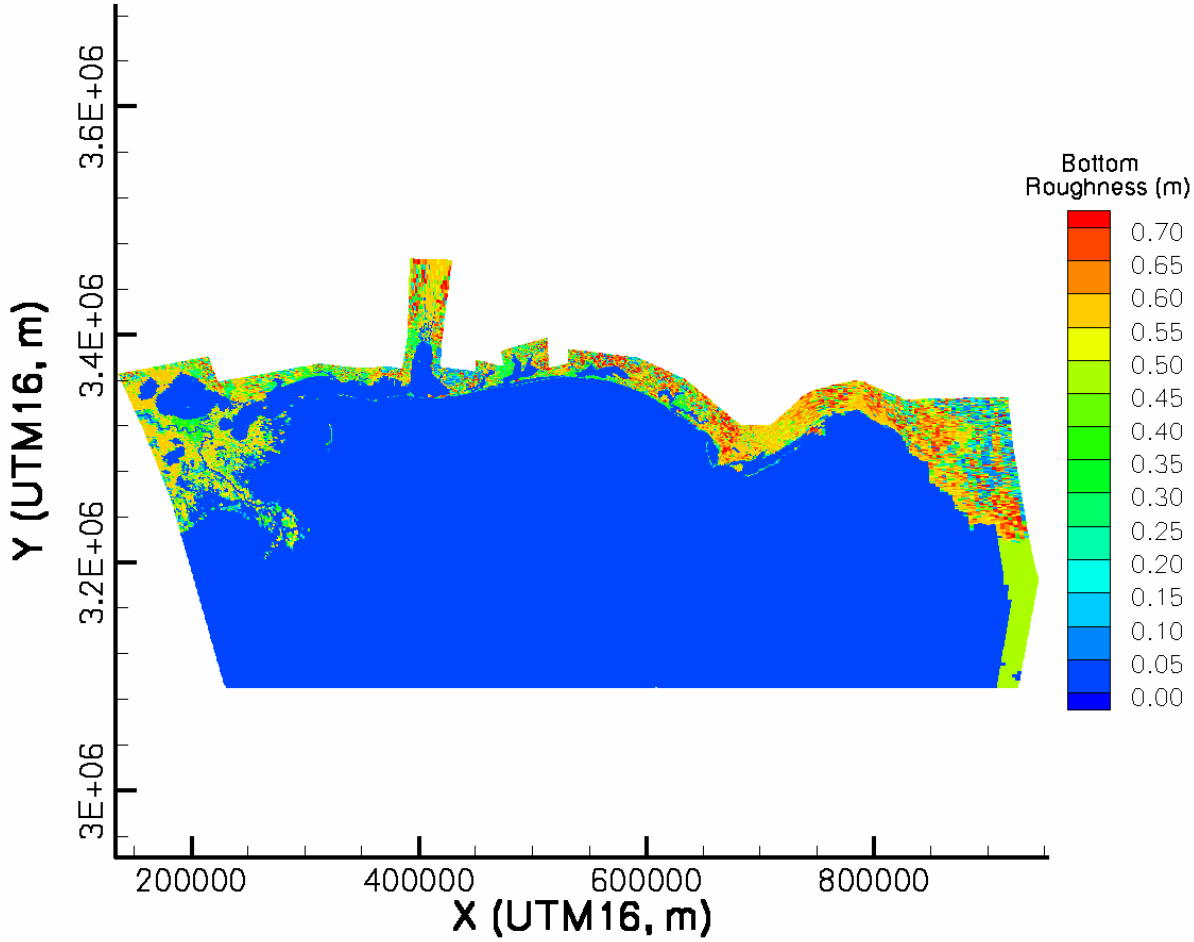

Figure 4-6. Bottom roughness of water and land for Hurricane Dennis.

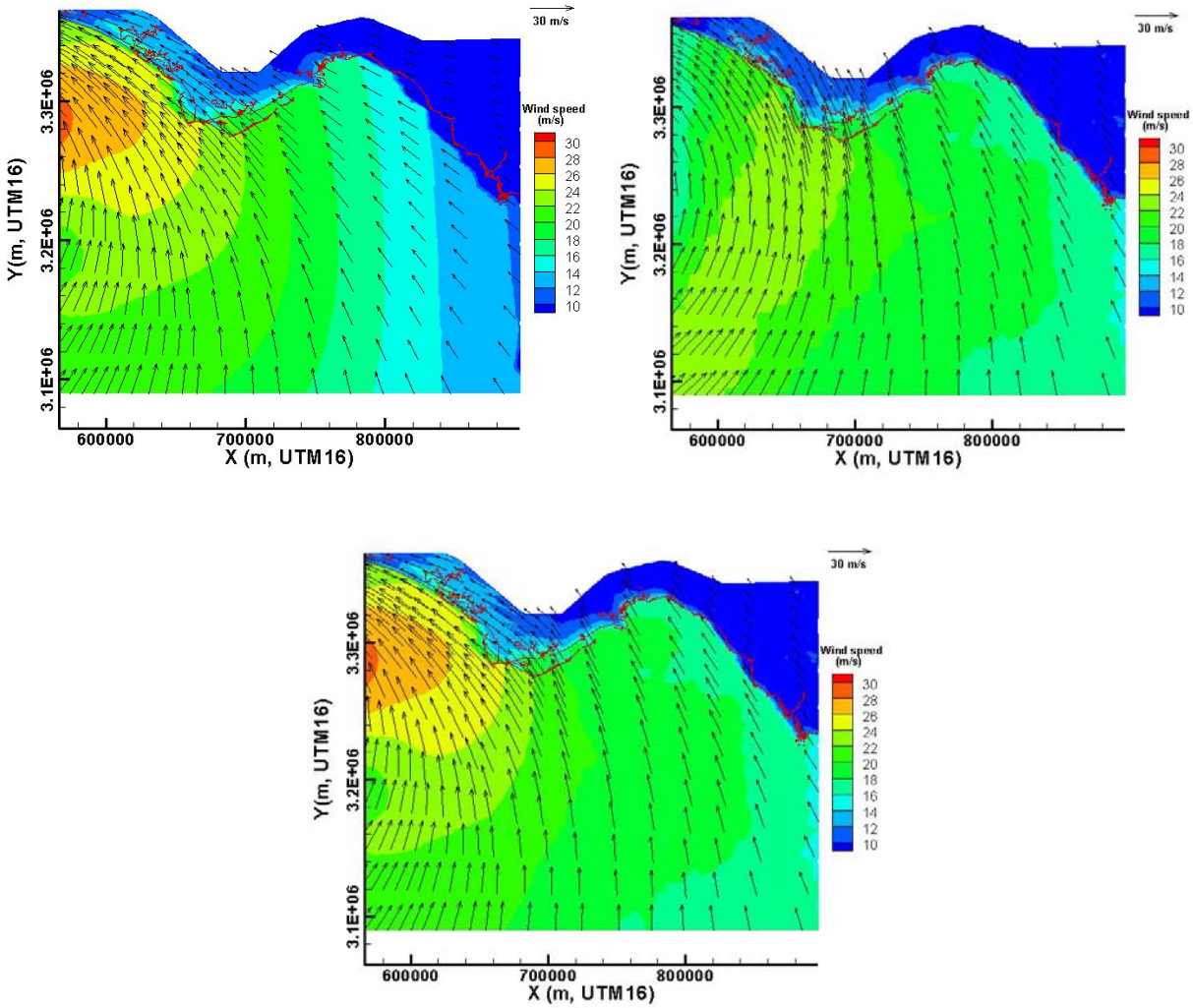

Figure 4-7. Wind field at west coast of Florida at 16:30, July 10th, 2005, UTC. The top left panel is from HRD wind; the top right panel is from WNA wind; the bottom panel is from combination of HRD and WNA wind.

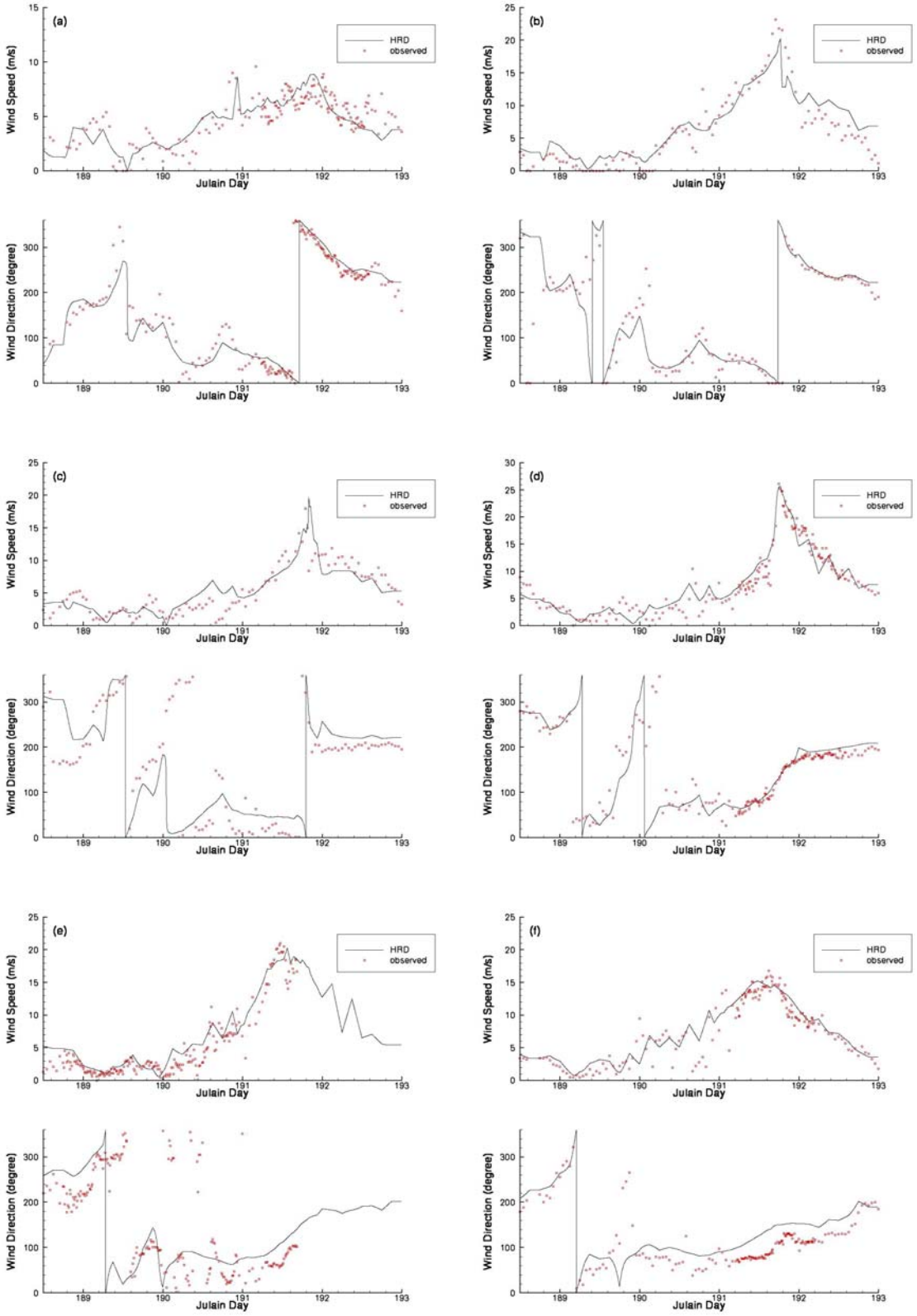

Figure 4-8. Wind comparison for Hurricane Dennis at (a). Waveland; (b). Dauphin Island; (c). Pensacola; (d). Panama City Beach; (e). Apalachicola; (f). Cedar Key.

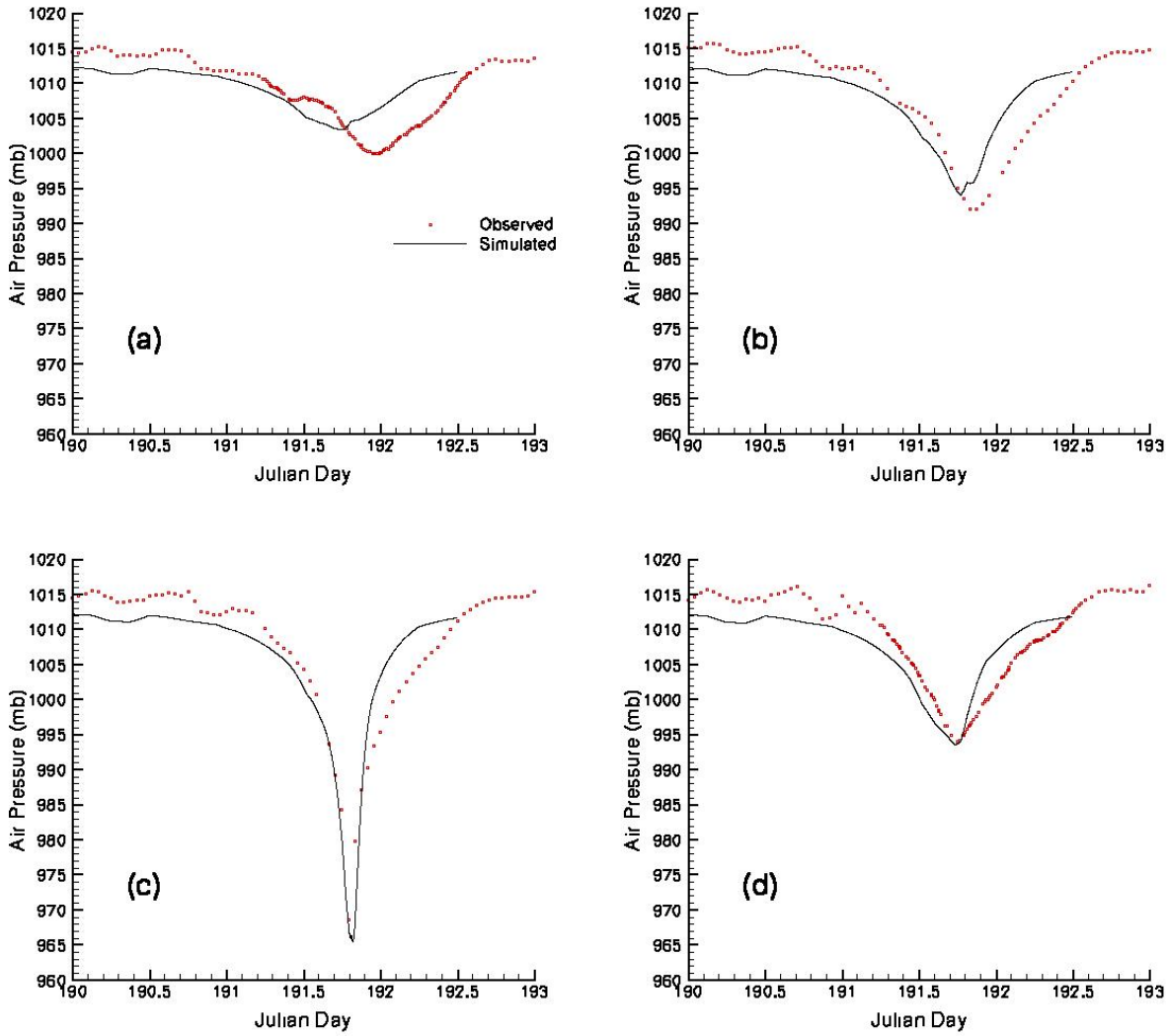

Figure 4-9. Atmospheric pressure comparison for Hurricane Dennis at (a). waveland; (b). Biloxi; (c). Pensacola; (d). Panama City Beach.

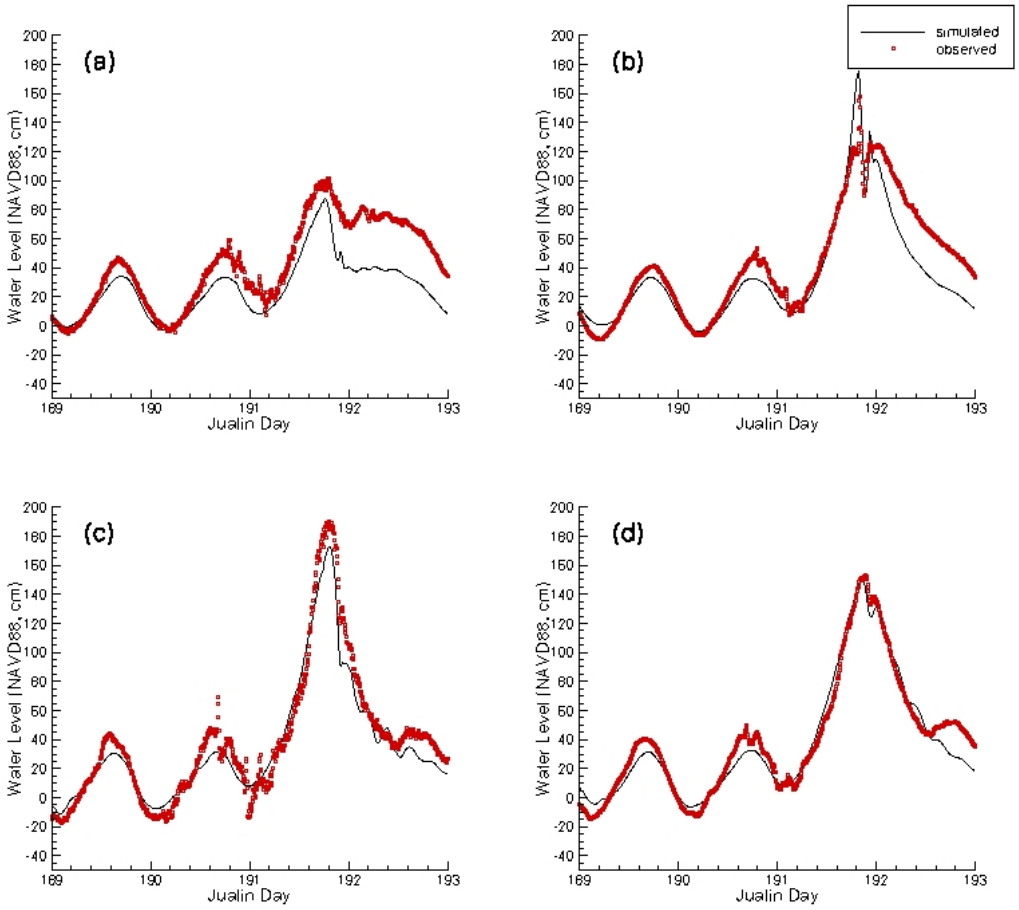

Figure 4-10. Water level comparison for Hurricane Dennis at (a). Dauphin Island; (b). Pensacola; (c). Panama City Beach; (d). Panama City; (e). Apalachicola; (f). Cedar Key; (g). Waveland. (h). Biloxi

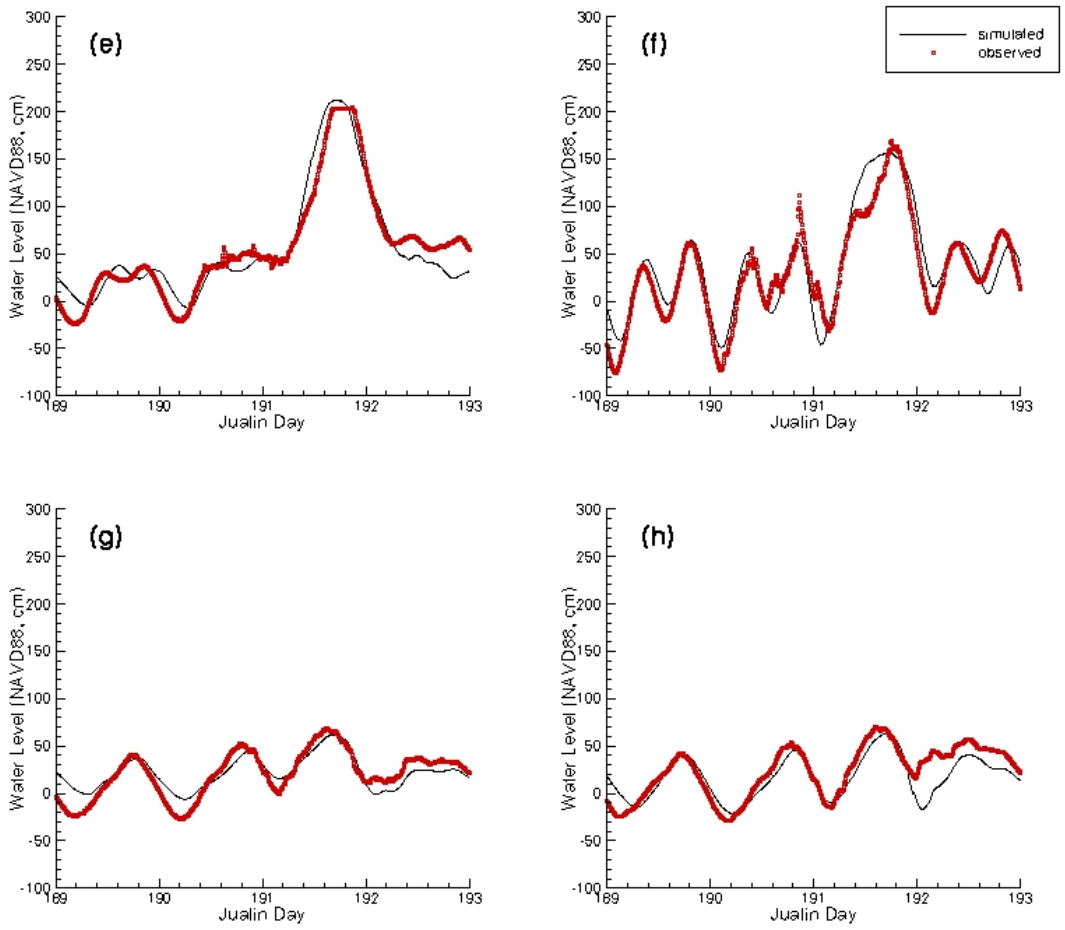

Figure 4-10 (continued)

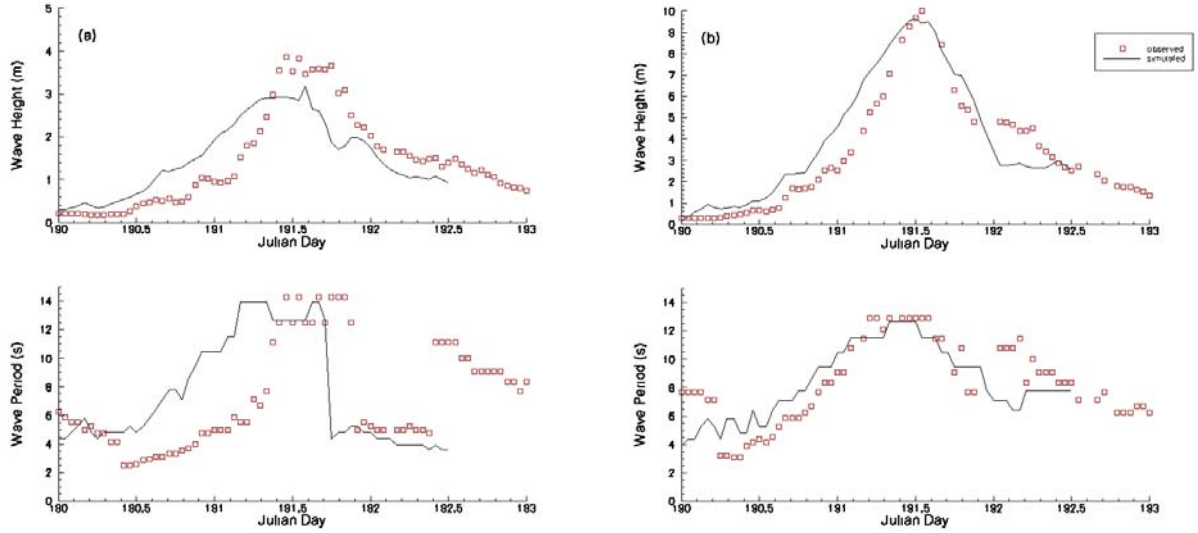

Figure 4-11. Wave comparison for Hurricane Dennis at (a). 42007; (b). 42037.

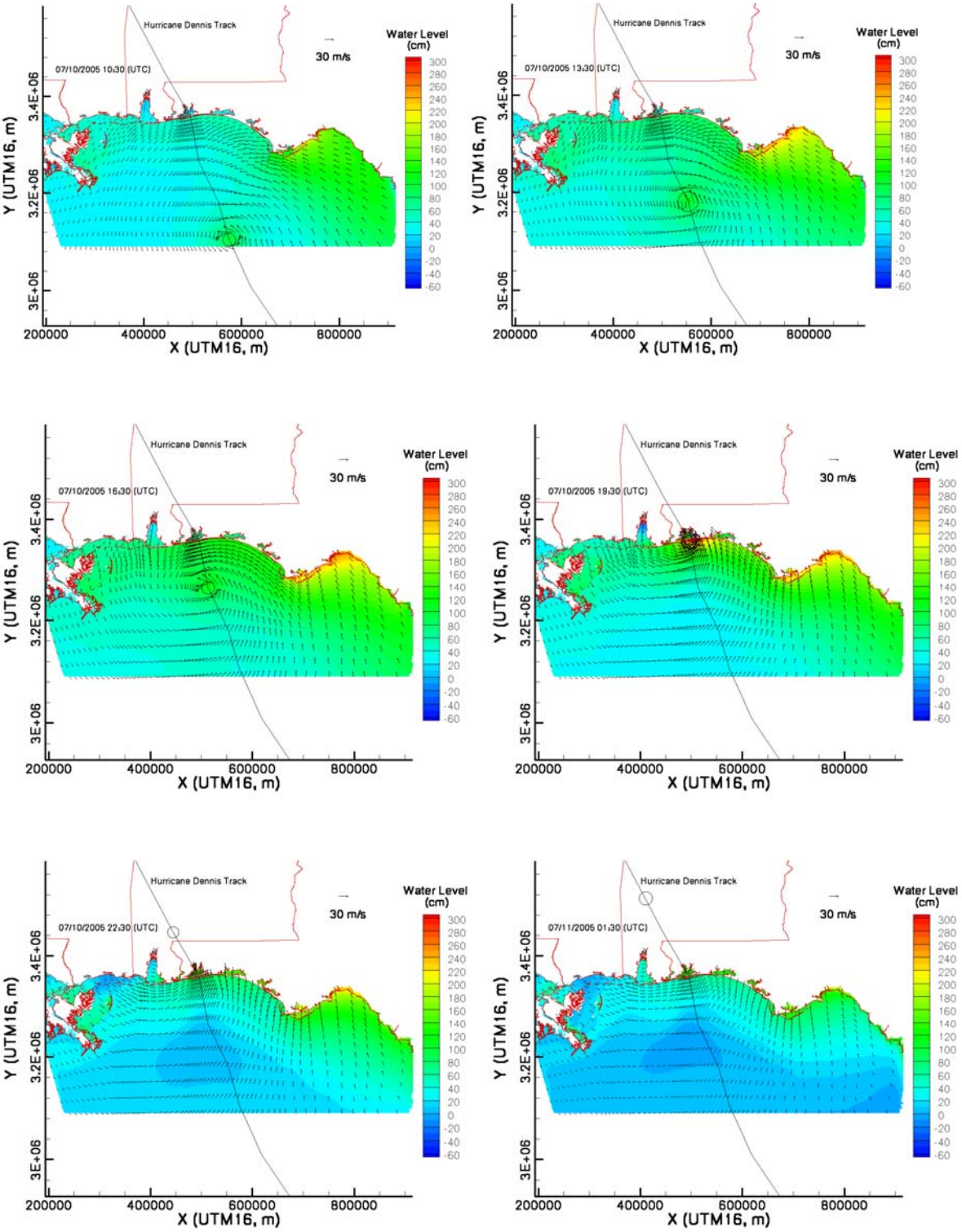

Figure 4-12. Snapshots of water level for Hurricane Dennis before and after landfall.

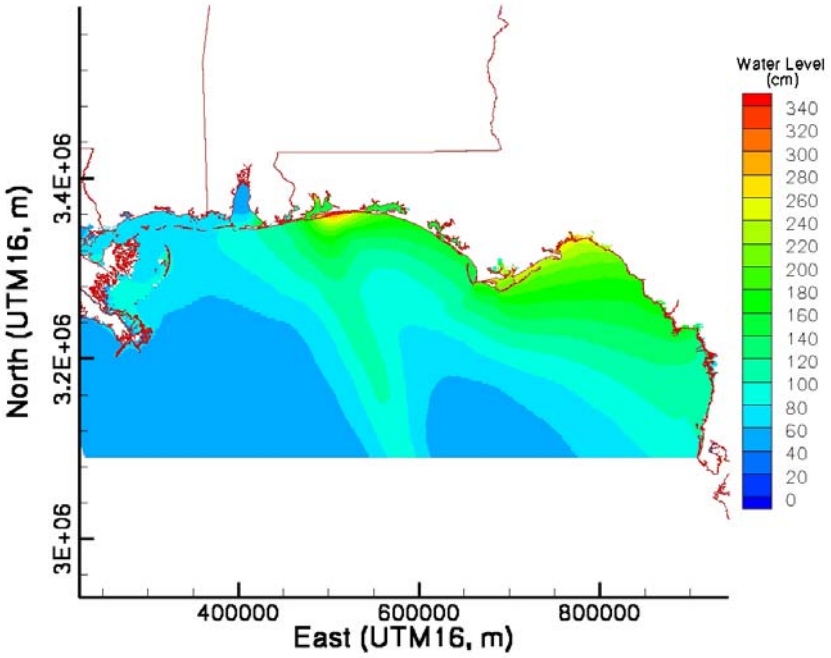

Figure 4-13. Envelop of High Water from Hurricane Dennis simulation using CH3D-SSMS.

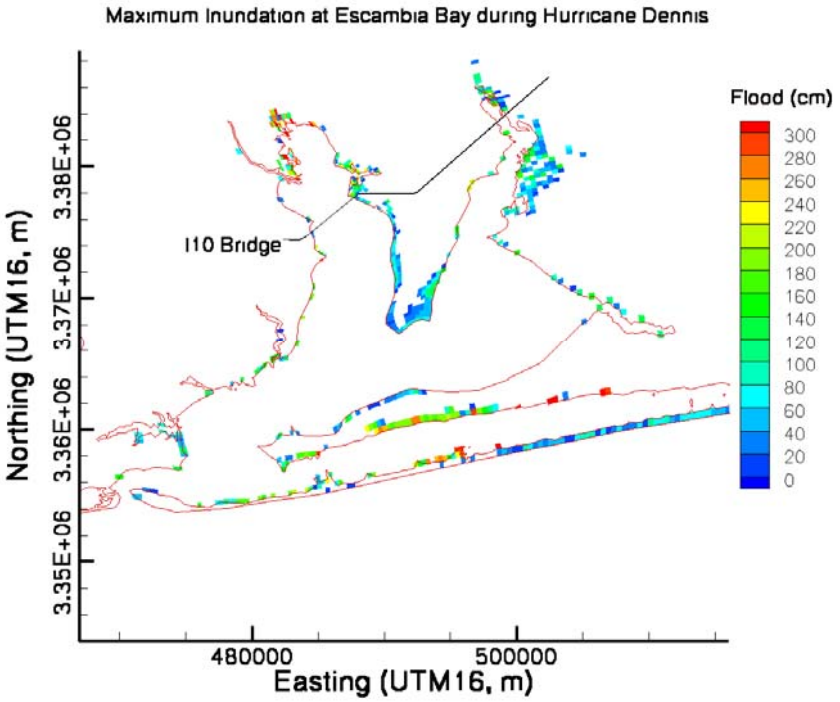

Figure 4-14. Maximum Inundation around Escambia Bay by Hurricane Dennis.

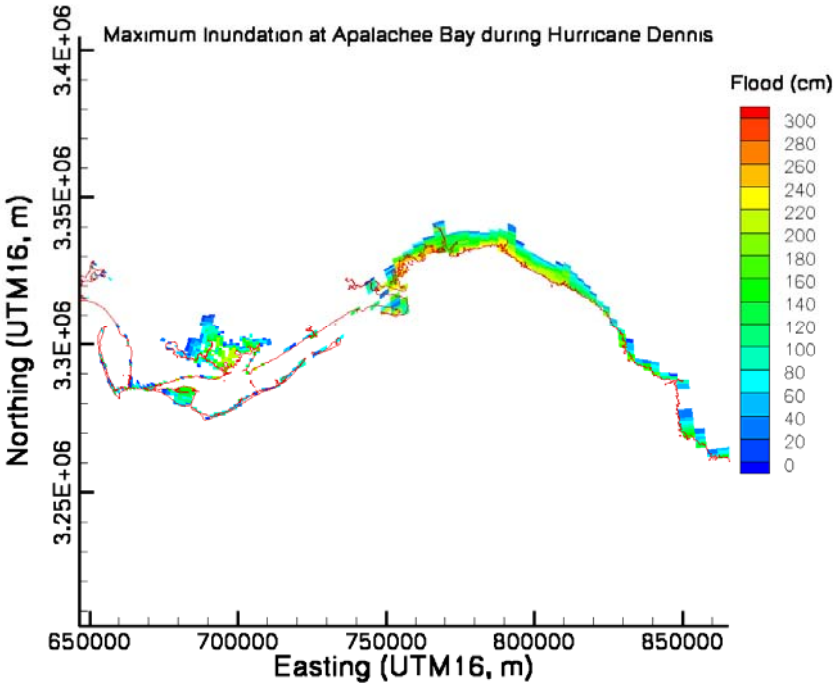

Figure 4-15. Maximum Inundation around Apalachee Bay by Hurricane Dennis.

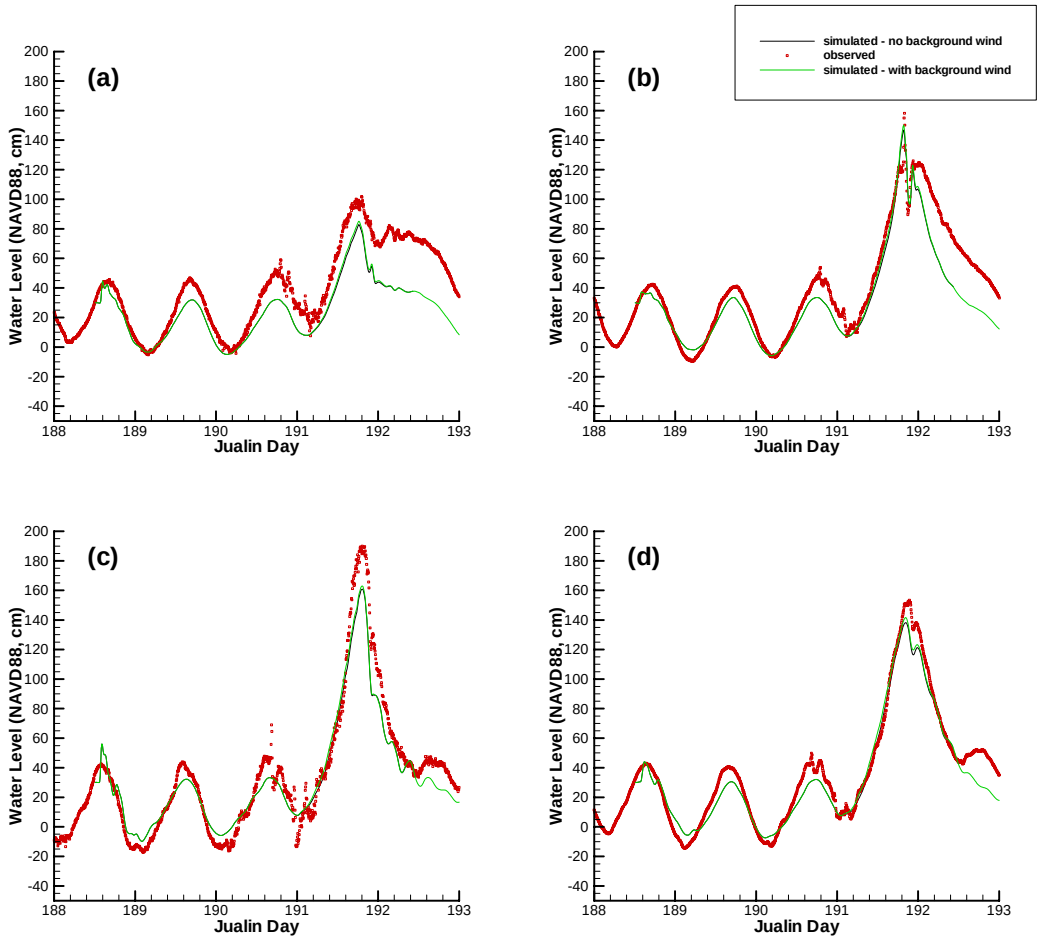

Figure 4-16. Water level comparison for Hurricane Dennis without wave effect at (a). Dauphin Island; (b). Pensacola; (c). Panama City Beach; (d). Panama City: (e). Apalachicola; (f). Cedar Key. (g). Waveland. (h). Biloxi

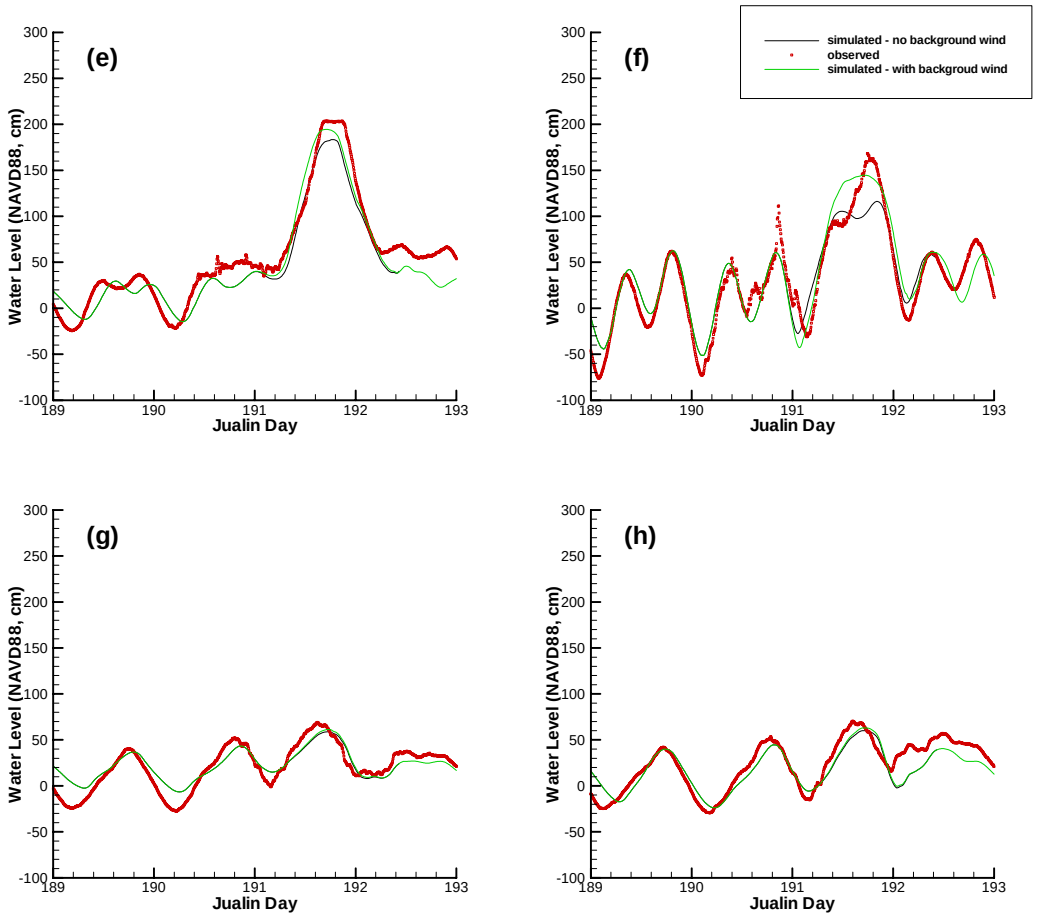

Figure 4-16 (continued).

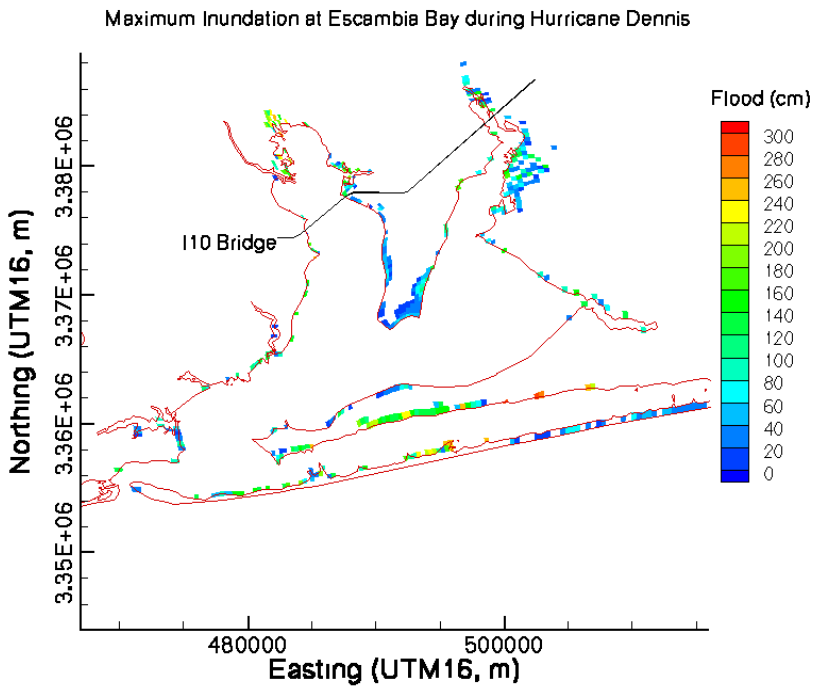

Figure 4-17. Maximum Inundation around Escambia Bay by Hurricane Dennis without wave effect.

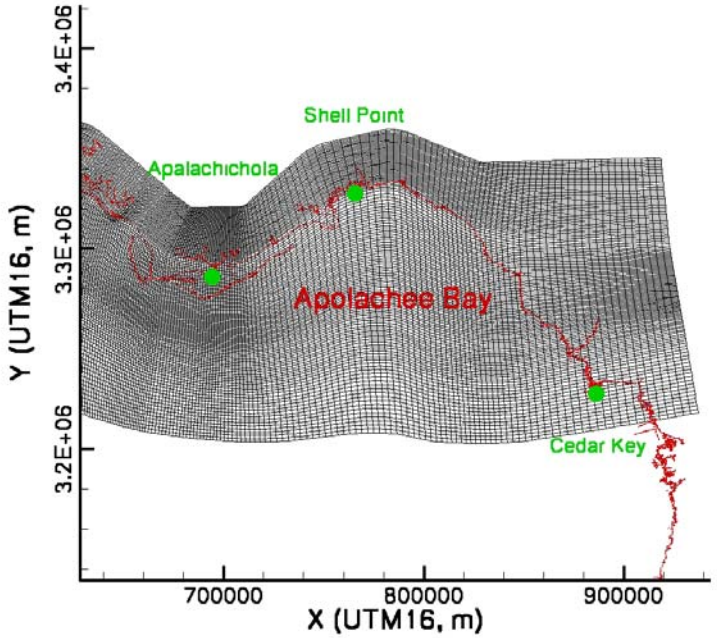

Figure 4-18. Reduced grid system for Hurricane Dennis simulation.

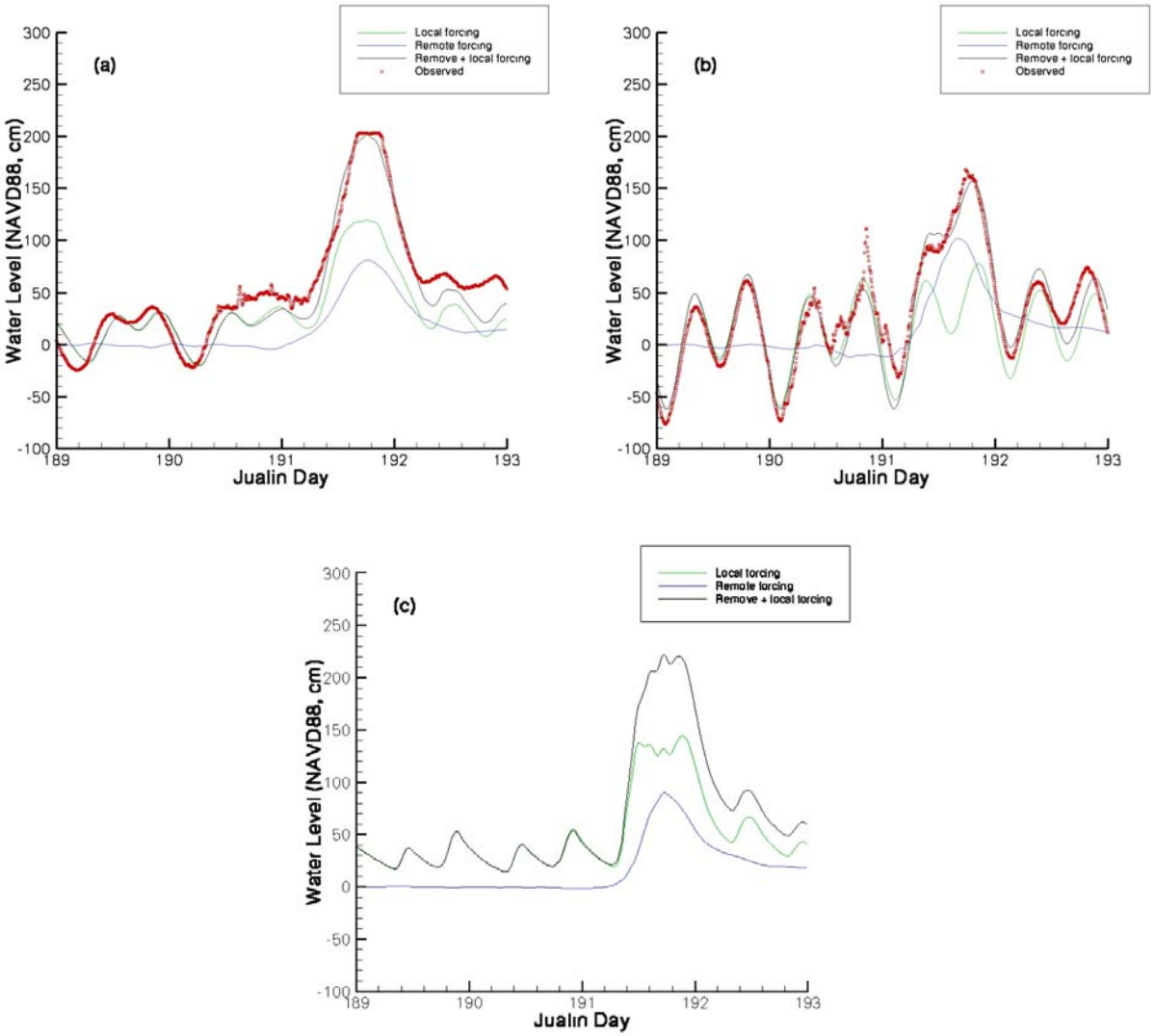

Figure 4-19 Water level comparison for simulations by local forcing, remote forcing and both for Hurricane Dennis at station: (a). Apalachicola; (b). Cedar Key; (c). Shell Point

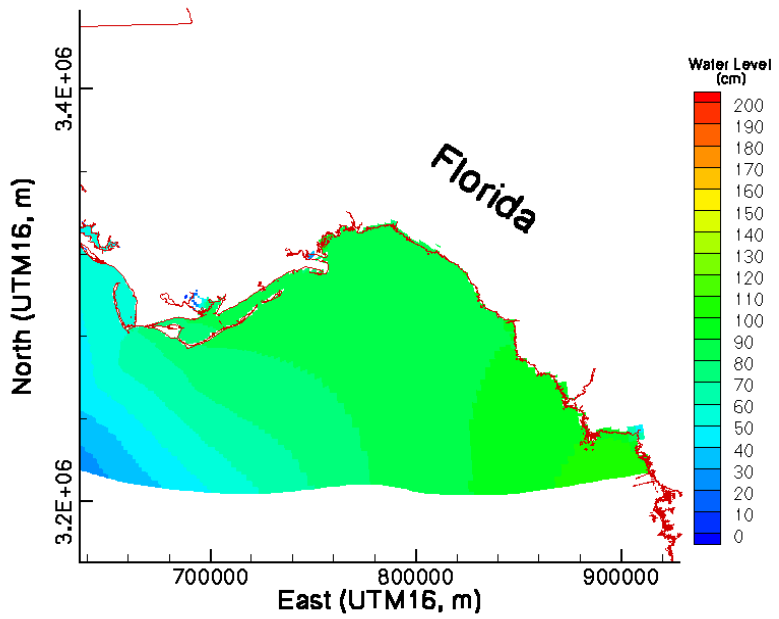

Figure 4-20. Maximum water level from simulation by remote forcing for Hurricane Dennis

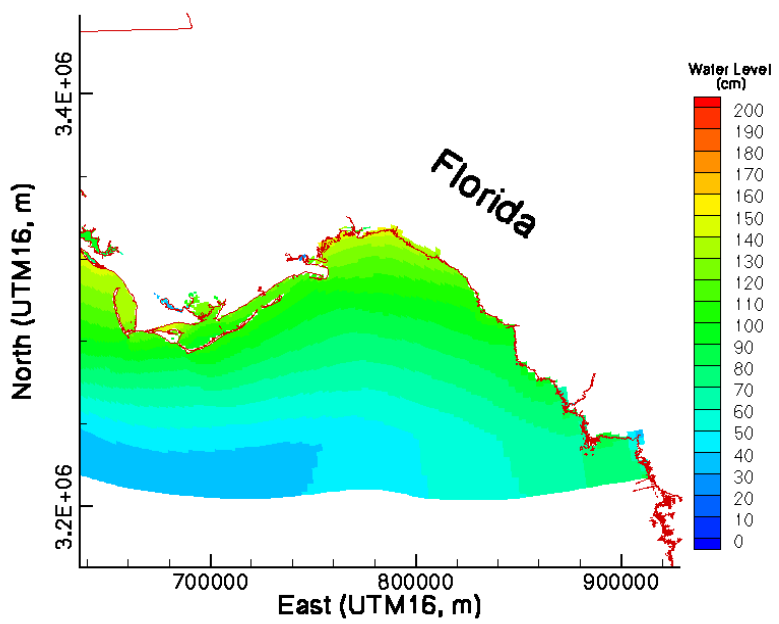

Figure 4-21. Maximum water level from simulation by local forcing for Hurricane Dennis

Table 4-1. Observe Data Stations of Hurricane Dennis

Data Source	Station Name	Station ID	Station Location (Long/Lat)	Data Type			
				Wind	Water Level	Wave	Atmospheric pressure
NOAA	Pensacola	8729840	-88.2117/30.4033	x	x		x
	Dauphin Island	8735180	-88.0733/30.2483	x	x		x
	Panama City	8729108	-85.6667/30.1517		x		
	Panama City Beach	8729210	-85.8800/30.2133	x	x		x
	Biloxi	8744117	-88.9033/30.4117		x		
	Waveland	8747766	-89.3667/30.2817	x	x		x
	Apolachicola	8760922	-84.9817/29.7267	x	x		x
	Cedar Key	8761724	-83.0317/29.1350	x	x		x
	Port Fourchon	8762075	-89.4067/28.9317	x	x		
NDBC	Mobile South	42007	-88.7686/30.0903	x		x	
	PEnsacola	42039	-86.0214/28.7939	x		x	

CHAPTER 5
SUMMARY AND CONCLUSIONS

Summary

In this dissertation, two major hurricanes, Ivan and Dennis, were simulated using CH3D Storm Surge Modeling System – CH3D-SSMS. The simulated wind, wave, water level and High Water Marks were validated against observed data. The wave forces on the I-10 Bridge over Escambia Bay were calculated to analyze the mechanism that caused the collapse of the bridge. The inundation maps for both hurricanes were presented to assess the extent of flooding in the coastal zone. A set of sensitivity tests were made on a few major parameters for the Hurricane Ivan simulation to determine the relative importance in storm surge simulation. Risk analysis simulations were conducted by varying hurricane intensity, size, speed, and direction of approach and landfall locations to study the various surge responses in strong storm events like Hurricane Ivan. A ranking system was then developed for assessing the vulnerability of coastal highways and bridges to storm surge and wave damages in extreme hurricanes like Ivan.

The first chapter gave a brief review of current development in storm surge modeling. Various wind, wave, and surge models were discussed with their merits and disadvantages. With recent increases in the loss of money and lives, more effort has been made to develop robust storm surge forecasting and hind-casting systems to accurately predict and assess hurricane-caused surges and provide useful information to reduce coastal flooding and human loss. CH3D-SSMS is one of these models that have been validated for several hurricanes and is under further development.

Chapter Two provides the detailed description of physical processes in CH3D-SSMS for storm surge simulation. The main mechanisms in the model include astronomical tide, wind stress, barometric pressure, and wave setup. The interactive coupling system dynamically

couples regional surge model – ADCIRC, local wave model SWAN, and local surge model CH3D to simulate coastal surge using high resolution bathymetry and topography data. CH3D-SSMS was validated by analytical solutions and has been successfully used to simulate Hurricanes Isabel (2003), Charley (2004), Francis (2004) and Wilma (2005) (Alymov, 2005; Sheng et al., 2005) and Hurricanes Ivan (2004) and Dennis (2005) in this study.

The CH3D-SSMS integrated modeling system is applied to simulate storm surge and waves during Hurricane Ivan and Hurricane Dennis to study hurricane storm surge reaction and potential for the Northeast Gulf coasts, including the Florida Panhandle, Alabama, and Mississippi. A detailed curvilinear, boundary-fitted grid system focusing on the Escambia Bay, FL, was developed using high resolution bathymetry and topography data from GEODAS and SEAMLESS, USGS. The CH3D-SSMS, with the capability of flooding and drying, is able to simulate both surges and waves by dynamically coupling with a local wave model SWAN (Holthuijsen et al., 2000). The coupled modeling system receives water level information along open boundaries of the model domain from a basin-scale storm surge model ADCIRC (Luettich et al., 1992) and a basin scale wave model WAVEWATCH-III (Tolman, 1999). The HRD wind of NOAA and the WNA wind from NCEP/NOAA are applied in the model with consideration of land reduction effect. The Lagrangian interpolation technique is used to improve interpolation accuracy between wind snapshots, especially around hurricane centers. The analytical Holland model is used to generate atmospheric pressure field for the model based on NHC best hurricane track.

In chapter three, the CH3D-SSMS is successfully calibrated and validated for Hurricane Ivan (2004) by comparing the results of the simulation to observed data. Ivan is a large scale, high intensity hurricane that caused significant flooding and damage at the coastal region. The

highest surge of over 4 m was observed at the north end of Escambia Bay and is captured by CH3D-SSMS. The time series of wind, atmospheric pressure, and storm surge at multiple NOAA stations were successfully compared with simulated water level, both in magnitude and trend of surge development. The maximum surge errors are around 10% at most stations. In addition, the simulated highest surges also agree well with several measured HWMs from USGS near the Pensacola Bay area. The simulated time series of significant wave height, peak wave period, and mean wave direction by SWAN agreed well with available observed data at the offshore station Mobile South. The extent of flooding during Hurricane Ivan was described in an inundation map. The most flooded domains were found to the east of Pensacola Bay and to the east of Blackwater Bay. The comparisons of simulated storm surge are similar between 3D model and 2D model. However, the 3D model produces much more accurate flow field, especially when pressure gradient is in the opposite direction with wind stress which causes stratified flow in the vertical direction. The surges of the Hurricane Ivan simulation illustrate that CH3D-SSMS is able to accurately simulate storm surge with a good set of bathymetry/topography, accurate wind data, and water level at open boundary with minimal calibration.

With validated surge and wave in Escambia Bay, the wave loads were calculated on the I-10 Bridge deck in both horizontal and vertical direction during Hurricane Ivan. The component of wave force includes buoyancy, drag force, inertial force, and slamming force. The analysis revealed that, on top of high surge, the wave crest is able to attack the bridge with enough strength to break the connection force and deck weight and push bridge deck into water. The slamming force is the major component of the total vertical force. The sensitivity test implied that the wave force on bridge deck is very sensitive to surge height. With slightly decreased surge levels, the wave force could be significantly reduced to keep the bridge undamaged.

Over ten sensitivity tests were made for Hurricane Ivan to determine the roles various important parameters play in storm surge simulation. These parameters include wind, land reduction effect on wind, deficit atmospheric pressure, tidal open boundary conditions, bottom friction, and wave setup effect. Four kinds of wind were considered including HRD wind, WNA wind, WINDGEN wind, and analytical Holland wind. The results showed that simulated storm surge is very sensitive to wind field used in the model. Different simulated water levels were obtained from each of the four wind fields. At some individual stations the difference is even bigger than 50% of total surge. Land reduction effect on wind is important for domains where wind blow from inland. The selection of tide level at open boundary has small effect on simulated surge as tidal amplitude is relatively small during Hurricane Ivan. Predicted tide produced slightly better surge than that from using ADCIRC tidal constituents. However, tidal boundary could be an important factor when hurricanes arrive together with high tide. The consideration of deficit atmospheric pressure added about additional seventy centimeters along the hurricane track and reduced exponentially to a few centimeters at remote domain away from the track. The wave effect on surge is also important. The wave setup contributed up to seventy centimeters inside Escambia Bay where the highest surge was observed.

Risk analysis tests were made for Hurricane Ivan by varying hurricane landfall location, intensity, size, speed, and direction of approach. The analytical Holland wind model is used as the driving force. It was found that all factors are able to cause very significant local surge changes within Pensacola Bay, Escambia Bay, and Mobile Bay. A ranking system was developed to assess the vulnerability of coastal highways and bridges along the northeast gulf coasts based on high surge level. The I-10 Bridge over Escambia Bay and The I-10 Bridge over Blackwater Bay are the most vulnerable ones based on total of 12 risk analysis tests. The bridge

of US98 and the bridge of SR281 over Pensacola Bay are the second group that could be damaged in extreme hurricanes like Ivan. The I-10 Bridge over north Mobile Bay is in danger only for case when the track of Ivan is shifted 50 kms from the original track, thus significantly large surges near north Mobile Bay may cause severe flooding and potential damage to bridges. Bridges and highways located further either west or east are relatively safe in storms with similar intensity and track like Ivan. No severe damage is observed from risk analysis tests at those locations.

In chapter four, CH3D-SSMS was applied to simulate storm surges and waves during Hurricane Dennis (2005). Compared to Hurricane Ivan, Dennis had similar track and landfall location but with weaker intensity slightly to the east, faster moving speed, and a more compact size. As a result the storm surged generated is lower and the damage caused by Dennis is not as severe as Ivan, the maximum observed surge is about 2-3 m. In order to simulate Hurricane Dennis, the grid system for Hurricane Ivan was extended extensively to the northwest Florida coast to include more storm-effected domain. Extra bathymetry, topography, and land use data were downloaded and incorporated into the grid. Similar procedures for the preparation of wind, deficit atmosphere atmospheric pressure, water level, and wave at open boundaries described in Hurricane Ivan were repeated for Dennis.

The simulation of the storm surge was quite successful for Hurricane Dennis. The simulated water level at multiple NOAA stations over 300 miles of northeast Gulf coast, from Cedar Key, FL to Waveland, MS, agreed well with observations. The difference of highest surge between simulation and observation is around 10%. In addition, both simulated wind and atmospheric pressure at most stations compared reasonably well with measurement. The waves simulated by SWAN were successfully validated at a couple of offshore stations during

Hurricane Dennis. The inundation maps showed that serious flooding occurred at northwest Florida Apalachicola Bay and inside Pensacola Bay. The high storm surge in Apalachee Bay is caused by both the shelf waves and local wind setup during Hurricane Dennis, each of them contributes about 50% of the total surge.

The current grid used in CH3D-SSMS is a structured curvilinear grid system. It could resolve reasonably well of interested inlets, shoreline, and other detailed morphological features for particular interested area. However, the nature of structured grid requires similar resolution along both the X and Y coordinate directions, which leads to quick increase of the total number of cells. For the Hurricanes Ivan and Dennis simulations, the resolution in open water is about 1 km and 100 m within Pensacola Bay, FL. This is fairly good for open water circulation and over land inundation simulation. The unstructured grid is able to resolve detailed shoreline with finer elements and open water with coarser elements simultaneously to keep the overall number of cells relatively low. As an example, the finite element model ADCIRC uses an unstructured grid to represent the irregular shoreline. However, its computation speed is limited by a stringent stability condition associated with the "explicit" numerical scheme for wave propagation and nonlinear advection. Very small time steps have to be used for very fine grid, resulting in significantly increased simulation time. The UnTRIM model uses semi-implicit time integration and an Eulerian-Lagrangian method for to allow larger time step to be used without badly reducing accuracy. Compared to structured models, the unstructured model requires much more effort to generate orthogonal unstructured grids.

For storm surge simulation in this study (Ivan and Dennis), the most sensitive factor is the wind field used in the model as wind shear stress is proportional to square of wind speed. Various winds could produce quite different surges. Wind drag coefficients have a similar effect

on wind stress but with a linear relationship. The bottom friction coefficient (Manning's n for 2D and bottom roughness for 3D) is also an important factor. This is especially true for shallow water. For the Hurricane Ivan simulation, both spatially-vary Manning's coefficients between 0.015-0.025 based on bottom sand characteristics and a constant Manning's coefficient of 0.02 were used. The simulated storm surge used was improved for spatial-varying case but the improvement is not very big. The effect of using a different method of wind field interpolation is limited to domains close to the hurricane center. Therefore, if the study location is close to a hurricane track, it is important to use Lagrangian interpolation to obtain more accurate wind fields. The storm surge is directly related to the accuracy of tide simulation. The same error from tide simulation would be transferred to total surge simulation. For Hurricane Ivan, the amount of error is about 10 cm. Storm surge simulation is also sensitive to grid resolution, especially in a shallow bay or lagoon. When an important shoreline feature, such as an inlet, can not be represented well, large error can be found in storm surge simulation. The water level is not sensitive to river flow. For the Ivan simulation, the surge barely changed if the Mississippi River discharge is included in the simulation. The model time step is mainly determined by advection stability criteria. The simulated surge varied slightly for different time steps used. For Hurricane Ivan/Dennis simulation, 60 second time step and 10 second time step were used for CH3D-SSMS 2D and 3D simulation, respectively. CH3D treats the propagation of surface gravity wave with a "semi-implicit" scheme as opposed to the "explicit" scheme of ADCIRC, hence a much less stringent time step limit is required compared to ADCIRC.

To accurately simulate storm surge, three major things have to be prepared well: a large scale high resolution grid with a good set of bathymetry/topography data, a robust storm surge model, and accurate description of driving forces. After preparing the grid, a sensitivity test is

made first to determine bottom roughness and tidal open boundary. During this process, the possible errors related to grid and tidal open boundaries are identified and removed. Then, each component of driving force: wind, atmospheric pressure, surge at open boundaries, and waves should be tested and validated separately. Among them, wind is the most complicated factor that involves selection of wind field, wind spatial and temporal interpolation, and consideration of land reduction effect. In general, HRD wind with Langrangian temporal interpolation and inclusion of land reduction effect provides the best fit of field measurement. When HRD wind is not available, WNA can be used to fill the gap. Atmospheric pressure is calculated based on best track and hurricane strength using the Holland analytical model. Surges at open boundaries are obtained by coupling with the ADCIRC regional surge model. Waves are provided by the SWAN wave model. The error from open boundaries can be reduced by extending the computational domain, but it also demands more computing resource at the same time. Consequently, these two factors are compromised to consider the grid system with large domain but acceptable computing efficiency.

From the Hurricane Ivan simulation, it is found that estuaries play an important role in affecting the storm surge and inundation in coastal bays or lagoons. The shallow water induced larger surge and delayed the peak of the surge. The maximum simulated storm surge at the north rim of Pensacola Bay is about 1.7 m higher than the simulated surge at mouth of Pensacola Bay with 1.5 hour delay. As the storm surge advanced within the bay, water levels gradually increased and were maximized at the north end. The abnormally elevated water caused extensive flooding at the low-land areas along the bay coast zone. The effect on the storm surge and inundation from estuaries is normally small for open water, coastal shores, and barriers islands. The affected zone is limited to locations around the inlet between the bay and open water.

As for model efficiency, the computational time step for 2D simulation is around 1-2s/time step without coupling with the SWAN wave model for the Hurricane Ivan and Hurricane Dennis simulation. As a result, a 6-day storm surge simulation takes about 3-6 hours to finish. This is fast enough for both forecasting and hind casting simulations. However, much longer time is needed if the SWAN wave model is added. If the SWAN simulation is made every one hour, which is sufficient to keep accuracy and efficiency, then the total simulation time is at least a few times more. For other grid systems with different grid resolution and total number of grid cells, this time would change accordingly.

Besides high resolution grid and robust model, it is the forcing inputs that make the difference on storm surge simulations. These include bottom roughness, water level (tide and surge) at open boundary, wind, and deficit atmospheric pressure. The bottom roughness and tide at open boundaries must be determined first from calibration test. There is no certain rule what tide is better. ADCIRC tidal base may perform well for one particular period but may also behave badly at some other time. For one particular time, preliminary simulation is necessary to select from interpolated measured water levels and ADCIRC tidal constituents based on performance. For the same reason, wind is selected from different models by comparing measured data at stations.

For storm surge simulation, the advantages of 3D mode over 2D mode include resolved current structure in the vertical direction, more correct bottom friction and more accurate nonlinear, diffusion and Coriolis terms. The 3D model results have shown improved simulated storm surge for the Hurricane Ivan using CH3D-SSMS. However, because of the mode splitting technique used in 3D mode, the bottom friction has to be calculated in explicit mode, which requires reduced time step to keep numerical stability. For Hurricane Ivan simulation, as small as

10 second is used in 3D model compared to 60 second in 2D model. In addition, solving for velocities in each vertical layers also require addition computing time. Therefore, implementation of 3D mode in storm surge simulation is somehow traded off by the significantly increased simulation time. Under some circumstances, the 2D model might be a better choice because of its reasonably good water level simulation and efficiency, such as storm surge forecast simulation.

There are two methodologies implemented in CH3D-SSMS to calculate wave enhanced bottom stress. The first one is the Grant and Madsen (1979) theory described in a simplified form by Signell et al. (1990) and second one is the lookup table produced from a one-dimensional wave-current bottom boundary layer model (Sheng and Villaret, 1989). When applied to the Hurricane Ivan, both methods showed similar but very limited effects on simulated storm surge. Inclusion of wave enhanced bottom stress normally reduced the simulated water level by a few centimeters.

Conclusions

The main conclusions drawn from this study are summarized as followings:

1. CH3D-SSMS was successfully calibrated and validated for Hurricane Ivan and Hurricane Dennis. The simulated highest surge is around 10% error at most stations.

2. The consideration of land reduction on hurricane wind could significantly improve surge simulation at local stations with wind coming from inland.

3. Wind forcing is the primary factor in storm surge modeling.

4. The water level at open boundary, deficit atmospheric pressure, bottom friction and wave setup are all important for storm surge simulation.

5. Extensive waves on top of high surge caused the I-10 Bridge over Escambia Bay collapse during Hurricane Ivan.

6. Wave loads on bridge deck is very sensitive to surge level, a slightly decreased surge may considerably reduce wave loads.

7. A series of risk analyses were conducted to assess storm surge response by varying hurricane parameters of intensity, size, landfall location, speed, and direction of approach according to Hurricane Ivan. Results proved that all these factors are important and may result in very different local surge development.

8. A ranking system was developed to describe the vulnerability of coastal highways and bridges around the Florida Panhandle to storm surge in extreme hurricanes like Ivan.

9. The shelf waves over local wind setup caused the high surge in Apalachee Bay during Hurricane Dennis.

CHAPTER 6
FUTURE WORK

In this study, CH3D-SSMS was successfully applied to simulate the storm surges caused by Hurricane Ivan and Hurricane Dennis. Good agreements were achieved between simulation and observation for wind, wave, deficit atmospheric pressure and high surge. However, CH3D-SSMS is not a perfect model yet. With further development, the model could work more efficiently and more accurately. Possible future work is suggested in this chapter.

Wind is a key factor in storm surge simulation. Ideally, the wind should be a continuous set of accurate, high resolution, large scale wind that covers both over water and land. However, this is very difficult to achieve in reality. The best hind cast wind so far is the HRD wind by NOAA, which are normally 3-hour snapshots with coverage of 4 degrees from hurricane center. The land reduction effect is limited to open terrain closure for wind over land. After landfall, HRD wind is normally not available. Therefore, there is plenty of room to improve wind in several aspects. More frequent, larger coverage, more accuracy and inclusion of wind after landfall are all beneficial to both waves and storm surge simulation.

The bottom friction is also an important term in storm surge simulation. However, there is little knowledge about the drag coefficients over land and vegetated shallow water area. In this study, those areas are treated the same as other domains. This may lead to locally overestimated storm surge. Incorporation of scientific advancement of the friction calculation over land and vegetated area will improve the accuracy of storm surge modeling at those domains.

The water level at the open boundary is obtained by coupling with ADCIRC. Thus the quality of storm surge simulation inside domain using local surge model CH3D is partially controlled by the results from ADCIRC. In this study, the EC 2001 grid system used by ADCIRC is relatively coarse and the coastline cannot be accurately resolved. If a more-detailed

grid was available in the future, the open boundary could be better represented which could lead to improvement of storm surge simulation inside local surge model domain.

Local wave model SWAN has been widely used to simulate wave characteristics in near shore coastal waters. It was coupled dynamically with CH3D-SSMS to provide wave parameters for local surge models. However, it is well recognized by slow iteration procedures to get accurate wave solution. Its slowness is the bottle neck of CH3D-SSMS simulation time. During the Hurricane Ivan and Hurricane Dennis simulation, including SWAN slowed the program by at least 5 times over comparing the cases without wave simulation. It is therefore important to find ways to reduce the simulation time by SWAN and thus keep the total simulation time within a more reasonable range. There are a few possible solutions for this. First, a coarser grid could be considered for SWAN instead of the same current grid with same resolution as local surge model. In this way, SWAN can be controlled with comparable simulation time to local surge model or even less. The reduction of simulation accuracy, however, should be considered and further investigation should be made to check if it still could provide reasonable good wave parameters for local surge model. Another method that could be considered is to perform SWAN wave simulation only within a specified domain where wave setup is important. The challenge is to define the proper domain boundary for complex shoreline and provide accurate wave boundary condition for SWAN.

APPENDIX A
SAFFIR-SIMPSON SCALE, VERTICAL DATUM AND HURRICANE TRACK

The Saffir-Simpson Hurricane Scale

The Saffir-Simpson Hurricane Scale is a 1-5 rating based on the hurricane's present intensity. This is used to give an estimate of the potential property damage and flooding expected along the coast from a hurricane landfall. Wind speed is the determining factor in the scale, as storm surge values are highly dependent on the slope of the continental shelf and the shape of the coastline, in the landfall region. Note that all winds are using the U.S. 1-minute average (NOAA, 2006d). The detailed range of wind speed, atmospheric pressure and associated storm surge height for each Saffir-Simpson Hurricane Scale is listed in Table A-1.

The vertical datum

The vertical datum in current storm surge simulation is NAVD88. For station with water level data that are not in NAVD88, a datum conversion is applied to convert station results into NAVD88 system. For the locations where datum information is not available, a linear interpolation technique is used to estimate datum conversion from near NOAA stations with vertical datum conversion. The relationship between NAVD88 and MSL at northern Gulf of Mexico is available at several NOAA stations (NOAA, 2006a) (Table A-2). Considering the datum difference is less than 20 cm over several hundred miles along open boundary, the interpolation should not introduce significant error. In both Ivan and Dennis storm surge simulations, water levels along open boundary from ADCIRC model are converted from MSL to NAVD88 before they are used by CH3D-SSMS.

The Best Track of Hurricanes Ivan and Dennis

According to NOAA, the best track of hurricane is a subjectively-smoothed representation of a tropical cyclone’s location and intensity over its lifetime. The best track contains the

cyclone's latitude, longitude, maximum sustained surface winds, and minimum sea-level pressure at 6-hourly intervals. Best track positions and intensities, which are based on a post-storm assessment of all available data, may differ from values contained in storm advisories. They also generally will not reflect the erratic motion implied by connecting individual center fix positions (NOAA, 2004e). The detailed best track for Hurricane Ivan and Hurricane Dennis are listed in Table A-3 and Table A-4, respectively.

Table A-1. The Saffir-Simpson Hurricane Scale

Saffir-Simpson Category	Maximum sustained wind speed		Minimum surface pressure	Storm surge
	mph	m/s	mb	ft
1	74-95	33-42	> 979	4-5
2	96-110	43-49	965-979	6-8
3	111-130	50-58	945-964	9-12
4	131-155	59-69	920-944	13-18
5	>155	>69	<920	>18

Table A-2. Vertical Datum Difference at Northeast of Gulf of Mexico

Station Name	MSL (m)	MLLW (m)	NAVD88 (m)	MSL to NAVD88 (m)
Panama City, FL	0.0	-0.103	-0.033	0.033
Dauphin Island, AL	0.0	-0.172	-0.102	0.102
Waveland, MS	0.0	-0.244	-0.178	0.178
Port Fourchon, LA	0.0	-0.198	-0.159	0.159

Table A-3. Best track for Hurricane Ivan, 2-24 September 2004

Date/Time (UTC)	Latitude (°N)	Longitude (°W)	Pressure (mb)	Wind Speed (kt)	Stage
03 / 0600	9.7	30.3	1005	35	tropical storm
03 / 1200	9.5	32.1	1003	40	“
03 / 1800	9.3	33.6	1000	45	“
04 / 0000	9.1	35.0	999	45	“
04 / 0600	8.9	36.5	997	50	“
04 / 1200	8.9	38.2	997	50	“
04 / 1800	9.0	39.9	994	55	“
05 / 0000	9.3	41.4	991	60	“
05 / 0600	9.5	43.4	987	65	hurricane
05 / 1200	9.8	45.1	977	85	“
05 / 1800	10.2	46.8	955	110	“
06 / 0000	10.6	48.5	948	115	“
06 / 0600	10.8	50.5	950	110	“
06 / 1200	11.0	52.5	955	110	“
06 / 1800	11.3	54.4	969	90	“
07 / 0000	11.2	56.1	964	90	“
07 / 0600	11.3	57.8	965	95	“
07 / 1200	11.6	59.4	963	100	“
07 / 1800	11.8	61.1	956	105	“
08 / 0000	12.0	62.6	950	115	“
08 / 0600	12.3	64.1	946	120	“
08 / 1200	12.6	65.5	955	120	“
08 / 1800	13.0	67.0	950	120	“
09 / 0000	13.3	68.3	938	130	“
09 / 0600	13.7	69.5	925	140	“
09 / 1200	14.2	70.8	919	140	“
09 / 1800	14.7	71.9	921	130	“
10 / 0000	15.2	72.8	923	130	“
10 / 0600	15.7	73.8	930	125	“
10 / 1200	16.2	74.7	934	125	“
10 / 1800	16.8	75.8	940	120	“
11 / 0000	17.3	76.5	926	135	“
11 / 0600	17.4	77.6	923	130	“
11 / 1200	17.7	78.4	925	125	“
11 / 1800	18.0	79.0	920	145	“
12 / 0000	18.2	79.6	910	145	“
12 / 0600	18.4	80.4	915	135	“
12 / 1200	18.8	81.2	919	135	“
12 / 1800	19.1	82.1	920	130	“
13 / 0000	19.5	82.8	916	140	“
13 / 0600	19.9	83.5	920	140	“
13 / 1200	20.4	84.1	915	140	“
13 / 1800	20.9	84.7	912	140	“

Table A-3. Continued

Date/Time (UTC)	Latitude (°N)	Longitude (°W)	Pressure (mb)	Wind Speed (kt)	Stage
14 / 0000	21.6	85.1	914	140	“
14 / 0600	22.4	85.6	924	140	“
14 / 1200	23.0	86.0	930	125	“
14 / 1800	23.7	86.5	931	120	“
15 / 0000	24.7	87.0	928	120	“
15 / 0600	25.6	87.4	935	120	“
15 / 1200	26.7	87.9	939	115	“
15 / 1800	27.9	88.2	937	115	“
16 / 0000	28.9	88.2	931	110	“
16 / 0600	30.0	87.9	943	105	“
16 / 1200	31.4	87.7	965	70	“
16 / 1800	32.5	87.4	975	50	tropical storm
17 / 0000	33.8	86.5	986	30	tropical depression
17 / 0600	34.7	85.7	991	25	“
17 / 1200	35.4	84.0	994	20	“
17 / 1800	36.2	82.3	996	20	“
18 / 0000	37.0	80.5	999	20	“
18 / 0600	37.7	78.5	998	15	“
18 / 1200	38.4	76.7	1000	15	“
18 / 1800	38.0	75.5	1002	25	extratropical
19 / 0000	37.5	74.0	1003	35	“
19 / 0600	36.0	74.0	1005	35	“
19 / 1200	34.5	74.5	1008	35	“
19 / 1800	32.8	75.8	1008	35	“
20 / 0000	31.0	77.5	1008	35	“
20 / 0600	29.0	78.5	1008	35	“
20 / 1200	27.5	78.7	1009	30	“
20 / 1800	26.4	79.1	1009	25	“
21 / 0000	26.1	79.7	1009	25	“
21 / 0600	25.9	80.6	1009	25	“
21 / 1200	25.8	81.7	1009	25	“
21 / 1800	25.2	82.8	1010	25	low
22 / 0000	24.8	84.1	1010	25	“
22 / 0600	25.1	86.1	1010	25	“
22 / 1200	26.0	87.3	1010	25	“
22 / 1800	26.5	88.6	1008	30	tropical depression
23 / 0000	27.1	89.5	1007	35	tropical storm
23 / 0600	27.9	91.0	1007	35	“
23 / 1200	28.9	92.2	998	50	“
23 / 1800	29.2	92.7	1003	40	“
24 / 0000	29.6	93.2	1003	30	tropical depression
24 / 0600	30.1	94.2	1009	25	“
24 / 1200					dissipated inland

Table A-4. Best track for Hurricane Dennis, 4 – 13 July 2005

Date/Time (UTC)	Latitude (°N)	Longitude (°W)	Pressure (mb)	Wind Speed (kt)	Stage
04 / 1800	12.0	60.8	1010	25	tropical depression
05 / 0000	12.2	62.5	1009	30	“
05 / 0600	12.5	64.2	1008	30	“
05 / 1200	13.0	65.9	1007	35	tropical storm
05 / 1800	13.6	67.3	1005	40	“
06 / 0000	14.3	68.5	1000	45	“
06 / 0600	14.7	69.7	995	50	“
06 / 1200	15.1	70.9	991	55	“
06 / 1800	15.6	71.9	989	60	“
07 / 0000	16.2	73.0	982	70	hurricane
07 / 0600	16.7	74.1	972	80	“
07 / 1200	17.6	74.9	967	90	“
07 / 1800	18.5	76.1	957	100	“
08 / 0000	19.4	77.1	951	120	“
08 / 0600	20.3	78.4	953	110	“
08 / 1200	20.9	79.5	938	130	“
08 / 1800	22.0	80.6	941	120	“
09 / 0000	22.7	81.6	960	100	“
09 / 0600	23.4	82.5	973	75	“
09 / 1200	24.3	83.4	967	80	“
09 / 1800	25.2	84.2	962	90	“
10 / 0000	26.1	85.0	942	110	“
10 / 0600	27.2	85.8	935	125	“
10 / 1200	28.5	86.3	930	120	“
10 / 1800	29.9	86.9	942	110	“
11 / 0000	31.5	87.7	970	45	tropical storm
11 / 0600	32.6	88.5	991	30	tropical depression
11 / 1200	33.9	88.8	997	25	“
11 / 1800	35.3	89.1	1002	20	“
12 / 0000	36.4	89.2	1003	20	“
12 / 0600	37.1	89.0	1005	15	“
12 / 1200	37.7	88.7	1007	15	“
12 / 1800	38.1	88.3	1008	15	“
13 / 0000	38.5	87.8	1009	15	“
13 / 0600	38.9	87.2	1010	15	“
13 / 1200	39.2	86.5	1010	15	remnant low
13 / 1800	39.2	85.8	1010	15	“
14 / 0000	39.2	85.7	1009	10	“
14 / 0600	39.0	85.6	1009	10	“
14 / 1200	38.7	85.6	1010	10	“
14 / 1800	38.4	85.6	1010	10	“
15 / 0000	38.1	85.9	1009	10	“
15 / 0600	37.9	86.2	1010	10	“

Table A.4. Continued

Date/Time (UTC)	Latitude (°N)	Longitude (°W)	Pressure (mb)	Wind Speed (kt)	Stage
15 / 1200	38.1	86.4	1012	10	“
15 / 1800	38.4	86.6	1012	10	“
16 / 0000	38.6	86.8	1011	10	“
16 / 0600	39.4	86.5	1013	10	“
16 / 1200	40.2	86.2	1014	10	“
16 / 1800	40.8	85.2	1014	10	“
17 / 0000	41.3	84.1	1013	10	“
17 / 0600	42.2	83.2	1013	10	“
17 / 1200	43.1	82.3	1013	10	“
17 / 1800	43.9	81.4	1012	10	“
18 / 0000	44.6	80.5	1010	10	“
18 / 0600	45.8	79.8	1009	10	“
18 / 1200					absorbed by larger low
04 / 2100	12.1	61.6	1009	30	landfall on Grenada
08 / 0245	19.9	77.6	956	120	landfall near Punta del Ingles, Cuba
08 / 1845	22.1	80.7	941	120	landfall just west of Punta Mangles Altos, Cuba
10 / 1930	30.4	87.1	946	105	landfall on Santa Rosa Island, Florida, 10 miles west of Navarre Beach
10 / 1200	28.5	86.3	930	120	minimum pressure
08 / 1200	20.9	79.5	938	130	maximum wind

APPENDIX B
TIDAL SKILL ANALYSIS

In order to quantify a model's performance on tidal simulation, several statistics on tidal time series and extrema analysis are used by comparison with observed data (Hess, et al., 1993). Given time series of observed and simulated tidal elevation, the root mean square (rms) difference can be calculated as:

$$D_{rms} = \left[\sum_{i=1}^{n} (\hat{y}_i - y_i)^2 / n \right]^{1/2} \tag{B-1}$$

Where y_i and $\hat{y}_i$ are observed and simulated tidal elevation at the same time, n is the number of available data. Since observed tidal ranges can vary widely from station to station, a more meaningful statistics is the ratio of the rms difference to the mean observed range, or relative difference:

$$D'_{rms} = D_{rms} / R \tag{B-2}$$

where R is observed range which can be calculated as:

$$R = (2 / N) \sum_{j=1}^{N} \left| Y_j \right| \tag{B-3}$$

Where Y_j is either maximum water level at high tides or minimum water level at low tides with total of number of N occurrence. A weighted gain (G_w) characterized the modeled range relative to the observed range:

$$G_w = (2 / R) \sum_{j=1}^{\hat{N}} \left| \hat{Y}_j \right| / \hat{N} \tag{B-4}$$

with $\hat{Y}_j$ representing simulated high tide and low tide.

Following above all time rms difference calculation, similar analysis procedures can be applied to determine times and amplitudes rms error for tidal extrema. For one extreme observed

water level, the closest modeled extrema (denoted by prime) with same sign and within 3 hours, if it exits, will be used to calculate rms difference for amplitude extrema:

$$A_{rms} = \left[\sum_{j=1}^{M} (\hat{Y}_{ji} - Y_j)^2 \ / \ M \right]^{1/2} \tag{B-5}$$

Then the mean time lag (L_m) and rms lag (L_{rms}) can be defined to describe phase difference;

$$L_m = \left[\sum_{j=1}^{M} (\hat{T}_j - T_j) \ / \ M \right]^{1/2} \tag{B-6}$$

and

$$L_{rms} = \left[\sum_{j=1}^{M} (\hat{T}_j - T_j)^2 \ / \ M \right]^{1/2} \tag{B-7}$$

where T_j represent times of extreme water level for each pair.

With definitions of relative peak and lag values:

$$A'_{rms} = A_{rms} \ / \ R \ \text{ and } \ L'_{rms} = L_{rms} \ / \ 6.21 \tag{B-8}$$

where 6.21 hours (one-half an M2 tidal period) approximates the mean time between extrma, the three skill parameters for tidal comparison can be used to quantify model accuracy:

$$\begin{aligned} S_D &= 1 - D' \\ S_A &= 1 - A' \\ S_L &= 1 - L' \end{aligned} \tag{B-9}$$

where S_D is hourly difference skill, S_A is extrema amplitude skill and S_L is extrema time skill.

A 30-day pre-storm period was selected to calibrate model on bottom coefficient and tidal boundary condition. Observed water level from several NOAA stations was downloaded first. Then non-tidal components, both high frequency noise and low frequency surge, were removed using Chebyshev Type II filtering program. Two tidal boundaries were tested in the study. First, predicted tides from NOAA stations were used along open boundary using inverse-distance

interpolation technique. The second method is to apply tidal constituents from ADCIRC tidal database. As for bottom friction coefficient, three constant Manning's coefficients were tested.

In open channel hydraulics study, Chow (1959) suggested Manning's coefficient range from 0.016 for clean channel and 0.033 for channels with short grass. An recent summary by Hess and Bosley (1993) from USGS also gave similar range of Manning's for stable channels and flood plain. The minimum Manning's n is 0.012 for concrete channel, 0.017-0.020 for medium sand and 0.025-0.035 for firm soil and coarse sand. A sedimentary study of the Mississippi Sound and adjacent coastal waters (Upshow, et al, 1966; Sheng, 1983) has shown that southwest of Mobile Bay the open water bottom is covered by sand, while to east sediment size gradually reduces from sand to sandy silt to silt. A set of sensitivity tests (Table B-1 to B-7) using different Manning's coefficients further proved the overall trend of sediment distribution of Hurricane Ivan computational domain. At the Pensacola station, the bottom sediment type is sand, accordingly Manning's coefficient of 0.022 produces best results. Located on the west computational domain, Station Waveland has the finest sediment (silt) and smaller Manning's coefficient to simulate water level well. Station Biloxi and station Dauphin Island locate in between, thus a transitional Manning's coefficient around 0.020 perform well. Based on sensitivity test and sedimentary study (Upshow, et al, 1966; Sheng, 1983), a spatial-varying Manning's coefficients, approximately increasing from 0.016 to 0.022 from west to east, were made over Hurricane Ivan computational domain and then were used for later storm surge simulation.

Table B-1. Calibration of tidal simulation for Ivan using Manning's 0.015 and predict tide

Station	Mean Tidal Range R (cm)	rms difference D_{rms} (cm)	Extrema amplitude rms difference A_{rms} (cm)	Extrema phase difference L_m (hour)	Extrema phase rms difference L_{rms} (hour)	Hourly difference skill S_D	Extrema amplitude skill S_A	Extrema time skill S_L
Wave land	41.12	5.20	3.87	0.393	0.836	0.874	0.906	0.865
Biloxi	43.18	4.92	4.43	0.003	0.799	0.886	0.897	0.871
Dauphin Island	31.3	2.75	2.16	-0.328	0.898	0.912	0.931	0.855
Pensacola	34.29	4.06	4.58	-0.009	0.717	0.880	0.867	0.884
Panama City Beach	31.45	4.06	4.58	-0.009	0.717	0.880	0.867	0.884

Table B-2. Calibration of tidal simulation for Ivan using Manning's 0.020 and predict tide

Station	Mean Tidal Range R (cm)	Rms difference D_{rms} (cm)	Extrema amplitude rms difference A_{rms} (cm)	Extrema phase difference L_m (hour)	Extrema phase rms difference L_{rms} (hour)	Hourly difference skill S_D	Extrema amplitude skill S_A	Extrema time skill S_L
Wave land	41.12	6.80	5.71	0.714	1.138	0.835	0.861	0.817
Biloxi	43.18	5.51	5.65	0.355	0.847	0.872	0.869	0.864
Dauphin Island	31.3	3.07	3.77	0.222	0.927	0.902	0.880	0.851
Pensacola	34.29	3.07	2.20	0.617	0.905	0.911	0.936	0.854
Panama City Beach	31.45	3.06	3.59	-0.200	1.037	0.903	0.886	0.833

Table B-3. Calibration of tidal simulation for Ivan using Manning's 0.025 and predict tide

Station	Mean Tidal Range R (cm)	Rms difference D_{rms} (cm)	Extrema amplitude rms difference A_{rms} (cm)	Extrema phase difference L_m (hour)	Extrema phase rms difference L_{rms} (hour)	Hourly difference skill S_D	Extrema amplitude skill S_A	Extrema time skill S_L
Wave land	41.12	8.02	7.15	0.942	1.195	0.805	0.826	0.808
Biloxi	43.18	6.58	6.56	0.636	0.998	0.848	0.848	0.839
Dauphin Island	31.3	3.65	4.69	0.222	0.916	0.884	0.851	0.852
Pensacola	34.29	3.47	2.09	0.829	1.020	0.899	0.939	0.836
Panama City Beach	31.45	3.09	3.69	-0.282	1.032	0.902	0.883	0.834

Table B-4. Calibration of tidal simulation for Ivan using spatial-varying Manning's and predict tide

Station	Mean Tidal Range R (cm)	Rms difference D_{rms} (cm)	Extrema amplitude rms difference A_{rms} (cm)	Extrema phase difference L_m (hour)	Extrema phase rms difference L_{rms} (hour)	Hourly difference skill S_D	Extrema amplitude skill S_A	Extrema time skill S_L
Wave land	41.12	6.88	5.27	0.759	1.102	0.833	0.872	0.822
Biloxi	43.18	5.69	5.76	0.412	0.898	0.868	0.866	0.855
Dauphin Island	31.3	3.02	3.68	0.234	0.915	0.904	0.883	0.853
Pensacola	34.29	3.47	2.09	0.829	1.021	0.899	0.939	0.836
Panama City Beach	34.29	3.09	3.69	-0.282	1.032	0.902	0.883	0.834

Table B-5. Calibration of tidal simulation for Ivan using Manning's 0.020 and ADCIRC Constituents

Station	Mean Tidal Range R (cm)	Rms difference D_{rms} (cm)	Extrema amplitude rms difference A_{rms} (cm)	Extrema phase difference L_m (hour)	Extrema phase rms difference L_{rms} (hour)	Hourly difference skill S_D	Extrema amplitude skill S_A	Extrema time skill S_L
Wave land	41.12	6.84	6.20	0.422	1.008	0.834	0.849	0.837
Biloxi	43.18	7.15	6.50	0.174	0.893	0.834	0.849	0.856
Dauphin Island	31.3	4.28	4.84	-0.372	0.950	0.864	0.846	0.847
Pensacola	34.29	5.03	4.96	0.090	0.773	0.853	0.855	0.876
Panama City Beach	31.45	5.24	6.13	-0.126	1.027	0.833	0.805	0.835

APPENDIX C
ANNULAR TEST

Tidal forcing is one of the most important parts of estuarine hydrodynamic modeling. In this appendix a tidal forcing problem is studied and the simulation results are compared with analytical solution for model verification.

Lynch and Gray (1978) derived analytical solutions for tidally forced estuarines of various geometries and depths. Neglecting friction, nonlinear, diffusion and Coriolis terms, the vertically averaged equation of motion in a Cartesian coordinate system are:

$$\frac{\partial u}{\partial t} = -g\frac{\partial \zeta}{\partial x} \tag{C-1}$$

$$h\frac{\partial u}{\partial x} = -\frac{\partial \zeta}{\partial t} \tag{C-2}$$

where u is velocity, ζ is surface elevation, h is the water depth and g is gravitational acceleration. Letting l represent the basin length, the tidally forced rectangular basin has the following boundary conditions:

$$\zeta(x,t)\big|_{x=x_0} = a\cos(\omega t) \tag{C-3}$$

$$\left.\frac{\partial \zeta}{\partial x}\right|_{x=l} = 0 \tag{C-4}$$

where a and ω are the tidal amplitude and frequency, respectively.

With these boundary conditions, the solutions for a flat bottom basin of uniform width can be written as:

$$\zeta(x,t) = \mathrm{Re}\left[ae^{i\omega t}\frac{\cos(\beta(x-x_l))}{\cos(\beta l)}\right] \tag{C-5}$$

$$u(x,t) = \mathrm{Re}\left[-\frac{i\omega t}{\beta H_0}e^{i\omega t}\frac{\sin(\beta(x-x_l))}{\cos(\beta l)}\right] \tag{C-6}$$

where H_0 is the basin depth and

$$\beta = \sqrt{\frac{\omega^2}{gH_0}} \tag{C-7}$$

For an annular basin, the analytic solution determined by Lynch and Grey (1978) can be written as:

$$\zeta(r,t) = \mathrm{Re}\left[(AJ_0(\beta r) + BY_0(\beta r)e^{i\omega t}\right] \tag{C-8}$$

$$u(r,t) = \mathrm{Re}\left[(-AJ_1(\beta r) - BY_1(\beta r)\frac{i\omega}{\beta H_0}e^{i\omega t}\right] \tag{C-9}$$

where J_0, J_1, Y_0, Y_1, are Bessel function and

$$A = \frac{aY_1(\beta r_1)}{\left[J_0(\beta r_2)Y_1(\beta r_1) - Y_0(\beta r_2)J_1(\beta r_1)\right]} \tag{C-10}$$

$$B = \frac{-aJ_1(\beta r_1)}{\left[J_0(\beta r_2)Y_1(\beta r_1) - Y_0(\beta r_2)J_1(\beta r_1)\right]} \tag{C-11}$$

The numerical grid (42x5 cells) chosen for annular section test is shown in Figure A3.1. The parameters used in the test are:

$$\begin{aligned} &a = 50 \text{ cm} \\ &\omega = \frac{2\pi}{9000s} \\ &\varphi = 20 \\ &r_1 = 20 \text{ km} \\ &r_2 = 83 \text{ km} \\ &H_0 = 100 \text{ m} \\ &\Delta t = 30 \text{ s} \end{aligned} \tag{C-12}$$

The model was run for 10 cycles before attaining steady state conditions. Figure C-1 shows the comparison of the maximum surface elevation and velocity between analytical solution and numerical results.

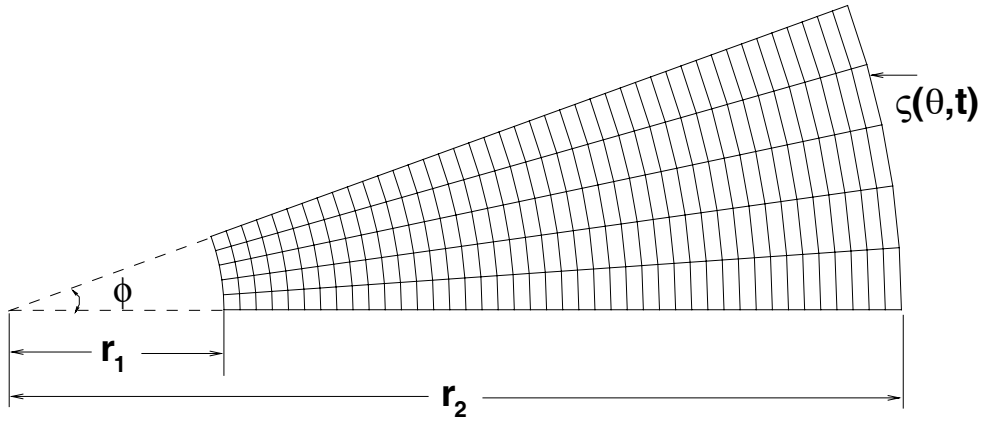

Figure C-1. The 42x5 annular section grid

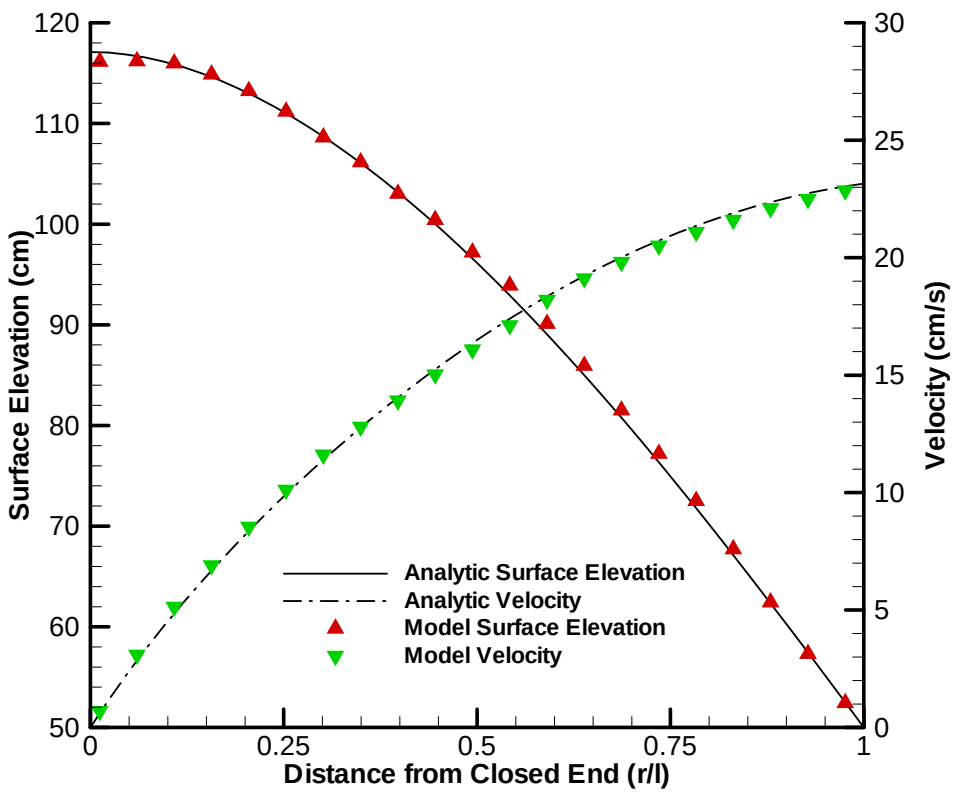

Figure C-2. Comparison between simulated surface elevation and velocity and analytical solutions for tidally forced flat-bottom annular section.

APPENDIX D
ADDITIONAL HURRICANE IVAN RESULTS

The inundation at Escambia Bay without wave effect from 2D simulation is shown in Figure D-1.

The time series of simulated water level for Hurricane Ivan at NOAA monitoring stations from 3D simulation without wave effect is shown in Figure D-2. Overall, the magnitude and trend of simulated surges agreed well with the measurement. However, the highest surges at Dauphin Island and Panama City Beach were slightly underestimated. Even though the flow field varied quite a bit between the 3D model and 2D model (Chapter 3), the simulated surges were very close to each other.

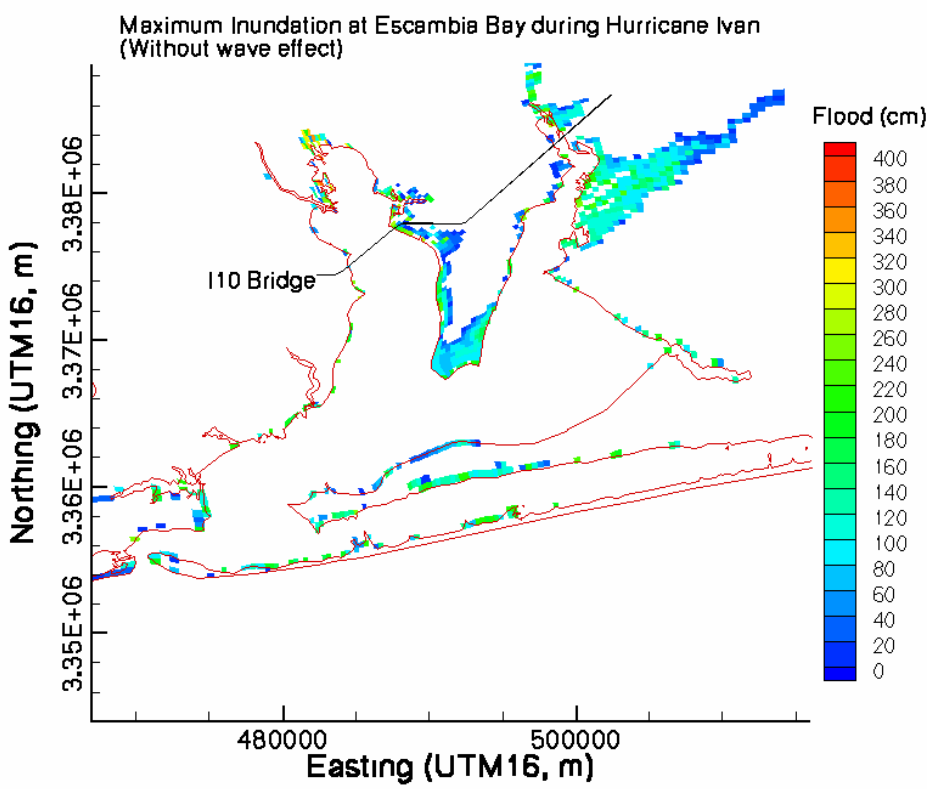

Figure D-1. Maximum Inundation around Pensacola Bay and Escambia Bay for Hurricane Ivan without wave effect.

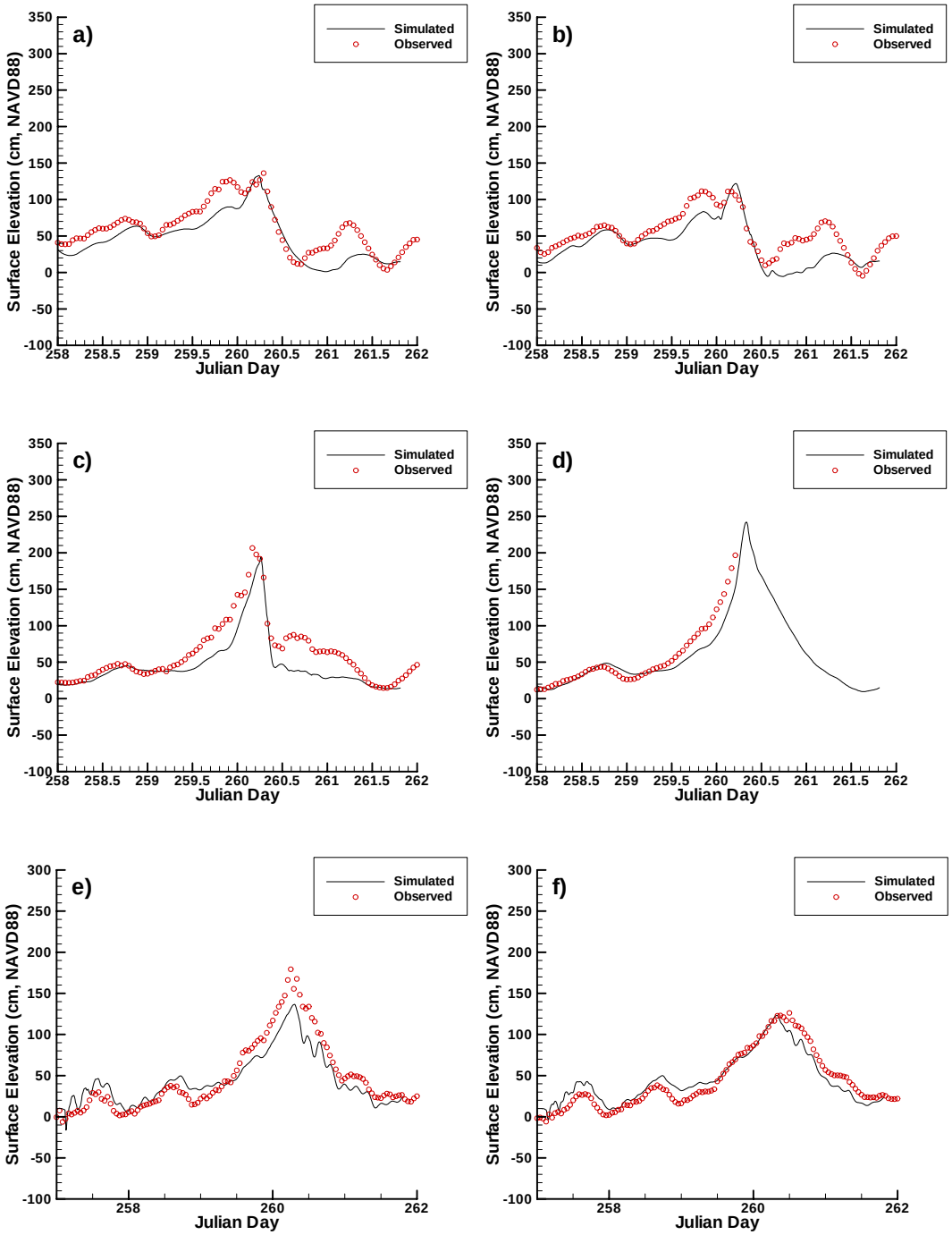

Figure D-2. Water level comparison for Hurricane Ivan from 3D simulations without wave effect at (a). Biloxi; (b). Waveland; (c). Dauphin Island; (d). Pensacola; (e). Panama City Beach; (f). Panama City.

APPENDIX E
RADIATION BOUNDARY CONDITION

The open boundary conditions for circulation models can be classified into several categories. The first kind is the clamped boundary condition, where water levels are specified as $\eta = \eta_0$. These water levels may come from tidal constituents, measurement or other model's results. For the second kind of open boundary condition, the transport (Velocity) is specified at boundary: $u = u_0$. This open boundary is seldom used in real cases as the velocity is not normally available for the entire open boundary cells. Another practice is to apply radiation boundary at open waters. This technique is able to transport water level disturbance freely out of the computational domain. This methodology has been developed and used for circulation, tsunami and storm surge simulations in slightly different forms (Sommerfeld, 1949; Reid & Bodine, 1968; Orlanski, 1976; Blumberg and Kantha,1985; Flather, 1976, 1993). In this study, the Flather Open Boundary Condition is introduced into CH3D-SSMS and applied for the Hurricane Dennis simulation.

Following Flather (1976, 1993), the Flather open boundary condition can be written in the form of:

$$u = u_0 \pm \sqrt{\frac{g}{H}}(\varsigma - \varsigma_0) \tag{E-1}$$

Where u is velocity at open boundary;
u_0 is prescribed velocity at open boundary;
g is gravity;
H is the total water depth at open boundary;
ζ is water level at open boundary;
ζ_0 is prescribed water level at open boundary;
± is determine by direction, - is for west/south boundary and + is for east/north boundary;

In order to incorporate Flather boundary condition into CH3D-SSMS, the continuity equation is used to include and calculate mass flux across open water boundary cells. This

process adds additional terms and slightly changes the formation of the matrix solving for water levels. When velocity u is set equal to prescribed velocity u_0, it reduces to clamped boundary condition.

To test the Flather open boundary condition, the same Annular test represented in Appendix C was adopted here. The initial water level, prescribed water level and velocity at open boundary were provided by analytical solution. Two kinds of simulations were made using both the clamped boundary condition and the Flather condition. Time series of water level at four different stations (Figure E-1) are compared with analytical solution (Figure E-2).

The Flather boundary condition is further applied for the Hurricane Dennis simulation in this study. The prescribed velocity and water level come from the combination of tide and surge. The tidal-only case was setup first to obtained velocity and water from tidal-driven circulation only. Then, the complete simulation was made by further adding the velocity and water level from surge from regional circulation model ADCIRC from coupling process. The time series of simulated water level using the Flather boundary condition at several NOAA stations is shown in Figure E-3. The simulated highest surges are close to measured data and only a few centimeters from simulation using clamped open boundary condition. The difference comes from the additional velocity information considered by the Flather boundary condition. This practice implies that the maximum storm surge is not very sensitive to the boundary condition for Hurricane Dennis in this study.

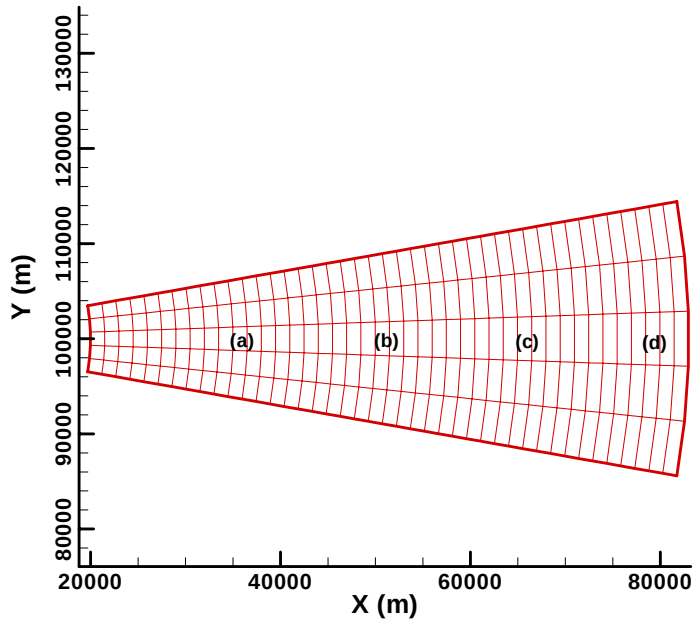

Figure E-1. The 42x5 annular section grid with four output stations.

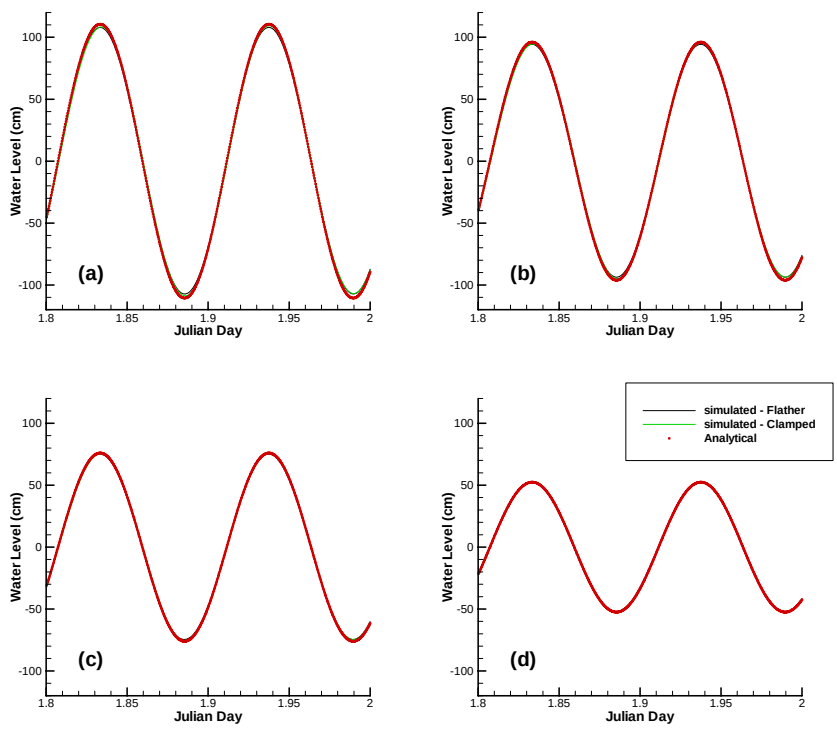

Figure E-2. Water level comparison at four stations for Annular grid using Flather open boundary conditions.

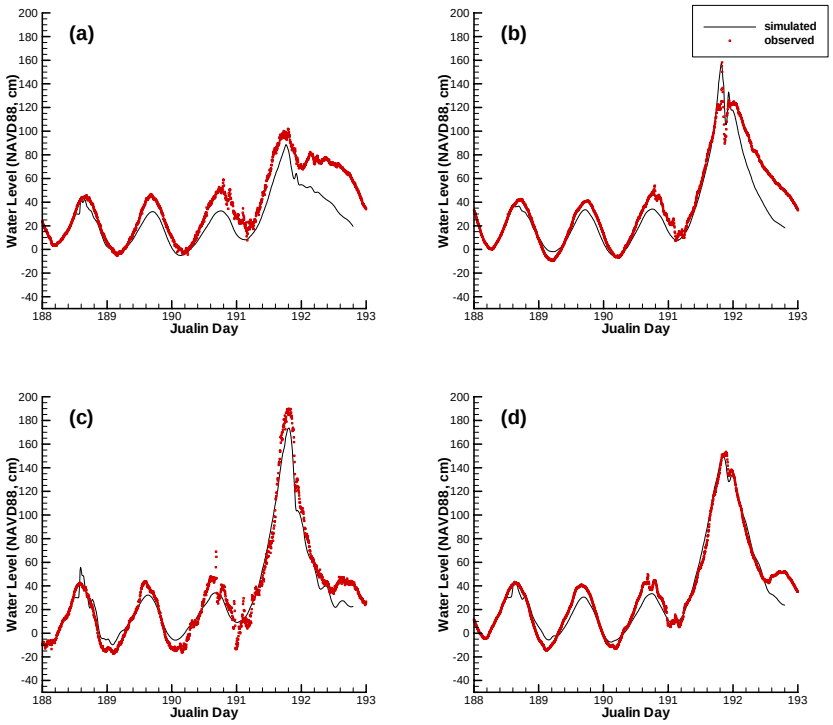

Figure E-3. Water level comparison for Hurricane Dennis with Flather radiation boundary at (a). Dauphin Island; (b). Pensacola; (c). Panama City Beach; (d). Panama City.

APPENDIX F
WAVEWATCH-III SIMULATION

The wave open boundary conditions for Hurricane Ivan and Dennis simulation are obtained from the operational wave model WW3 by NCEP/NOAA. The results of WW3 model are downloaded from the NOAA website (NOAA-3) and then interpolated onto the boundary cells of local wave model SWAN. In this appendix, the WW3 model is compiled and applied for Hurricane Ivan to simulate storm waves in the ocean. The simulated waves are similar to the results downloaded from NCEP/NOAA.

The grid system and associated bathymetry for WW3 simulation are shown in Figure F-1. The grid covers the entire Gulf of Mexico and partially northwest Atlantic Ocean with 0.2 degree resolution. It has to be noticed that the simulation by NCEP/NOAA has slightly coarser grid resolution of 0.25 degree. The WNA wind by NECP for Hurricane Ivan is also used here to drive the WW3 model. A linear interpolation technique is used to apply WNA wind onto this WW3 grid. The wind speed over land cells is set to zero. The time step used by WW3 is ten minutes. As the purpose of the simulation is to provide wave condition for local wave model SWAN, the simulated waves at open boundary cells in the northeast Gulf of Mexico are saved. The time series of wave heights at three selected stations (Figure F-2) are compared to the results downloaded from NCEP (Figure F-3). The close comparison implies that new WW3 simulation is successful. The difference of wave height should come from the variation of grid system and wind field used in the model.

Another WW3 simulation is made for Hurricane Ivan risk analysis test case 4. The wind field is calculated from the analytical Holland wind model. The obtained wave parameters are then used as open boundary condition for local wave model SWAN. The simulated wave height at I10 Bridge is about 1.5 m, which is close to 1.6 m from Hurricane Ivan simulation.

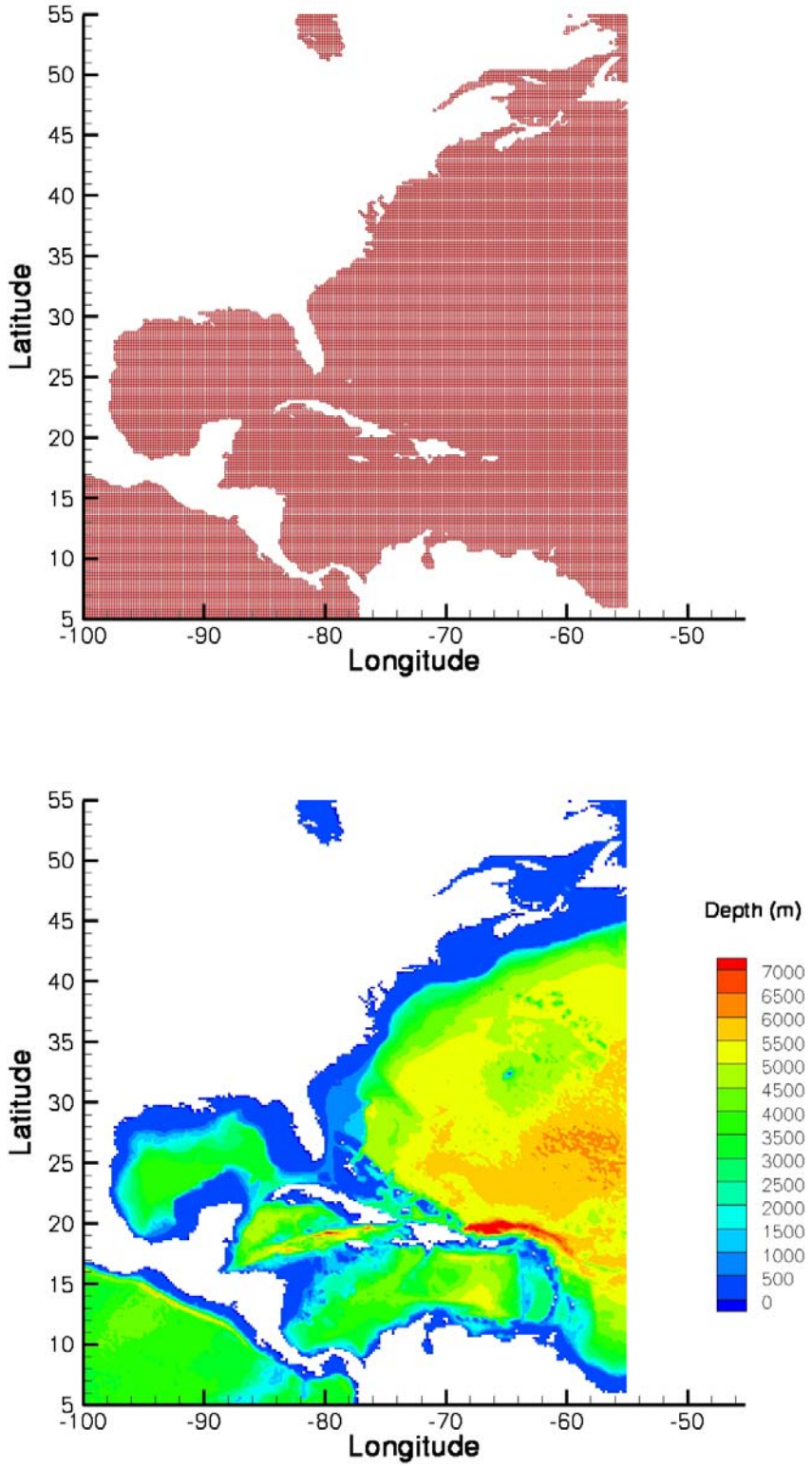

Figure F-1. The grid system (up panel) and bathymetry (lower panel) for WW3 wave model.

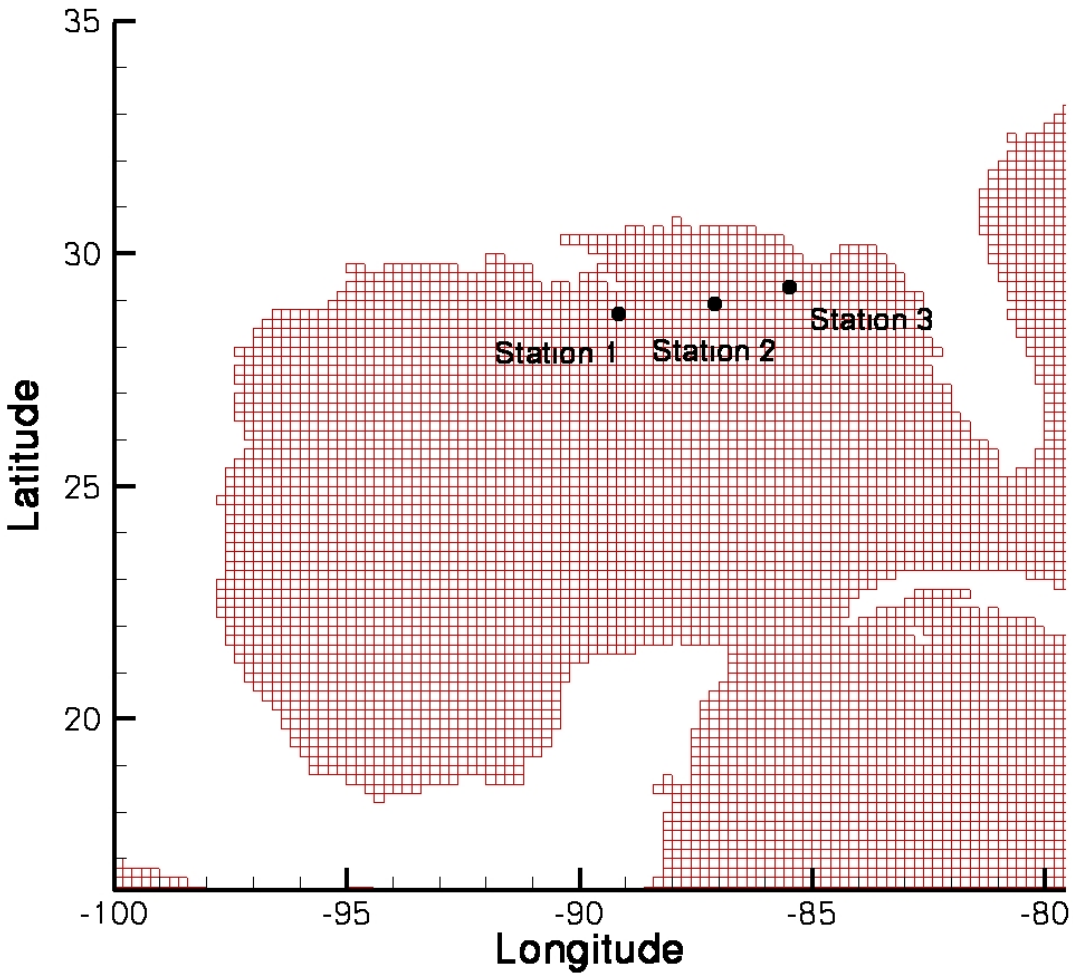

Figure F-2. The output station locations for Hurricane Ivan simulation using wave model WW3.

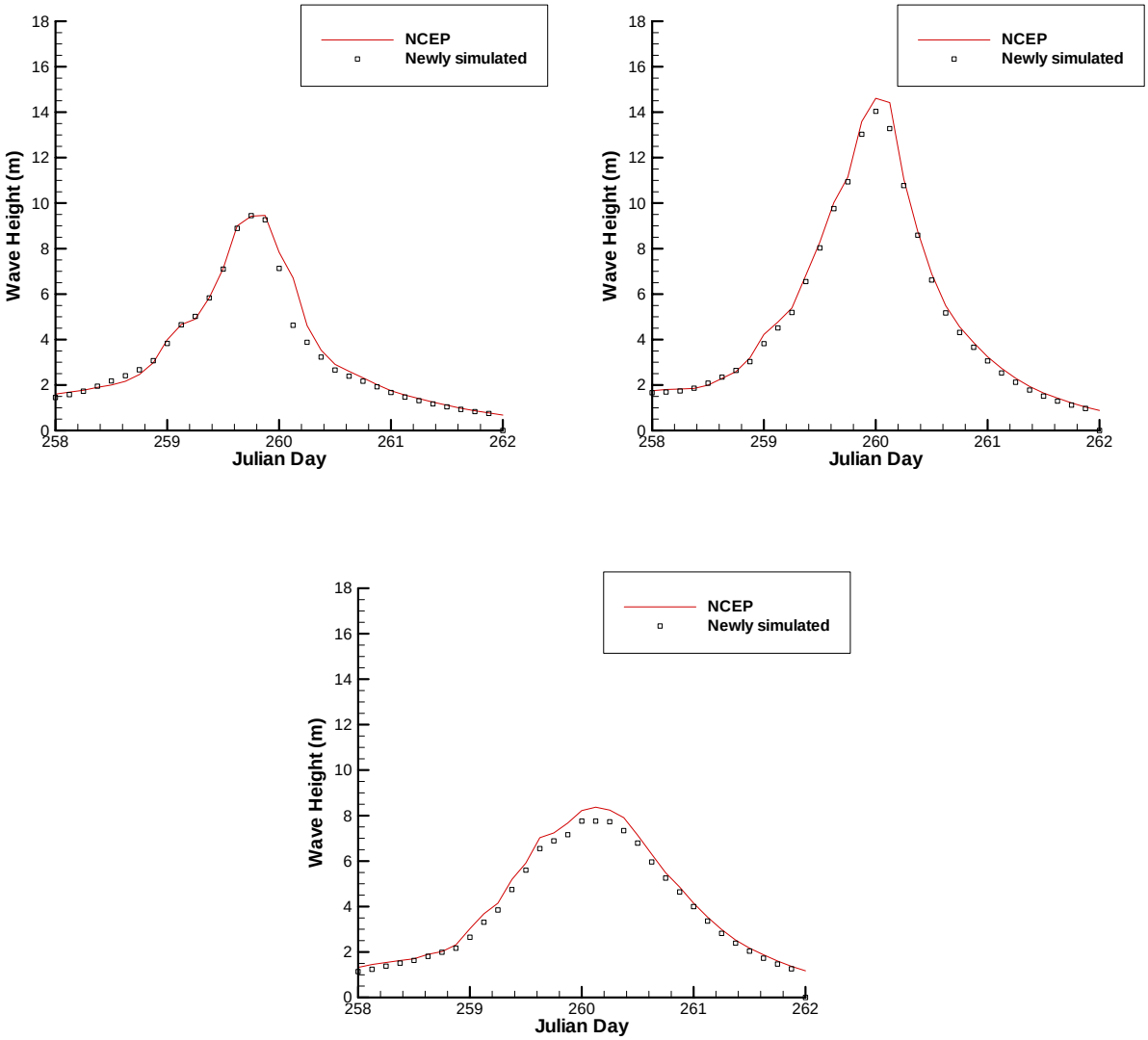

Figure F-3. The time series comparison of wave height between NCEP results and WW3 simulation at Station 1 (top left), Station 2 (top right) and Station 3 (bottom).

LIST OF REFERENCES

Arcement, G.J. and V.R. Schneider. Guide for selecting Manning's roughness coefficients for natural channels and flood plains. United States Geological Survey Water-Supply Paper 2339.

Alymov, V. V., 2005. Integrated modeling of storm surge during Hurricanes Isabel, Charley and Frances. Dissertation, University of Florida, Gainesville.

ADCIRC, 2006. http://www.unc.edu/ims/ccats/tides/tides.htm. Viewed on March, 2006.

Baptista, A.M. and Zhang, Y.-L., Chawla, A., Zulauf, M.A., Seaton, C., Myers, E.P., Kindle, J., Wilkin, M., Burla, M. and Turner, P.J., 2005. A cross-scale model for 3D baroclinic circulation in estuary-plume-shelf systems: II. Application to the Columbia River. Continental Shelf Research, 25, pp. 935-972.

Bea, R. G., 1996. Nonlinear performance of offshore platforms in extreme storm waves. Journal of Waterways, Port, Coastal & Ocean. Engineering, ASCE, 122(2), pp. 68-74.

Bea R. G., Xu T., Stear J. and Ramos R., 1999. Wave forces on decks of offshore platforms. Journal of Waterways, Port, Coastal & Ocean Engineering, ASCE, 125(3), pp. 136-144.

Blain, C.A., J.J. Westerink, R.A. Luettich, Jr. and N.W. Scheffner, 1994. ADCIRC: an advanced three-dimensional circulation model for shelves coasts and estuaries, report 4: hurricane storm surge modeling using large domains. Dredging Research Program Technical Report, DRP-92-6, U.S. Army Engineers Waterways Experiment Station, Vicksburg, MS.

Blumberg, A.F., and L.H. Kantha,1985. An open boundary condition for circulation models. Journal of Hydraulics, ASCE, 111, pp. 237-255.

Blumberg, A. F. and G. L. Mellor, 1987. A description of a three-dimensional coastal ocean circulation model. Three-dimensional coastal ocean models. Coastal and estuarine sciences, Volume 4, edited by N. Heaps, American Geophysical Union, Washington, D.C., pp. 1–16.

BMRC, 2006. Bureau of Meteorology Research Center, Australia. http://www.bom.gov.au/bmrc/pubs/tcguide/ch4/ch4_2.htm. Viewed on April, 2006.

Carrere, L. andF. Lyard, 2003. Modeling the barotropic response of the global ocean to atmospheric wind and pressure forcing –comparisons with observations. Geophysical Research Letters, 30 (6), 1275. doi:10.1029/2002GL016473.

Casulli, V. and R. T. Cheng, 1992. Semi-implicit finite difference methods for three-dimensional shallow water flow. International Journal for Numerical Methods in Fluids, 15, pp. 629-648.

Casulli, V. and R.A.,Walters, 2000. An unstructured grid, three-dimensional model based on the shallow water equations. International Journal on Numerical Methods in Fluids, 32, pp. 331-248.

Cardone, V. J., Greenwood, C. V., and Greenwood, J. A., 1992. United program for the specification of hurricane boundary layer winds over surfaces of specified roughness. Contract Report CERC-92-1, Corps of Engineers, Vicksburg, MS.

Cheng, R. T., V. Casulli, and J. W. Gartner, 1993. Tidal, residual, intertidal mudflat (TRIM) model and its applications to San Francisco Bay, California. Estuarine, Coastal, and Shelf Science, Vol. 36, pp. 235-280.

Choi, B.H., 1980. A tidal model of the Yellow Sea and the Eastern China Sea. Korea Ocean Research and Development Institute, Technical report 80-02, pp 72.

Choi, B. H., H. M. Eum and S. B. Woo, 2003. A synchronously coupled tide-wave-surge model of the Yellow Sea. Coastal Engineering, 47, pp. 381-398

Chow, S., 1971. A study of the wind field in the planetary boundary layer of a moving tropical cyclone. Master's Thesis, New York University, New York.

Chow, V.T., 1959. Open Channel Hydraulics. New York, McGraw-Hill Book Co.

Cuomo G., N. W. H. Allsop and K.L. McConnell, 2003. Dynamic wave loads on coastal structures: Analysis of impulsive and pulsating wave loads. Proc. Conf. Coastal Structures 2003, AASCE/CPRI, Portland, pp. 356-368

Davis, J. R., 1996. Hydrodynamic modeling in shallow water with wetting and drying. Master's Thesis, University of Florida, Gainesville.

Davis, J. D., 2001. High performance modeling of circulation and transport in the Indian River Lagoon, Florida. Dissertation, University of Florida, Gainesville.

Dean, R. G. and R. A. Dalrymple, 1991. Water wave mechanics for engineers and scientists. Advanced Series on Ocean Engineering, World Scientific, Vol.2.

Denson, K. H., 1978. Wave forces on causeway-type coastal bridges. Water Resources Research Institute, Mississippi State University.

Denson, K. H., 1980. Wave forces on causeway-type coastal bridges: Effects of angle of wave incidence and cross-section shape. Water Resources Research Institute, Mississippi State University.

Dietsche D., S. C. Hagen and P. Bacopoulos, 2007. Storm surge simulations for hurricane Hugo (1989): On the significance of inundation areas. Journal of Waterway, Port, Coastal, and Ocean Engineering, 133(3), pp. 183-191.

DHI, 2002. MIKE 21 Coastal Hydraulics and Oceanography, Hydrodynamic Module, Reference Manual. DHI Water and Environment, Hørsholm, Denmark.

Donelan, M. A., F. W. Dobson, S. D. Smith, and R. J. Anderson, 1993. On the dependence of sea-surface roughness on wave development. Journal of Physical Oceanography, 23, pp. 2143-2149.

Douglass, S.L., S. A. Hughes, S. Rogers and Q. Chen, 2004. The impact of Hurricane Ivan on the coastal roads of Florida and Alabama: A preliminary report. Coastal Transportation Engineering Research & Education Center, University of South Alabama.

Douglass, S.L., Q. Chen, J. Olsen, B. Edge, D. and Brown, 2006. Wave forces on bridge decks. Department of Civil Engineering, University of South Alabama, Texas A&M University, Dan Brown and Associates. Report prepared for U.S. Department of Transportation, Federal Highway Administration, office of Bridge Technology, Washington, D.C.

FEDP, 1998. Plans of final fender rehabilitation, state project no. 58002-3446, Florida Department of Transportation.

Flather, R. A., 1976. A tidal model of the northwest European continental shelf. Modern Society Royal Science Liege, Ser. 6, 10, pp. 141–164.

Flather, R. A., 1993. A storm surge prediction model for the Northern Bay of Bengal with application to the Cyclone disasters in April 1991. Journal of Physical Oceanography, vol 24, pp. 172-190.

French J.A., 1970. Wave uplift pressures on horizontal platforms. Proceedings of the Civil Engineering in the Oceans Conference, American Society of Civil Engineers, pp. 187-202.

GEODAS, NOAA, 2006. http://www.ngdc.noaa.gov/mgg/coastal/coastal.html. Viewed on March, 2006.

Graber, H.C. and V.J. Cardone, R.E. Jensen, D.N. Slinn, S.C. Hagen, A.T. Cox, M.D. Powell, and C. Grassl, 2006. Coastal Forecasts and Storm Surge Predictions for Tropical Cyclones: A Timely Partnership Program, Oceanography, 19(1), pp. 130-141.

Hess. K. and K. Bosley, 1993. Methodology for validation of a Tampa Bay circulation model. Estuarine and Coastal Modeling, pp. 83-94.

Holland, G. J., 1980. An analytic model of the wind and pressure profiles in hurricanes. Monthly Weather Review, 108, pp. 1212-1218.

Holthuijsen, L.H., N. Booij, R.C. Ris, IJ.G. Haagsma, A.T.M.M. Kieftenburg, E.E. Kriezi, and M. Zijlema, 2003. SWAN Cycle III version 40.20, User Manual (not the short version). Delft University of Technology, DELFT, The Netherlands.

HRD, 2006. http://www.aoml.noaa.gov/hrd/Storm_pages/ivan2004/wind.html. Viewed on March, 2006.

HUBBERT, G.D. and KYL., MCINNEs, 1999. A storm surge inundation model for coastal planning and impact studies. Journal of Coastal Research, 15, pp. 168-185.

IPET, 2006. Performance evaluation of the New Orleans and Southeast Louisiana hurricane protection system. Draft Final Report of the Interagency Performance Evaluation Task Force, US Army Corps of Engineers.

Jelesnianski, C. P., 1972. SPLASH (Special Program List Amplitudes of Surges From Hurricanes). NOAA Technical Memorandum, MWS TDL-46, National Oceanic and Atmospheric Administration, Silver Spring, MD.

Jelesnianski, C. P., J. Chen, W. A. Shaffer and A.J. Gilad, 1984. SLOSH: Sea, lake, and overland surges from hurricanes. Oceans 84, Marine Technology Society, Washington D.C.

Jelesnianski, C. P., J. Chen, and W. A. Shaffer, 1992. SLOSH: Sea, Lake, and Overland Surges from Hurricanes. NOAA Technical Report NWS 48, United States Department of Commerce, NOAA, NWS, Silver Springs, MD., pp. 71.

Kaplan, P., Murray , J.J., and Yu, W.C., 1995. Theoretical analysis of wave impact forces on platform deck structure. Proceedings of the 14th International Conference on Offshore Mechanics and Arctic Engineering, American Society of Mechanical Engineers, vol. 1-A, pp. 189-198.

Kerenyi, K., 2005. Wave forces on bridge decks. Technical note, U.S. Department of Transportation; Federal Highway Administration.

Kliem N., J. W. Nielsen and V. Huess, 2006. Evaluation of a shallow water unstructured mesh model for the North Sea – Baltic Sea. Ocean Engineering, 15 pp. 124-136.

Luettich, R.A., J.J. Westerink and N.W. Scheffner, 1992. ADCIRC: an advanced three-dimensional circulation model for shelves coasts and estuaries, report 1: theory and methodology of ADCIRC-2DDI and ADCIRC-3DL. Dredging Research Program Technical Report DRP-92-6, U.S. Army Engineers Waterways Experiment Station, Vicksburg, NS.

Luettich, R.A. and J.J. Westerink, 2000. ADCIRC, A (Parallel) ADvanced CIRCulation model for oceanic, coastal and estuarine waters. http://www.marine.unc.edu/C_CATS/adcirc/document/users_manual_pdf_version/ADCIRC_manual.pdf.

Lynch, Daniel R. and G. Gray William, 1978. Analytic solutions for computer flow model testing. Journal of the Hydraulic Division, 36(2), pp. 135-153.

Madsen, H. and F Jakobsen, 2004. Cyclone induced storm surge and flood forecasting in the Northern Bay of Bengal. Coastal Engineering, 51, pp. 277-296.

Martin, P.J., 2000. A description of the Naval Coastal Ocean Model version 1.0. NRL report: NRL/FR/7322-009962, Naval Research Lab, pp. 39.

McConnell, K., Allsop, W., and Cruickshank, I., 2004. Piers, jetties, and related structures exposed to waves: Guidelines for hydraulic loadings. Thomas Telford Press, London.

Mellor, G., 2003. The three-dimensional current and surface wave equation. Journal of Physical Oceanography, 33, pp. 1978-1989.

Moon, I., 2000. Development of a coupled ocean wave-circulation model and its applications to numerical experiments for wind waves, storm surges and ocean circulation of the Yellow and East China Seas. Ph.D. Dissertation, Department of Oceanography, Seoul National University.

Moon, I., I. S. OH, T. Murty and Y. H. Youn, 2003. Causes of the unusual coastal flooding generated by Typoon Winnie on the west coast of Korea. Natural Hazards, 29, pp. 485-500.

Moon, I., 2005. Impact of a coupled ocean wave-tide-circulation system on coastal modeling. Ocean Modeling, 8, pp. 203-236.

Morey, S. L., S. Baig, M. A. Bourassa, D. S Dukhovskoy, and J. J. O'Brien, 2006. Remote forcing contribution to storm-induced sea level rise during Hurricane Dennis. Geophysical Research Letters, 33, L19603, doi:10.1029/2006GL027021.

Morison, J. R., M. P. O'Brien, J. W. Johnson and S. A. Shaaf, 1950. The force exerted by surface waves on piles. Petroleum Transactions, 189, pp. 149-157.

Myers, V. A. and Malkin, W., 1961. Some properties of hurricane wind fields as deduced from trajectories. National Oceanic and Atmospheric Administration, US Department of Commerce, National Hurricane Research Project Report 49, pp. 43.

Narendra, T., 1998. Design of modern highway bridges, NewYork: McGraw-Hill, ISBN 0070629978, pp. 197-198.

NDBC, 2006. http://www.ndbc.noaa.gov/Maps/WestGulf_inset.shtml. Viewed on March, 2006.

NED, USGS, 2006. http://seamless.usgs.gov/website/seamless/viewer.php. Viewed on March, 2006.

NHC, NOAA, 2004. http://www.nhc.noaa.gov/2004ivan.shtml. Viewed on March, 2006.

NOAA, 2006a. http://nauticalcharts.noaa.gov/csdl/vdatum.htm. Viewed on March, 2006.

NOAA, 2006b. http://tidesandcurrents.noaa.gov/index.shtm. Viewed on March, 2006.

NOAA, 2006c. http://polar.ncep.noaa.gov/waves/wavewatch/wavewatch.html. Viewed on March, 2006.

NOAA, 2006d. http://www.nhc.noaa.gov/aboutsshs.shtml. Viewed on May, 2006.

NOAA, 2006e. http://www.nhc.noaa.gov/aboutgloss.shtml. Viewed on May, 2006.

NOAA, 2006f. http://www.csc.noaa.gov/cots/progress_reports/scoop_semi06.pdf. Viewed on May, 2006.

NWP, 2004. http://www.bom.gov.au/nmoc/NWP.shtml. Viewed on May, 2006.

OEA, 2005. Hurricane impact analysis and development of design criteria for the I-10 Bridges over Escambia Bay County, Florida. Final report submitted to Florida Department of Transportation Drainage Design Office, Tallahassee, Florida, by Ocean Engineering Associates, INC, Gainesville, Florida.

Orlanski, I., 1976. A simple boundary condition for unbounded hyperbolic flows. Journal of Computational Physics, 21, pp. 251-269.

Overbeek, J., and Klabbers, I. M., 2001. Design of jetty decks for extreme vertical loads. Proceedings of the Ports 2001 Conference, American Society of Civil Engineers, pp. 10.

Peng, M., L. Xie and L. J. Pietrafesa, 2006. Tropical cyclone induced asymmetry of sea level surge and fall and its presentation in a storm surge model with parametric wind fields. Ocean Modelling, 14, pp. 81-101.

Peng, M., L. Xie and L. J. Pietrafesa, 2004. A numerical study of storm surge and inundation in Croatan-Albemarle-Pamlico estuary system. Estuarine Coastal and Shelf Research, 59, pp. 121-137.

Peng, M., L. Xie and L. J. Pietrafesa, 2006. A numerical study of hurricane-induced storm surge and inundation in Charleston Harbor, South Carolina. Journal of Geophysical Research, 111, C08017, 10.1029/2004JC002755.

Powell, M. D., S. H. Houston, L. R. Amat, and N. Morisseau-Leroy, 1998. The HRD real-time hurricane wind analysis system. Journal of Wind Engineering. 77&78, pp. 53-64.

Powell, M. D. and S. H. Houston, 1996(a). Hurricane Andrew's landfall in South Florida. Part I: standardizing measurements for documentation of surface wind fields. Weather and Forecasting, 11, pp. 304-328.

Powell, M. D. and S. H. Houston, 1996(b). Hurricane Andrew's landfall in South Florida. Part II: Surface wind fields and potential real-time applications. Weather and Forecasting, 11, pp. 329–349.

Reid, R. O., and B. R. Bodine, 1968. Numerical model for storm surges in Galveston Bay. ASCE, Journal of Waterway, Harbors, Coastal Engineering Division, 94, pp. 33–57.

SCOOP, 2006. The Southeastern Universities Research Association (SURA) Coastal Ocean Observing and Prediction (SCOOP). http://scoop.sura.org/. Viewed on March, 2006.

Shen, J., H. Wang, M. Sisson and W. Gong, 2006(a). Storm tide simulation in the Chesapeake Bay using an unstructured grid model. Estuarine Coastal & Shelf Science, 68, pp. 1 –16.

Shen, J., K. Zhang, C. Xiao and W. Gong, 2006(b). Improved prediction of storm surge inundation with a high-resolution unstructured grid model. Journal of Coastal Research, 22(6), pp. 1309 –1319.

Shen, J., W. Cong, and H. Wang, 2006(c). Water level response to 1999 Hurricane Floyd in the Chesapeake Bay. Continental Shelf Research, 26, pp. 2484 –2502.

Sheng, Y.P., 1983. Mathematical modeling of three-dimensional coastal currents and sediment dispersion: Model development and application. US Army Corps of Engineers.

Sheng, Y. P., 1986. A three-dimensional numerical model of coastal and estuarine circulation and transport in generalized curvilinear grids. Technical Report No.587.

Sheng, Y. P., 1987. On modeling three-dimensional estuarine and marine hydrodynamics. Three-dimensional models of marine and estuarine dynamics, pp. 35-54.

Sheng, Y. P., 1989. Evolution of a three-dimensional curvilinear-grid hydrodynamic model for estuaries, lakes and coastal waters: CH3D. Estuarine and Coastal Modeling, pp. 40-49.

Sheng, Y. P., 1994. Modeling hydrodynamics and water quality dynamics in shallow waters. Proceedings of the First International Symposium on Ecology and Engineering, Taman Negara, Malaysia.

Sheng, Y.P. and D. Welter, 1995. A three-dimensional lagrangian particle trajectory model for coastal and estuarine applications. Report COEL/95/098. Coastal and Oceanographic Engineering Department, University of Florida. Gainesville, FL.

Sheng, Y. P., 1997. Development of a preliminary hydrodynamics and water quality model of the Indian River Lagoon. Final Report to the St. Johns River Water Management District, Coastal and Oceanographic Engineering Department, University of Florida, Gainesville, Florida

Sheng, Y. P., Y. Zhang, V., Alymov, and J. Lee, 2002. Implementation of wetting-and-drying algorithm to CH3D. Technical Report, Department of Civil and Coastal Engineering, University of Florida, Gainesville.

Sommerfeld, A., 1949. Partial differential equations. Academic Press, New York.

SSEC, 2004. Space Science and Engineering Center, University of Wisconsin-Madison. Viewed on 2005. http://www.ssec.wisc.edu/media/spotlight/ivan.html

Tolman, H. L., 1992. User manual for WAVEWATCH-II. NASA Goddard Space Flight Center, NASA.

Tolman, H. L., 1997. User manual and system documentation of WAVEWATCH-III version 1.15. NOAA / NWS / NCEP / OMB technical note 151, pp. 97.

Tolman, H.L., 1999. User manual and system documentation of WAVEWATCH-III Version 1.18. NOAA/MWS/NCEP/OMB technical note 166, pp. 110.

Upshow, G.F., W.B. Creath, and F.L. Brooks, 1966. Sediment and macrofauna off the coasts of Mississippi and adjacent States. Mississippi Geological Survey Bulletin, 106, pp. 127.

USACE, 2006. http://chps.sam.usace.army.mil/USHESdata/Assessments/2004Storms/Ivan/slosh/Ivan_slosh_report.htm Viewed on March, 2006.

WAMDI group, 1988. The WAM model - a third generation ocean wave prediction model. Journal of Physical Oceanography, 18, pp. 1775–1810.

Wang, H., 1970. Water wave pressure on horizontal plate. Journal of the Hydraulics Division, American Society of Civil Engineers, 96(10), pp. 1997-2017.

Watson, C. C.,1995. The arbiter of storms: a high resolution, GIS based storm hazard model. National Weather Digests, 20, pp. 2-9.

Watson, C. C. and M. E. Johnson, 1999. Design, implementation and operation of a modular integrated tropical cyclone hazard model. Proceeding 23rd conference on hurricanes and tropical meteorology, Dallas, TX.

Weaver, J, Robert, 2004. Effect of wave forces on storm surge. MS Thesis, Department of Civil and Coastal engineering, University of Florida, Gainesville.

Weisberg, R. and L. Zheng, 2006. Hurricane storm surge simulation for Tampa Bay. Estuaries and Coasts, 29(6A), pp. 899-913.

Westerink, J.J. and R.A. Luettich, 1991. Tide and storm surge predictions in the Gulf of Mexico using model ADCIRC-2D. Report to the US Army Engineer Waterways Experiment Station.

Westerink, J.J., J.C. Muccino and R.A. Luettich, 1992. Tide and storm surge computations for the Western North Atlantic and Gulf of Mexico. Estuarine and Coastal Modeling II, M. Spauling [ed]., ASCE, New York, N.Y.

Xie L., L. J. Pietrafesa and M. Peng, 2004. Incorporation of a mass-conservation inundation scheme into a three dimensional storm surge model. Journal of Coastal Research, 20(4), pp. 1209-1223.

Wikipedia, 2006. http://en.wikipedia.org/wiki/Hurricane_Ivan. Viewed on April, 2006.

Wikipedia, 2006. http://en.wikipedia.org/wiki/Hurricane_Dennis#Storm_history. Viewed on March, 2006.

Wilson, B. W.,1957. Hurricane wave statistics for the Gulf of Mexico. Department of Army Corps of Engineers. Technical Memorandum 98.

Wolf J. and R. A. Flather, 2005. Modelling waves and surges during the 1953 Storm. Philosophical Transactions of the Royal Society A: Mathematical, Physical and Engineering Sciences, 363, pp. 1359-1375.

Zhang, Y.-L. and Baptista, A.M. and Myers, E.P, 2004. A cross-scale model for 3D baroclinic circulation in estuary-plume-shelf systems: I. Formulation and skill assessment. Continental Shelf Research, 24, pp. 2187-2214.

BIOGRAPHICAL SKETCH

Yanfeng Zhang was born on December 19th, 1972 at Liaoyang, Liaoning Province, P. R. China. He obtained his Bachelor of Engineering in naval architecture in 1995 and Master of Science in ocean engineering in 1998 both from Tianjin University, P.R. China. In the summer of 2000, he came to USA to pursuit his Ph.D. in coastal and oceanographic engineering at Department of Civil & Coastal Engineering, University of Florida.